12-2010

Fabrication of Multi-Material Structures Using Ultrasonic Consolidation and Laser-Engineered Net Shaping

John Olorunshola Obielodan
Utah State University

FABRICATION OF MULTI-MATERIAL STRUCTURES USING ULTRASONIC CONSOLIDATION AND LASER-ENGINEERED NET SHAPING

by

John Olorunshola Obielodan

A dissertation submitted in partial fulfillment
of the requirements for the degree

of

DOCTOR OF PHILOSOPHY

in

Mechanical Engineering

Approved:

_____	_____
Dr. Brent Stucker Major Professor	Dr. Thomas Fronk Committee Member
_____	_____
Dr. Leijun Li Committee Member	Dr. Yibin Xue Committee Member
_____	_____
Dr. Randy Jost Committee Member	Dr. Byron R. Burnham Dean of Graduate Studies

UTAH STATE UNIVERSITY
Logan, Utah

2010

ABSTRACT

Fabrication of Multi-material Structures Using Ultrasonic Consolidation

and Laser-Engineered Net Shaping

by

John Olorunshola Obielodan, Doctor of Philosophy

Utah State University, 2010

Major Professor: Dr. Brent E. Stucker
Department: Mechanical and Aerospace Engineering

This research explores the use of two additive manufacturing processes for the fabrication of multi-material structures. Ultrasonic consolidation (UC) and laser-engineered net shaping (LENS) processes were used for parallel systematic investigations of the process parameters and methodologies for the development of multi-material structures.

The UC process uses ultrasonic energy at low temperature to bond metallic foils. A wide range of metallic materials including nickel; titanium; copper; molybdenum; tantalum; MetPreg®; silver; stainless steel; and aluminum alloys 1100, 3003, and 6061 were bonded in different combinations. Material domains are inherently discrete in ultrasonically consolidated structures. The mechanical properties of some of the bonded structures were characterized to lay the groundwork for their real-life applications.

LENS uses a laser beam to deposit metallic powder materials for the fabrication of fully dense structures. Mechanical testing was used to characterize the flexural and

tensile properties of dual-material structures made of Ti6Al4V/10wt%TiC composite and Ti6Al4V materials. Experimental results show that the strength of transition joints in multi-material structures significantly depends on the joint design.

Dual-material minimum weight structures, representing geometrically and materially complex structures, were fabricated using the results of the process parameters and fabrication methodologies developed in this work. The structures performed well under loading test conditions. It shows that function-specific multi-material structures ultrasonically consolidated and LENS fabricated can perform well in real-life applications.

(216 pages)

To my wife, Funmilayo, and my children, Rotimi, Busayo, Ibukun and Opemipo

ACKNOWLEDGMENTS

I would like to thank my major advisor, Dr. Brent Stucker, for his insightful guide and encouragements on my research and studies since inception. I also thank my other committee members, Dr. Thomas Fronk, Dr. Leijun Li, Dr. Yibin Xue, and Dr. Randy Jost, for their thoughtful advice on this research work.

My appreciation also goes to the staff of the department, especially Bonnie Ogden and Terry Zollinger who were of help during the course of my study. The assistance of Dr. Yanzhe Yang (James) and other research group members is deeply appreciated.

This research was funded by NSF through grant Nos. CMMI 061457 and CMMI 0522908 and the office of Naval research through grant No. N000140710633

Above all, I thank God, for the strength to begin this work and His sustaining grace that helped through to completion.

John Obielodan

CONTENTS

LIST OF TABLES

LIST OF FIGURES

CHAPTER 1

INTRODUCTION AND LITERATURE REVIEW

1.1 Research Motivation and Problem Statement

The engineering community has witnessed unprecedented innovations and development of new materials in recent history. This development spans all categories of materials ranging from polymers to ferrous and non-ferrous metals, ceramics and composites. Advanced materials for specialized applications have emerged while better understanding and new applications of the traditional ones are continuously been developed. Designers more than ever before have a broader data base of materials for new designs and also, for improving the performance and reliability of existing systems.

Emerging designs seek to use specific materials where they are functionally required either in a single component structure or in a sub-system or system assembly. The new trend is such that different types of materials may be required at different locations in a structure, enabling the structure to exhibit different functional material properties in required locations. A structure may be fabricated using a combination of ductile metal, a hard, wear resistant alloy of either the same base material or another compatible material, and a corrosion resistant material at another location. As an example, the surface properties of soft materials are changed appropriately by coating them with wear or corrosion resistant materials for applications in machineries and biomedical implants. In some other cases, different categories of materials may be required to perform respective functions in a component. An example is a design requiring the differing functional properties of metals, ceramics and/or polymers in a single structure. Dissimilar material components are particularly common in the power

generation, chemical, petrochemical, nuclear and electronics industries. The desire for fuel efficiency in the automotive and aerospace industries drives their continuous efforts at reducing weight by using new material combinations, and hence, new fabrication technologies in some cases [1, 2].

The revolution in materials development has, however, not been matched with manufacturing capabilities. The major challenge, and one of the cost drivers of multi-material design, is the joining of the different materials [1]. Today, fabrication techniques and capabilities for multi-materials processing fall far behind in development, such that the realizations of conceptual multi-material structural designs have been limited. The modern design trend of specifying materials where they are functionally required requires joining capabilities for optimal performance of fabricated structures. Also, the high cost of many advanced materials with specialized properties constrains them to be economically specified just at locations where they are required. These requirements impose several material interfaces in a structure, such that many inter-material joint designs become inevitable [3-7].

A critical factor in multi-material structures is ensuring that good strength is obtained at the material interfaces. The interfaces in many cases are the weakest locations in multi-material structures. Depending on the materials joined and the technology employed, the interface bond can be mechanical, chemical, or metallurgical. Obviously, the extent and nature of the material interactions at the interface affect the bond strength. Several other factors affect the strength of a structure at the joints, such as material compatibility, inter-diffusion and formation of brittle intermetallics (mostly in the case of some metals) [7].

1.2 Literature Review

Most of the multi-material structures currently in use are made by joining different materials using mechanical fasteners or welding. The materials of each of these structures are selected based on their functional requirements. They have applications in different industries like aerospace, automotive, biomedical, nuclear and many others. Although great advances have been achieved in some of the traditional manufacturing methods, they do not yet have the capabilities to effectively fabricate mixes of geometry and material complexities that satisfy the desired functional requirements of some proposed structures. Some of the technologies that have been used for several decades with capabilities for dissimilar material manufacturing are discussed in the following sections. This is followed by discussions on additive manufacturing technologies with multi-material fabrication capabilities.

1.2.1 Multi-Materials Forming Technologies

1.2.1.1 Injection Molding

Injection molding is a traditional polymer processing method developed in the nineteenth century. It involves forcing molten polymer into mold cavities with the application of pressure. It allows net shape manufacturing of intricate, high precision, three dimensional parts at high production rates. It has been used to successfully manufacture components to replace wood, glass and metals in many applications, thereby reducing weight and cost without compromising functionality. The major process parameters are: melt temperature, viscosity, shot size, plunger ram velocity/rate of cavity fill, and cavity pressure [8].

Advances in injection molding technology led to the development of capabilities for multi-material polymeric components manufacture. Some of the advantages include two-color aesthetics, soft touch texture, brand identification, and property modification for shock absorption, impact resistance, etc. [9]. In multi-material injection molding, different materials are combined to achieve desired combinations of properties in a single component. Such components have applications in domestic appliances, hand tools, electronics, surgical instruments, automobile interiors, and others. Different processing routes are used for the variants of multi-material injection molding. The three major categories are multi-component molding, multi-shot molding and over-molding [10-12].

In multi-component molding, we have three methods, as follows. *Co-injection molding* uses sequential injection of different materials into a mold through the same gating system. The first material forms the core while the second material forms a skin around the core. The first material, that is the core, is placed in another mold in order to inject the second material around the core. *Bi-injection molding* is the process in which different polymeric materials are injected into the mold through different gates simultaneously. In *Interval injection molding*, there is simultaneous injection of different materials through the same gate with limited mixing.

Multi-shot molding is used to describe any process in which multiple material shots are applied to produce a single component. Over-molding is a process in which components are placed in an injection mold as a core and then molded over with another material. The first material can be polymer, metal or ceramic. A common example is over-molding of a plastic handle on top of a metal piece to form simple tools such as screw drivers and scissors.

1.2.1.2 Powder Injection Molding (PIM)

PIM is an innovative process that combines powder metallurgy and injection molding technologies for producing net-shape metallic, ceramic or any hard to process materials into useful engineering components. It provides the geometric shape attributes associated with injection molding and the performance attributes associated with full density powder metallurgy and ceramic sintering. Components of varying degrees of complexities are fabricated at competitive costs with this method. It has been successfully used for single material as well as dual-material components. The process involves feedstock preparation, injection molding, de-binding and sintering [13-14]. Metal or ceramic powder is proportionately mixed with polymer and wax. The mixture is heated in a screw-heated barrel and forced under pressure into the mold cavity where it cools and is subsequently ejected. The green component is then thermally processed to remove the polymer and sintered to obtain a densified final product.

The PIM process is applicable for micro, meso and macro scale single and dual material component manufacture [13-16]. It is used to manufacture components for computer disk drives, cellular telephones, dental orthodontics, surgical tools, investment casting cores, military and sporting firearms, wrist watches, automotive and other industrial applications.

For a successful dual material component PIM manufacture, the materials should have similar thermal expansion, similar densification behavior, good chemical compatibility for inter-diffusion and exhibit good interfacial bonding characteristics. Component geometry should also be given good consideration in product design for PIM manufacture to avoid failures due to residual stresses and/or interfacial stress differential

during densification. Differences in shrinkage behavior between the two materials at the early stage of sintering lead to defect formation, as the component is at its weakest form at that stage.

1.2.2 Multi-Material Joining Technologies

1.2.2.1 Adhesive Bonding

Adhesive bonding is a process in which natural or synthetic adhesives are applied on the surfaces of two materials to bond them to each other. The process is applicable to a vast number of similar and dissimilar materials that cannot be easily joined by other methods. The process has a wide range of applications in aerospace structures joining, automobiles, and in surgery for teeth and bone repairs, among others [17-19]. Adhesive bonding has been used for the bonding of aircraft primary structures for more than six decades. It is still in use in some applications as an alternative to riveting. The process has been found to possess better fatigue resistance than equivalent mechanically fastened structures [17]. It is a joining method of choice when there is concern about contact corrosion between two dissimilar materials as a result of different electro-chemical potentials. With adhesive bonding, the materials joined are isolated from each other by the adhesive used [17-18, 20]. It performs well with higher surface to volume ratio materials, such as sheets.

1.2.2.2 Ultrasonic Welding

In ultrasonic welding, high frequency vibration energy is applied between two materials to produce metallurgical bonding between them. The materials to be welded are placed between the anvil and a vibrating sonotrode. The vibration and applied normal

force causes friction and temperature rise between the two materials to be joined. In metals the friction cleans the contact surface by pulverizing and partly removing contaminants and oxides from the faying surfaces, thereby establishing metallurgical bonds between them. The welding mechanism involves the normal and oscillating shear forces creating small spot welds, which progressively become a full weld on the weld surface, with less than 5% plastic deformation of the materials [21]. This technology has been used to weld a range of similar and dissimilar materials for several decades. In polymers, the parts to be joined are held together under pressure between the oscillating horn and an immobile anvil and are subjected to ultrasonic vibrations of 20 to 40 KHz frequency at right angles to the contact area. Alternating high frequency stresses generate heat and melting of the polymer materials at the joint interface to produce a good quality weld. Ultrasonically weldable materials include some similar and dissimilar metals, polymer and polymer composites; metal to ceramic materials, and metal to polymer composites [21-26]. When compared to other welding techniques, ultrasonic welding is characterized by low energy input. According to Daniels [21], the welding temperature developed is not more than 40% of the melting temperature of the parent material. This technology is applicable to welding sheet materials as well as wires to sheets or plates.

In ultrasonic metal welding, the vibration of the sonotrode is typically parallel to the interface between work pieces to be welded. The variables that influence the quality of welds are applied normal force, ultrasonic power and welding time. Frequency and ambient temperature are often fixed. The variables have to be optimized for every combination of materials welded. The conditions of the surfaces to be welded in terms of the roughness is very important; the lower the surface roughness, the better the weld. As

such, polished surfaces will yield stronger bonds than rougher surfaces. Cleaning the work piece is not critical, however clean surfaces yield better reproducibility. The energy required to weld a set of materials depends on their hardness and thickness. The harder the material, the higher the weld energy needed for effective weld. Also, for a given material, the thicker it is, the higher the weld energy required. Table 2.1 shows combinations of ultrasonically weldable metals as compiled by O'Brien [27].

Kruger et al. [23] demonstrated the capabilities of both ultrasonic metal welding and ultrasonic polymer welding techniques to join metals to polymer matrix composites. Aluminum and copper alloys were welded with fiber glass composite using the two processes with some success. Figure 1.1 shows the optical micrograph of the welds made using the two processes.

Table 1.1: Binary Combinations of Weldable Materials [27]

	Al	Be	Cu	Ge	Au	Fe	Mg	Mo	Ni	Pd	Pt	Si	Ag	Ta	Sn	Ti	W	Zr
Al Alloys	●	●	●	●	●	●	●	●	●	●	●	●	●	●	●	●	●	●
Be Alloys		●	●			●										●		
Cu Alloys			●		●	●	●	●	●	●	●		●	●		●	●	●
Ge					●						●							
Au						●			●	●	●	●	●			●	●	●
Fe Alloys									●	●	●		●	●		●	●	●
Mg Alloys							●						●			●		
Mo alloys								●	●		●			●		●	●	●
Ni Alloys									●	●	●			●		●	●	
Pd										●			●	●				
Pt Alloys											●	●		●		●	●	
Si													●	●				
Ag Alloys													●	●				●
Ta Alloys														●		●	●	
Sn															●			
Ti Alloys																●	●	
W Alloys																	●	
Zr Alloys																		●

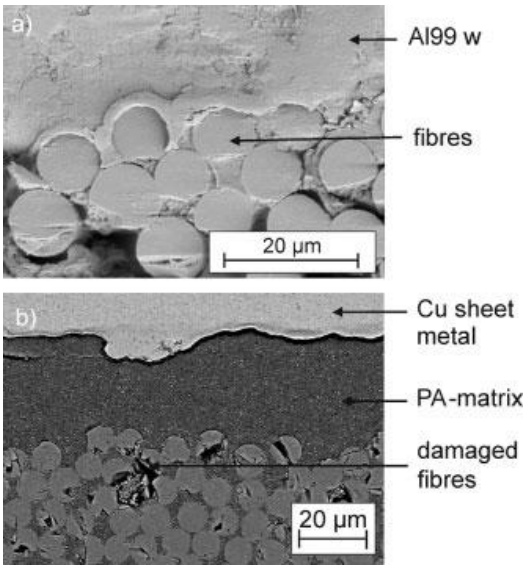

Figure 1.1: SEM images of (a) AlMg3/Al99w/composite joint by ultrasonic metal welding, and (b) Cu/composite joint by ultrasonic polymer welding [23].

1.2.2.3 Friction Stir Welding

Friction stir welding is a solid state joining process in which a non-consumable rotating tool with a specially designed pin and shoulder is inserted into the abutting edges of sheets or plates of material and translated from one point to the other along the line of contact, thereby joining the materials. The welding process was developed in 1991 at The Welding Institute (TWI), United Kingdom [28]. This welding technique is used to join both similar and dissimilar materials, especially materials that cannot be easily joined by the conventional fusion welding methods. A number of light weight materials suitable for the automotive, rail, marine, and aerospace transportation industries can be joined by friction stir welding [29]. As the tool rotates and moves through the interface region, it generates sufficient heat to cause plastic deformation of the materials being joined. The softened materials around the rotating and translating pin are continuously moved from the leading face of the pin to its trailing edge. The moving column of stirred hot metal consumes the interface of the abutting or lapping materials, disrupting and dispersing the

surface oxides. This process results in solid state joining of the materials. The intense plastic deformation at the ensuing elevated temperature generates fine equiaxed recrystallized grains, which results in good mechanical properties. The schematic is shown in Fig. 2.2. Friction stir welding is used for dissimilar material joining with good success [30-33].

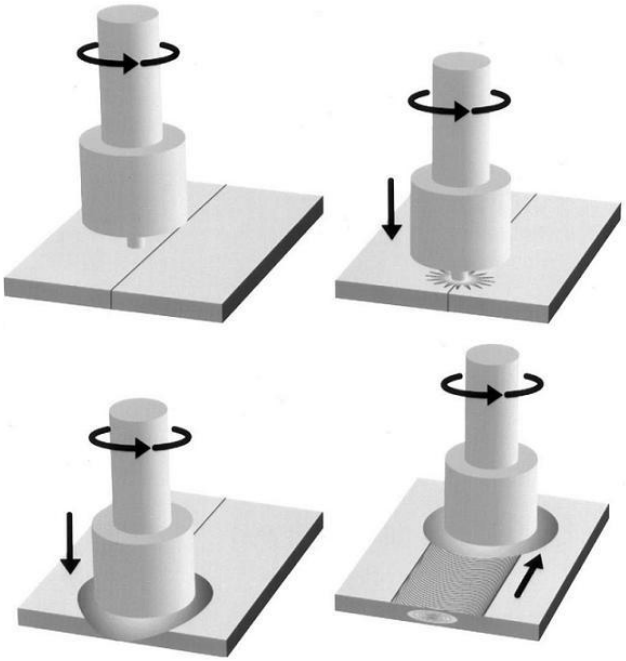

Figure 1.2: Schematic illustration of the friction stir welding process [41].

1.2.2.4 Diffusion Bonding

Diffusion bonding, as a subdivision of solid-state welding, is a joining process in which the principal mechanism is interdiffusion of atoms across the mating interfaces of materials. This method of fabrication has been used in a wide range of industries, from the electronics and nuclear fields to the manufacture of various engineering and aerospace components [34]. A driving force extending the use of diffusion bonding is the

increasing development of novel and advanced materials, such as metal matrix composites (MMCs), intermetallics and ceramics, where fusion processes are not applicable or are limited for joining [35-40].

Diffusion of most metals is conducted in vacuum or in an inert atmosphere (normally dry nitrogen, argon or helium) in order to reduce detrimental oxidation of the faying surfaces. In the process, two cleaned surfaces are brought into contact with the application of pressure and temperature for a period of time. The addition of heat permits deformation of the microscopic points of contact between the two materials, thus greatly increasing the true area of contact. If the surface contaminants are soluble in the base material, the contaminant will diffuse away into the bulk, permitting true inter-atomic bonding at the interface [6]. The primary variables controlling diffusion bonding are pressure, temperature, surface finish, surface cleanliness, and time. Contact pressures typically range from 3 – 35MPa at temperatures of 50 to 98% of the absolute melting temperature of the materials. Holding times can range from a few minutes to several hours, depending on the type of materials been bonded. The process can fabricate nearly ideal joints, similar to the base metal.

High temperatures can degrade the strength at the joints. This makes post bonding heat treatment inevitable in many cases [6,42]. Dissimilar materials are successfully joined using the process. The use of a suitable interlayer between materials to be joined has offered solution to most of the problems [43]. Transient liquid phase (TLP), a variant of diffusion bonding is commonly used to join difficult to weld metals and ceramics. TLP involve melting an interlayer between two materials to be joined. The liquid fills the voids, thus providing nearly complete contact and minimal pressure is thus required. The

interlayer materials always have relatively lower melting temperatures compared to the materials to be joined, and in some cases have constituent elements that can rapidly diffuse into the base metals. TLP produces joints with excellent strengths and reliability.

1.2.2.5 Laser Beam Welding

Laser welding uses the heating effects of a concentrated beam of coherent, monochromatic laser light to produce a fused weld bead. For a given joint and material combination, the principal processing parameters are beam power, focused spot size and welding speed [44]. The high energy density maintains a deeply penetrating weld pool, enabling through-thickness welds to be made rapidly in a single pass. Rapid cooling rates result in the formation of beneficial fine solidification microstructures and limited HAZ grain growth. Some non-equilibrium phases, some of which may be detrimental to mechanical properties, are also formed [44]. The heat affected zone is small, and cooling is very rapid with little distortion, and a high depth-to-width ratio for the fusion zone. The heat and fluid flow in the weld pool can extensively influence temperature gradients, cooling rates and solidification structure. In addition, the fluid flow and the convective heat transfer in the weld pool have been shown to control the penetration and shape of the fusion zone. The physical properties of materials that influence laser welding are thermal conductivity, absorptivity, density, specific heat capacity, coefficient of thermal expansion, and melting temperature. Chemical mismatches between joint components usually result in diffusion that can form undesirable phases and poor mechanical properties at the joints [44]. Table 1.2 shows the weldability of some binary metals, based on phase diagrams and practical experience [45].

The process has been widely used in the automotive industry for the welding of automotive body structures using similar materials joining. However, with the growing trend of multi-material structures designs, greater interest and research efforts are currently being directed at joining dissimilar materials using a laser beam. One major challenge is the formation of brittle intermetallic phases at the interface of most dissimilar materials that are fusion joined [45-51].

Table 1.2: Laser Weldability of Binary Metal Combinations (E=Excellent, G=Good, F=Fair, P=Poor, -=No Data Available) [45]

	W	Ta	Mo	Cr	Co	Ti	Be	Fe	Pt	Ni	Pd	Cu	Au	Ag	Mg	Al	Zn	Cd	Pb	Sn
W																				
Ta	E																			
Mo	E	E																		
Cr	E	P	E																	
Co	F	P	F	G																
Ti	F	E	E	G	F															
Be	P	P	P	P	F	P														
Fe	F	F	G	E	E	F	F													
Pt	G	F	G	G	E	F	P	G												
Ni	F	G	F	G	E	F	F	G	E											
Pd	F	G	G	G	E	F	F	G	E	E										
Cu	P	P	P	P	F	F	F	F	E	E	E									
Au	-	-	P	F	P	F	F	F	E	E	E	E								
Ag	P	P	P	P	P	F	P	P	F	P	E	F	E							
Mg	P	-	P	P	P	P	P	P	P	P	P	F	F	F						
Al	P	P	P	P	F	F	P	F	P	F	P	F	F	F	F					
Zn	P	-	P	P	F	P	P	F	P	F	F	G	F	G	P	F				
Cd	-	-	-	P	P	P	-	P	F	F	F	P	F	G	E	P	P			
Pb	P	-	P	P	P	P	-	P	P	P	P	P	P	P	P	P	P	P		
Sn	P	P	P	P	P	P	P	P	F	P	F	P	F	F	P	P	P	P	F	

1.2.3 Additive Manufacturing Processes

Additive Manufacturing (AM) Processes are a group of related advanced manufacturing technologies used to fabricate complex 3-dimensional solid objects directly from computer aided design (CAD) solid models without the use of molds. The technologies are also known by other names such as, solid freeform fabrication (SFF), rapid prototyping (RP), layered manufacturing (LM), digital manufacturing (DM) and e-

manufacturing [52]. A common feature of the processes is the numerical decomposition of the CAD solid models into thin horizontal layers as one of the preprocessing measures before data transfer to the machine for fabrication. During fabrication, the computer sequentially sends geometrical details of the layers starting from the bottom of the 3D model for direct physical replication by the AM machine until the final object is completely fabricated. Some of the AM techniques include stereolithography (SLA), selective laser sintering (SLS), fused deposition modeling (FDM), 3-dimensional object printing, laser-engineered net shaping (LENS), electron beam melting (EBM), laminated object manufacturing (LOM) and ultrasonic consolidation (UC). All the technologies produce objects by adding rather than removing materials. The major differences between them are: (1) materials used and (2) part building technique [52-55]. The technologies have been widely used for the fabrication of prototypes, as one of the design and development stages for product manufacture [53-54]. Other applications include rapid tooling (RT) [56-57], repairs of damaged mechanical components [58], medical implants and devices fabrication [59-61], and for other end-use functional components.

There are fundamental relationships that can naturally be drawn between many of the earlier discussed non-AM processes and AM processes. The underlying principles of some the non-additive processes are applied for direct 3D solid object manufacture in a layer-wise fashion. Table 1.3 shows some of the related processes.

The abilities of the AM technologies to fabricate complex objects without the use of molds offer designers a window of opportunities for novel designs that would otherwise have been impossible with traditional manufacturing techniques. High levels of geometrical complexities can now be designed for manufacture with little or no

restrictions. It also offers a wide range of possibilities including fabrication of structures with spatial material heterogeneity, direct build of multi-component assemblies, and the fabrication of materially graded structures – in density and composition [54,62]. There is also, the potential to deposit materials just where they are needed. The capabilities for high geometrical complexities and spatial heterogeneity of materials composition and density make AM much more preferable than the injection molding techniques and other technologies capable of dissimilar materials fabrication discussed earlier. The injection molding technologies are subject to many "design for manufacture rules," which are not required in the AM technologies, as molds are not needed for component fabrication. Also, there is a limit to material spatial heterogeneity in powder injection molding in contrast to its potentials in the AM techniques. Investments in molds are eliminated in AM. Other fabrication techniques earlier discussed have geometrical limitations, as most of them are restricted to planar and other simple geometries. This makes AM techniques most suitable in cases where geometrical complexities and spatial material heterogeneity are required.

Table 1.3: Corollaries Between Some Non-AM and AM Processes

	Traditional/Non-Additive Processes	**Additive Manufacturing Processes**
1	Adhesive bonding	Layer object manufacturing
2	Ultrasonic welding	Ultrasonic consolidation
3	Laser beam welding	Laser-engineered net shaping
4	Electron beam welding	Electron beam melting
5	Powder injection molding	Binder based powder processes such as: (a) Selective laser sintering/melting (b) Layer object manufacturing of ceramic tapes

1.2.3.1 Heterogeneous Material Solid Modeling

Solid modeling is the initial step in additive manufacturing. The current solid models contain geometry information stored as data and topology information incorporated in the data structure [63]. The models do not contain information about the interior of the object such as material variation, microstructure and other heterogeneities. They basically support homogenous material object modeling. This makes the fabrication of heterogeneous material objects a difficult task. Heterogeneous objects can be classified as objects with distinct material domains. The different domains might be homogeneous or heterogeneous. Those with homogeneous domains have definable material boundaries while those with heterogeneous domains do not have definable material boundaries. The material information of heterogeneous objects can be described and categorized in terms of two elements – composition and microstructure [64]. The ability to model heterogeneous solid materials holds the key to local composition and microstructure control required in some applications [61, 65-66].

Many alternative heterogeneous solid models for additive manufacturing have been proposed over the years [63-70]. There is a consensus that the use of the current stereolithography (STL) format is not adequate for complex object representation in terms of materials and microstructure distribution.

Some of the current attempts to fabricate multi-material structures with many of the existing AM technologies require a lot of skills and ingenuity of researchers. Currently, many CAD files are combined to fabricate multi-material structures. This necessitates interruptions of the build process to allow for change from one CAD file to the other. The processes are cumbersome, grossly inefficient and lead to under-utilization

of the capabilities of additive manufacturing processes. It is difficult for machine operators to precisely monitor the deposition of materials where they are needed during the build process in some cases. Besides developing heterogeneous material modelers, the current machines are in urgent need of upgrade to be able to interpret the material and microstructure attributes in heterogeneous solid models. They also need to be equipped with multiple material deposition facilities.

Overviews of selected AM technologies that have multi-material capabilities are presented below.

1.2.3.2 Three-Dimensional Object Printing

Three-dimensional object printing (3D printing) was developed in the early 1990s, as a direct extension of ink jet printing devices [57]. The printer head is the only element in common between ink jet printing and 3D printing. The printer head serves to shoot either droplets of binder, or liquid-to-solid compound to layers of a 3D object. The shooting of the actual building material (liquid-to-solid compound) is known as direct printing, while the shooting of droplets of binder on the powder material is called binder printing [71]. Binder materials are jet printed on thin layers of powder for selective binding until the 3D object is completely fabricated. The unbound powder material forms the support for the bonded areas. In this way, complex 3D geometries with overhangs, undercuts, and internal details (with provision for removing loose powder) can be fabricated. There is no geometrical limitation as long as unbounded powder can be removed after fabrication. The porous green body is strengthened by a pre-sintering process and then infiltrated. 3D printing can form any material that can be obtained as a powder, ranging from polymers to metals and ceramics. Because of its flexibility in

handling a wide range of materials, and its added ability to locally tailor the material composition, 3D printing offers potentials for the direct manufacture of structural components with unique microstructures. Monolithic components that integrate functions of multiple discrete components can be fabricated, thereby reducing the number of parts, saving space, and weight [62, 72, 73].

Objet Geometries Limited has been able to commercialize the 3D printing of dissimilar material end use products using polymer materials [74]. Objet's Connex^{TM} machines jets multiple materials simultaneously to fabricate a multi-material structure. Figure 1.3 shows a dual-material structure fabricated by Growit^{TM} using Objet's Connex^{TM} printers. Two acrylic-based polymers with different mechanical properties were used for the fabrications.

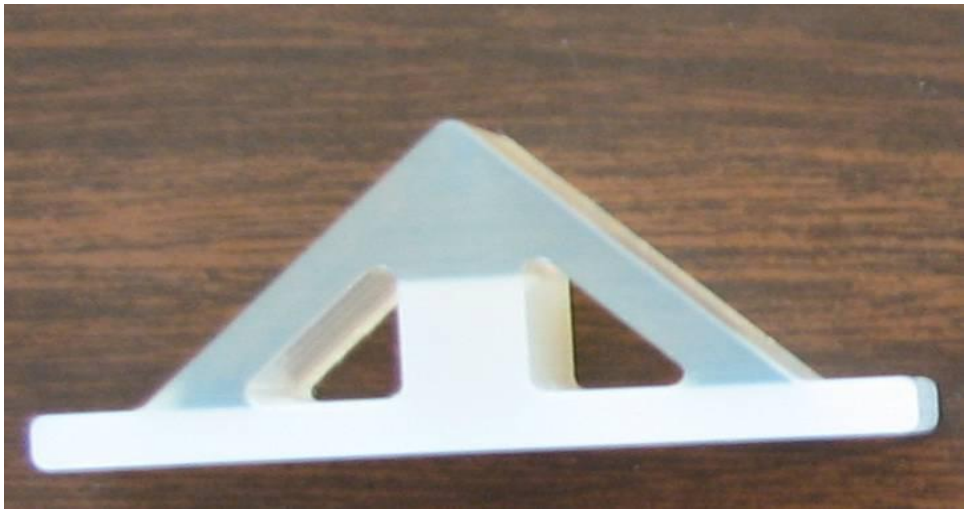

Figure 1.3: A dual material triangular structure fabricated using 3D printing.

1.2.3.3 Laser-Engineered Net Shaping (LENS)

Laser-engineered net shaping (LENS) is an additive manufacturing process that combines laser welding with layered manufacturing to fabricate three dimensional objects using metal powder. The process, which was developed by Sandia National Laboratory

and commercialized by Optomec Design Company of Albuquerque, New Mexico, uses a continuous wave neodymium-doped yttrium aluminum garnet (Nd:YAG) laser to directly melt metal particles in a layer-wise fashion to form solid objects. Newer versions of Optomec LENS machines use fiber lasers. LENS is one of several, similar direct metal deposition (DMD) processes, including direct light fabrication (DLF), epitaxial laser metal forming (E-LMF), laser direct forming (LDF), laser rapid forming (LRF) and others. Some of the DMD processes use powder feeders while others use wire feeders, or both. Like other AM technologies, a solid CAD model of the object is first numerically sliced into horizontal layers of specified thickness. The layers are used to develop a series of tool path patterns required to build the entire solid object [75,76]. In LENS, fully dense solid objects are fabricated by focusing the high-power laser beam onto a metal substrate (typically of similar composition) where streams of metallic powder are simultaneously injected. The particles are delivered through four coaxial nozzles by carrier gas to the focus of the laser [77-79]. The laser locally melts the powder in a molten pool on top of the surface of the growing part. The motion path generated using the sliced 3D solid model provides the control commands for the laser, powder feeder and motion system to produce linear beads of material that are laid side-by-side with a designated amount of overlap.

The build chamber of the LENS machine consists of an enclosure with controlled oxygen level, called the glove box. The closed system is filled with argon inert gas to bring oxygen levels to 2 – 5 parts per million for fabrication. The obvious advantage provided by the low oxygen level is to reduce oxidation of the deposited materials. The glove box offers a second advantage over an open-air deposition system that has safety

concerns [77]. In a three axes LENS machine, the deposition base plate or substrate on which components are fabricated is mounted on an x-y motion stage in the glove box. The laser and the deposition nozzles move as an integral unit in the z – axis, a distance equal to the layer thickness after every layer is deposited to maintain the stand-off distance. Features requiring material deposition at angled orientations to the substrate can be deposited by tilting the laser beam delivery head or tilting the work piece so that the beam axis is normal to the deposition plane; this usually requires more than three axes [79]. It may also be done by carefully selecting the right combination of process parameters in cases where the laser beam delivery head or the motion table cannot be tilted [80].

The basic process parameters that influence the quality of fabrications for a given material are laser intensity, laser power, travel speed, powder flow rate, layer thickness, and hatching space. Different combinations of these parameters determine the molten pool size, the depth of re-melt in the substrate and the thickness of the bead formed [81].

Another factor that determines the molten pool size is the substrate temperature and the reflectivity of the powder materials being processed. Higher rates of heat dissipation from the molten pool result in smaller pool width. Control of the molten pool size and solidification rate determines the microstructure of the component, which in turn determines its mechanical properties. Higher solidification rates result in smaller grain sizes and higher strength [79, 82-85]. Tensile data show that the as-deposited strength of materials fabricated are equivalent to those of their wrought materials and in some cases better properties are obtained as a result of rapid solidification and grain refinement [76-77, 79, 82, 86].

The capabilities of the LENS process for dissimilar materials fabrication have been demonstrated by various researchers. Studies documented in the literature include LENS fabrication of composites [83-85, 87-88] and gradient compositions such as stainless steel and inconel 690 [88], titanium and titanium carbide [89-90], titanium and inconel [91] and others. The number of steps required to form composite materials by most other fabrication processes like ingot metallurgy and subsequent thermo-mechanical processing are considerably reduced in the LENS process. New material compositions specifically tailored for desired properties can easily be deposited by appropriate blends of the needed materials. Metal powders can either be blended before deposition or multiple powder feeders can be employed to feed different materials at predetermined flow rates to achieve desired compositions at different locations in the component. Figure 1.4 shows the volume percent of the major constituents of the materials in a SS316/In690 graded materials composition [91].

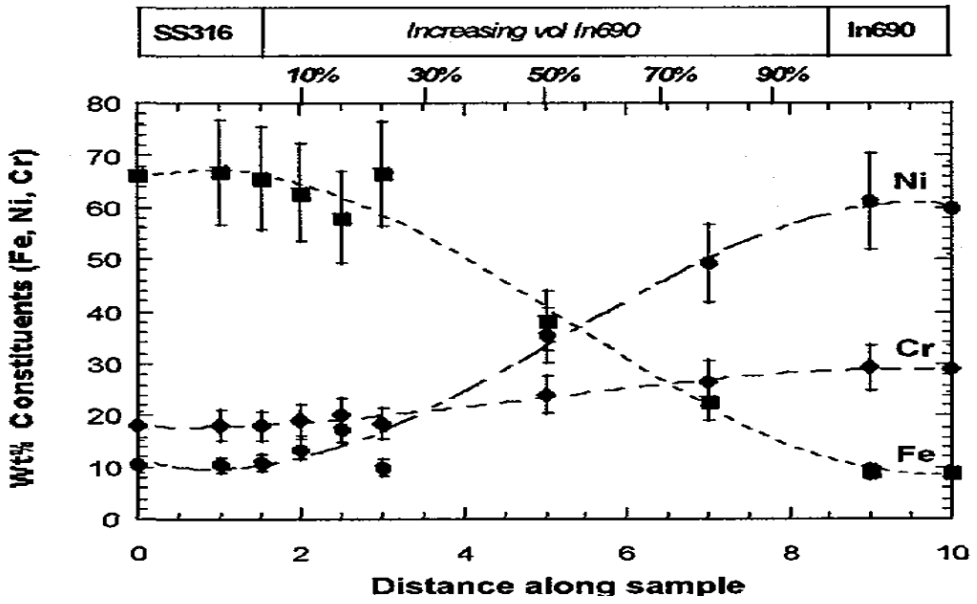

Figure 1.4: Alloyed constituent results for blending In690 into SS316 from 0 – 100 volume percent [89].

1.2.3.4 Ultrasonic Consolidation

Ultrasonic consolidation (UC) is a solid-state fabrication process that combines ultrasonic metal welding and layered manufacturing techniques to produce three-dimensional objects. The process uses the power of high frequency ultrasonic vibration at low amplitude to bond thin foils of materials to form solid objects. It combines normal and oscillating shear forces on mating foils on the one hand and the resulting friction forces between the materials to fracture and displace surface oxides from the materials. These atomically clean surfaces are then brought into direct contact under modest pressure and temperatures that are less than 50% of the melting point of the materials. The materials are thus metallurgically bonded [92]. Fractured oxides and surface impurities in the materials are distributed in the bond zone. The process combines the layer-by-layer addition of foils with contour milling using the integrated 3-axis computer numerical control (CNC) machining facilities to produce desired component geometry. It is therefore both an additive and subtractive process.

Apart from removing the substrate upon which the deposition is made after fabrication is completed, no further machining of the part is required, making it a net shape fabrication process. Some notable advantages of the solid state UC process are as follows [92].

- No process associated high-temperature or airborne powder safety hazards.
- No atmospheric control is required.
- As low temperature is involved on the small volume of material affected, less energy is needed.

- Embrittlement, residual stress, distortion and dimensional changes are greatly reduced with low temperature processing.

The UC machine consists of a welding horn, also known as a sonotrode, which exerts normal force and oscillatory high-frequency vibration on the materials to be welded. Welding takes place on a substrate fixed on a heated plate. The UC machine is designed for automatic foil material feed, but materials can also be fed manually.

Previous work has demonstrated other potential applications of UC. These include honeycomb structure fabrications [93]; embedding shape memory alloy (SMA) fibers and silicon carbide fibers in an aluminum matrix [92-98]; and embedded electronics structures [99]. The multi-material capabilities of UC have also been demonstrated [92, 100; see chapter 2]. The primary process parameters in UC fabrications are [94]

(i) vibration,

(ii) amplitude,

(iii) temperature,

(iv) welding speed, and

(v) normal force.

Other parameters that can affect weld quality include welding sonotrode roughness, materials surface finish [101], and sonotrode displacement relative to machine specified materials width in an automated material feed system [see chapter 4]. The optimum process parameters for different materials like aluminum alloys 3003 and 6061; stainless steel 316L; and Al/SiC metal matrix composite have been experimentally determined in earlier work [93-94, 96-98, 100, 102].

The bonding mechanism of ultrasonically consolidated foils has not been fully understood. Many authors believe that the surface oxides on foils have to be broken and displaced to facilitate bonding [94,102; chapter 4]. Johnson [103], in his work, however observed high oxygen content at the interface between UC bonded foils, suggesting that there may still be unbroken oxides after consolidation. The dominant factor influencing the bonding of mating foils is the cyclic softening due to ultrasonic energy. Acoustic softening enhances plastic deformation of the materials. According to Obielodan et al. [chapter 2] at least one of the two materials being bonded at any time must be plastically deformable under the action of the normal and oscillating shear forces of the sonotrode.

1.3 Research Goal and Objectives

The goal of this work is to establish methodologies for fabricating multi-material structures having effective inter-material joint strength using additive manufacturing technologies. The objectives are as follows.

(i) The first objective of this work is to establish the weldability of selected multi-materials using ultrasonic consolidation and laser-engineered net shaping.

(ii) The second objective is to establish, experimentally, the methodologies for fabricating bondable dissimilar material structures using the two processes.

(iii) The third objective is to fabricate and test dual-material minimum weight structures using UC and LENS.

UC and LENS were selected for this work because they are metal based processes and possess the capabilities for fabricating load bearing structures. UC represents low temperature laminate based AM processes while LENS represents high temperature

powder based AM processes. Both processes possess capabilities for multi-material structures fabrication. Material variation in UC is discrete but LENS has capabilities for both discrete and continuous material variation. Also, LENS fabricated structures have good microstructures and mechanical properties.

1.4 Structure of the Dissertation

This dissertation is prepared based on a multi-paper format in accordance to the publications policy of the Graduate School, Utah State University. The general structure is shown in Fig. 1.5 while Table 1.4 shows the publication details. Chapters 2 to 6 consist of articles generated from this research work. Chapter 2 explores the weldability of various multi-materials using UC. UC bonded multi-materials were qualitatively analyzed using metallographic studies. This is followed by the optimization of the shear strengths of ultrasonically consolidated Ti/Al 3003 dual-material structures in Chapter 3. Chapter 4 is focused on minimizing defects between adjacent foils in UC fabricated parts and Chapter 5 discusses methodologies for fabricating dual-material minimum weight structures, a representation of geometrically and materially complex structures. In Chapter 6, the characterization of the strengths of various material transition joint designs in LENS fabricated multi-material parts is presented. Chapter 7 discusses major conclusions from this work and identified future work.

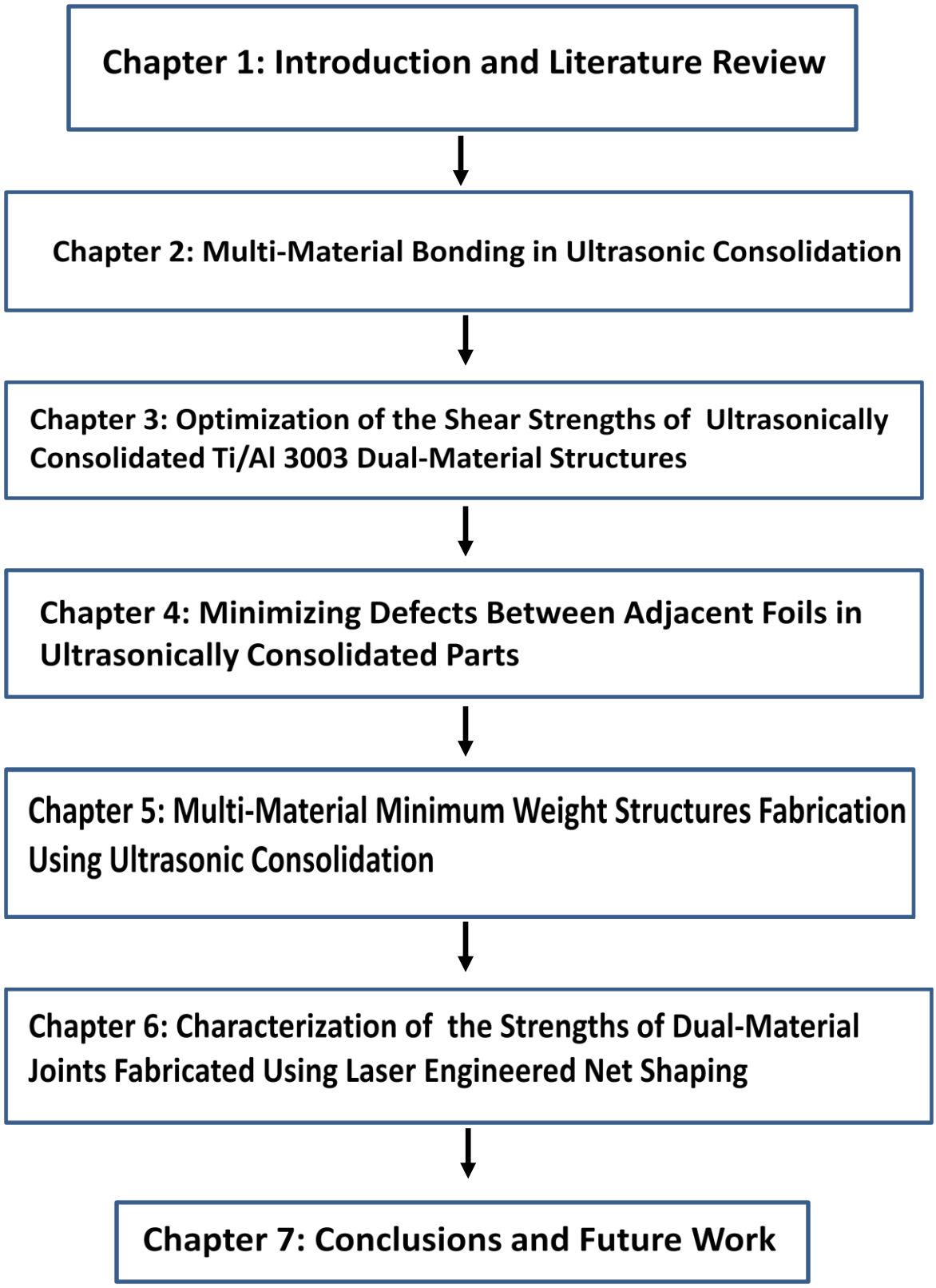

Figure 1.5: General structure of this dissertation.

Table 1.4: Details of the Articles in this Dissertation

Authors	Article Title	Journal	Status	Chapter in Thesis
Obielodan, J.O., Ceylan, A., Murr, L.E. and Stucker, B.E.	Multi-materials bonding in ultrasonic consolidation	Rapid Prototyping Journal	Published	Chapter 2
Obielodan, J.O., Stucker, B.E., Martinez, E., Martinez, J.C., Hernandez, D.H., Ramirez, D.A., and Murr, L.	Optimization of the shear strengths of ultrasonically consolidated Ti/Al 3003 dual-material structures	Journal of Materials Processing Technology	Submitted	Chapter 3
Obielodan, J.O., Janaki Ram, G.D., Stucker, B.E., and Taggart, D.G.	Minimizing defects between adjacent foils in ultrasonically consolidated parts	Journal of Engineering Materials and Technology	Published	Chapter 4
Obielodan, J.O. and Stucker, B.E.	Multi-material structures fabrication using ultrasonic consolidation	Journal of Materials Processing Technology	To be Submitted	Chapter 5
Obielodan, J.O. and Stucker, B.E.	Characterization of the strengths of dual-material joints fabricated using laser-engineered net shaping	Journal of Engineering Materials and Technology	To be Submitted	Chapter 6

References

[1] Lesemann, M.A., Bröckerhoff, M., and Urban, P., 2008. "The Prospects of Multi-Material Design," ATZ Autotechnology, **8**, pp. 15-20.

[2] Sun, Z., and Ion, J.C., 1995, "Laser Welding of Dissimilar Metal Combinations," J. Mater. Sci., **30**, pp. 4205-4214.

[3] Eagar, T.W., 1990, "Joining Technology," Adv. Mater. Process., **137(**1), pp. 65, 81.

[4] Messler, R.W., 2000, "Trends in Key Joining Technologies for the Twenty-First Century," Assembly Automation, **20(**2), pp. 118-128.

[5] Eagar, T.W., Baeslack, W.A., and Kapoor, R., 1994, "Joining of Advanced Materials, an Overview," Encyc. Adv. Mater., Pergamon Press, Oxford, pp. 1207-1211.

[6] Eagar, T.W., and Baeslack, W.A., 1994, "Joining Processes, Advanced," Encyc. Adv. Mater., Pergamon Press, Oxford, pp. 1221-1225.

[7] Eagar, T.W., 1990, "Challenges in Joining Emerging Materials," *Proceedings of international conference on advances in joining newer structural materials*, Montreal, Canada, July 23-35.

[8] Agrawal, A.R., Pandelidis, I.O., and Pecht, M, 1987, "Injection-Molding Process Control – A Review," Polym. Eng. and Sci., **27(**18), pp. 1345-1357.

[9] Hansen, M., 2006, "Overmolding: A Multifaceted Medical Device Technology," Medical Devices & Diagnostic Industry.

[10] Goodship, V., and Love, J.C., 2002, "Multi-Material Injection Moulding," Rapra Review Reports, **13(**1).

[11] Aurrekoetxea, J., Castillo, G., Cortes, F., Sarrionandia, M.A., Urrutibeascoa, I., 2006, "Failure of Multi-Material Fusion Bonding Interface Generated During Over-Injection Molding/Thermoforming Hybrid Process', J. Applie. Polym. Sci., **102**, pp. 261-265.

[12] Arzondo, L.M., Pino, N., Carella, J.M, Pastor, J.M. Merino, J.C., Poveda J., and Alonso, C., 2004, "Sequencial Injection Over-Molding of an Elastomeric Ethylene-Octene Copolymer on a Polypropylene Homopolymer Core," Polym. Eng. Sci., **44**(11), pp. 2110-2116.

[13] Zauner, R., 2006, "Micro-Powder Injection Moulding," Microelectr. Eng., **83**(4-9), pp. 1442-1444.

[14] Johnson, J.L., Tan, L.K., Suri, P., and German, R.M., 2003, "Design Guidelines for Processing Bi-Material Components via Powder-Injection Molding," J. Mater., **55(**10), pp. 30-34.

[15] Imgrund, P., Rota, A., Petzoldt, F., and Simchi, A., 2007, "Manufacturing of Multi-Functional Micro Parts by Two-Component Metal Injection Moulding," Int. J. Adv. Technol., **33**(1-2), pp. 176-186.

[16] Imgrund, P., Rota, A., Petzoldt, F., and Simchi, A., 2008, "Microinjection Moulding of 316L/17-4PH and 316L/Fe Powders for Fabrication of Magnetic – Nonmagnetic Bimetals," J. Mater. Process. Technol., **200**(1-3), pp. 259-264.

[17] Davis, M., and Bond, D., 1999, "Principles and Practices of Adhesive Bonded Structural Joints and Repairs," Int. J. Adhesion & adhesives, **19**(2), pp. 91-105.

[18] Yanagida, H., Taira, Y., Shimo,e S., Atsuta, M., Yoneyama, T., and Matsumura, H., 2003, "Adhesive Bonding of Titanium-Aluminum-Niobium Alloy with Nine Surface Preparations and Three Self-Curing Resins," European J. Oral sci., **111** (2), pp. 170-174.

[19] McCabe, J.F., Carrick, T.E., and Kamohara, H., 2002, "Adhesive Bond Strength and Compliance for Denture Soft Lining Materials," Biomaterials, **23**(5), pp. 1347-1352.

[20] Higgins, A., 2000, "Adhesive Bonding of Aircraft Structures," Int. J. Adhesion & Adhesives, **20**(5), pp. 367-376.

[21] Daniels, H.P.C., 1965, "Ultrasonic Welding," J. Ultrasonics, **3**(4), pp. 190-196.

[22] Jones, J.B., and Powers, J.J. (Jr), 1956, "Ultrasonic Welding," J. Ultrasonics, **35**, pp. 761-766.

[23] Kruger, S., Wagner, G., and Eifler, D., 2004, "Ultrasonic Welding of Metal/Composite Joints," Adv. Eng. Mater., **6**(3), pp. 157-159.

[24] Balle, F., Wagner, G.,and Eifler, D., 2007, "Ultrasonic Spot Welding of Aluminum Sheet/Carbon Fiber Reinforced Polymer – Joints," Materialwissenschaft und werkstofftechnik, **38**(11), pp. 934-938.

[25] Kuckert, H., Born, C., Wagner, G., and Eifler, D., 2003, "Residual Stress Distributions in Glass/Metal Joints Produced by Ultrasonic Torsion Welding," Materialwissenschaft und Werkstofftechnik, **34**(1), pp. 30-33.

[26] Jacobs, M., 2007, "Glass-Metal Joining in Nuclear Environment: The State of the Art," External Report of the Belgian Nuclear Research Center.

[27] O'Brien, R.L. 1991, "Welding Processes," Welding Handbook, 8th Ed., American Welding Society, Miami, FL, Volume 2.

[28] Mishra, R.S., and Ma, Z.Y., 2005, "Friction Stir Welding and Processing," Mater. Sci. Eng., **50**(1-2), pp. 1-78.

[29] Thomas, W.M., and Nicholas, E.D., 1997, "Friction Stir Welding for the Transportation Industries," Mater. & Design, **18**(4-6), pp. 269-273.

[30] Shigematsu, I., Kwon, Y.J., Suzuki, K., Imai, T., and Saito, N., 2003, "Joining of 5083 and 6061 Aluminum Alloys by Friction Stir Welding," J. Mater. Sci. Lett., **22**(5) pp. 353-356.

[31] Li, Y., Murr, L.E., and McClure, 1999, "Flow Visualization and Residual Microstructures Associated with the Friction-Stir Welding of 2024 Aluminum to 6061 Aluminum," Mater. Sci. Eng. A, **271**(1-2), pp. 213-223.

[32] Li, Y., Trillo, E.A., and Murr, L.E., 2000, "Friction-Stir Welding of Aluminum Alloy 2024 to Silver," J. Mater. Sci. Lett., **19**(12), pp. 1047-1051.

[33] Ouyang, J., Yarrapareddy, E., and Kovacevic, R, 2006, "Microstructural Evolution in the Friction Stir Welded 6061 Aluminum Alloy (T6-Temper Condition) to Copper", J. Mater. Process. Technol., **172**(1), pp. 110-122.

[34] Xun, Y.W, and Tan, M.J., 2000, "Applications of Superplastic Forming and Diffusion Bonding to Hollow Engine Blades," J. Mater. Process. Technol., 99(1-3), pp. 80-85.

[35] Elssner, G., and Petzow, G., 1990, "Metal/Ceramic Joining," ISIJ Int., **30**(2), pp. 1011-1032.

[36] Jadoon, A.K., Ralph, B., and Hornsby, P.R., 2004, "Metal to Ceramic Joining Via a Metallic Interlayer Bonding Technique," J. Mater. Process. Technol., **152**(3), pp. 257-265.

[37] Travessa, D., Ferrante, M., and Ouden, G.D., 2002, "Diffusion Bonding of Aluminum Oxide to Stainless Steel Using Stress Relief Interlayers," Mater. Sci. Eng. A., **337**(1-2), pp. 287-296.

[38] Esposito, L., Bellosi, A., and Celotti, 1997, "Silicon Nitride Nickel Joints Through Diffusion Bonding," Acta Metall., **45**(12), pp. 5087-5097.

[39] He, P., Feng, J.C., Zhang, B.G., and Qian, Y.Y., 2003, "A New Technology for Diffusion Bonding Intermetallic TiAl to Steel with Composite Barrier Layers," Material Characterization, **50**(1), pp. 87-92.

[40] Wu, G.Q., and Huang, Z., 2001, "Superplastic Forming/Diffusion Bonding of Laser Surface Melted TiAl Intermetallic Alloy," Scr. Mater., **45**(8), pp.895-899.

[41] Mahoney, M.W., Rhodes, C.G., Flintoff, J.G., Spurling, R.A., and Bingel W.H., 1998, "Properties of Friction-Stir-Welded 7075 T651 Aluminum," Metall. Mater. Trans. A, **29**(7), pp. 1955-1964.

[42] Nicholas, M.G., and Mortimer, D.A. 1985. "Ceramic/Metal Joining for Structural Applications," Mater. Sci. Technol., **1**(9), pp. 657-665.

[43] Kundu, S., Ghosh, M., Laik, A., Bhanumurthy, K., Kale, G.B., and Chatterjee, S., 2005, "Diffusion Bonding of Commercially Pure Titanium to 304 Stainless Steel Using Copper Interlayer," Mater. Sci. Eng. A, **407**(1-2), pp. 154-160.

[44] Sun, Z., and Ion, J.C., 1995, "Laser Welding of Dissimilar Metal Combinations," J. Mater. Sci., **30**(17), pp. 4205-4214.

[45] Belforte, D., and Levitt, M., 1989, "The Industrial Laser Annual Handbook," Pennwell Books, Laser Focus, Tulsa Oklahoma, USA.

[46] Borrisutthekul, R., Miyashita, Y., and Mutoh, Y., 2005, "Dissimilar Material Laser Welding Between Magnesium Alloy AZ31B and Aluminum Alloy A5052-O," Sci. Technol. of Adv. Mater., **6**, pp. 199-204.

[47] Theron, M., Van, R. C., and Ivanchev, L.H., 2007, "CW ND:YAG Laser Welding of Dissimilar Sheet Metals," *International Congress on Applications of Lasers & Electro-Optics*, Orlando, Florida, USA, October 29-November 1.

[48] Yao, C., Binshi Xu, B., Zhang, X., Huang, J., Fu, H., and Wu, Y., 2009, "Interface Microstructure and Mechanical Properties of Laser Welding Copper-Steel Dissimilar Joint," Optics and Lasers in Eng., **47**(7-8), pp. 807-814.

[49] Li, Z., and Fontana G., 1998, "Autogenous Laser Welding of Stainless Steel to Free-Cutting Steel for the Manufacture of Hydraulic Valves," J. Mater. Process. Technol., **74**(1-3), pp. 174-182.

[50] Sepold, G., and Kreimeyer, M., 2003, "Joining of Dissimilar Materials," *Proceedings of SPIE,* Osaka, Japan, Vol. 4831.

[51] Mian, A., Newaz, G., Vendra, L., Rahman, N, and Georgiev, D.G., 2005, "Laser Bonded Micro-joints between Titanium and Polyimide for Applications in Medical Implants," J. Mater. Sci.: Mater. in Medicine, **16**(3), pp. 229-237.

[52] Jacobs, P.F., "A Brief History of Rapid Prototyping & Manufacturing: The Early Years," *Proceedings of the 2002 International Conference on Metal Powder Deposition for Rapid Manufacturing*, Newport Beach, California, USA, October 28 – 29.

[53] Yan, X., and Gu P., 1996, "A Review of Rapid Prototyping Technologies and Systems," Computer-Aided Design, **28**(4), pp. 307-318.

[54] Dutta, D. , Prinz, F.B., Rosen, D., and Weiss, L., 2001, "Layered Manufacturing: Current Status and Future Trends," J. Comput. Inform. Sci. in Eng., (ASME), **1**(1), pp. 60-71.

[55] Santos, E.C., Shiomi, M., Osakada, K., and Laoui, T., 2006, "Rapid Manufacturing of Metal Components by Laser Forming," Int. J. Mach. Tool and Manufacture, **46**(12-13), pp. 1459-1468.

[56] Levy, G.N., Schindel, R.,and Kruth, J.P., 2003, "Rapid Manufacturing and Rapid Tooling with Layer Manufacturing (LM) Technologies, State of the Art and Future Perspectives," CIRP Annals – Manufact. Technol., **52**(2), pp. 589-609.

[57] Karapatis, N.P., Van Griethuysen, J.P.S., and Glardon, R., 1998. "Direct Rapid Tooling: A Review of Current Research," Rapid Protot. J., **4**(2), pp. 77-89.

[58] Bohrer, M., Basalka, H., Birner, W., Emiljanow, K., Goede, M., and Czerner, S., "Turbine Blade Repair with Laser Fusion Welding and Shape Recognition," *Proceedings of the 2002 International Conference on Metal Powder Deposition for Rapid Manufacturing*, Newport Beach, California, USA.October 28 – 29.

[59] Stevens, B., Yang, Y., Mohandas, A., Stucker, B., and Nguyen, K., 2008, "A Review of Materials, Fabrication Methods, and Strategies Used to Enhance Bone Regeneration Engineered Bone Tissues," J. Biomed. Mater. Res.: Part B – Applied Biomat., **85**(2), pp. 573-582.

[60] Wu, B.M., Borland, S.W., Giordano, R.A., Cima, L.G., Sachs, E.M., and Cima, M.J., 1996, "Solid Free-Form Fabrication of Drug Delivery Devices," J. Controlled Release, **40**(1-2), pp. 77-87.

[61] Hong, S.B., Eliaz, N., Sachs, E.M., Allen, S.M., and Latanisan, R.M., 2001, "Corrosion Behavior of Advanced Titanium-Based Alloys Made by Three-Dimensional Printing (3DP^{TM}) for Biomedical Applications," Corr. Sci., **43**(9), pp. 1781-1791.

[62] Cohen, D.L., Malone, E., Lipson, H., and Bonassar, L.J., 2006, "Direct Freeform Fabrication of Seeded Hydrogels in Arbitrary Geometries," Tissue Eng., 12(5), pp. 1325-1335.

[63] Dutta, D., and Shpitalni, M., 2000, "Heterogeneous Solid Modeling for Layered Manufacturing," CIRP Annals – Manufact. Technol., **49**(1), pp. 109-112.

[64] Kumar, V. and Dutta, D., 1998, "An Approach to Modeling & Representation of Heterogeneous Objects," J. Mech. Design, **120**(4), pp. 659-667.

[65] Rajagopalan, S., Goldman, R., Shin, k., Kumar, V., Cutkosky, M., and Dutta D., 2001, "Representation of Heterogeneous Objects During Design, Processing and Freeform Fabrication," Mater. and Design, **22**(3), pp. 185-197.

[66] Cho, W., Sachs, E.M., Patrikalakis, N.M., Cima, M., Liu, H., Serdy, J., and Stratton, C.C. "Local Composition Control in Solid Freeform Fabrication," *Proceedings of the 2002 NSF Design, Service and Manufacturing Grantees and Research Conference*, San Juan, Pueto Rico, January 5 – 7.

[67] Siu, Y.K., and Tan, S.T., 2002, "Modeling the Material Grading and Structures of Heterogeneous Objects for Layered Manufacturing," Comput.-Aided Design, **34**(10), pp. 705-716.

[68] Zhu, F., and Chen, K., 2003, "A CAD Modeling System for the Components Made of Multi Heterogeneous Materials," Materials & Design, **26**(2), pp. 113-126.

[69] Wei, S., 2000, "Multi-Volume CAD Modeling for Heterogeneous Object Design and Fabrication," J. Comput. Sci. & Technol., **15**(1), pp. 27-36.

[70] Wei, S., Fiang T., Lin F., 2004, "A Process Algorithm for Freeform Fabrication of Heterogeneous Structures," Rapid Protot. J., **10**(5), pp. 316-326.

[71] Hiller, J., Lipson, H., 2009, "STL 2.0: A Proposal for a Universal Multi-Material Additive Manufacturing File Format," *Proceedings of 20th International Solid Freeform Fabrication Symposium*, Austin, TX, USA, August 3-5.

[72] Cho ,W., Sachs, E.M., and Patrikalakis, N.M. 2001, "Solid Freeform Fabrication with Local Composition Control," Rapid Prototyping Association of Society of Manufacturing Engineers, **7**(2), pp. 1-5.

[73] Malone, E., Rasa, K., Cohen, D., Isaacson, T., Lashley, H., Lipson, H., 2004, "Freeform Fabrication of Zinc-Air Batteries and Electromechanical Assemblies," Rapid Protot. J., **10**(1), pp. 58-69.

[74] Growit Rapid Prototyping & Manufacturing, 2009. Available at: www.growit3d.com/services/multi-material-polyjet/. Accessed: October, 2009.

[75] Atwood, C.L., Ensz, M.T., Greene, D.L., Griffith, M.L., Harwell, L.D., Jeantette F.P., Keicher D.M., Oliver M.S., Reckaway D.E., Romero J.A., Schlienger M.E., and Smugeresky J.D., 1999, "Laser Spray Fabrication for Net-Shape Rapid Product Realization LDRD," Technical Report, Sandia National Labs.

[76] Choi, J., and Chang, Y., 2005, "Characteristics of Laser Aided Direct Metal/Material Deposition Process for Tool Steel," Int. J. Mach. Tool and Manufacturing, **45**(4-5), pp. 597-607.

[77] Keicher, F.P., and Smugeresky, J.D. 1997, "The Laser Forming of Metallic Components Using Particulate Materials," J. Mater., **49**(5), pp. 51-54.

[78] Vasinonta, A., Beuth, J.L., and Griffith, M.L., 2001, "A Process Map for Consistent Build Conditions in the Solid Freeform Fabrication of Thin-Wall Structures,"J. Manuf. Sci. and Eng., **123**(2-3), pp. 615-623.

[79] Lewis, G.K., and Schlienger, E., 2000, "Practical Considerations and Capabilities for Laser Assisted Direct Metal Deposition," Mater. and Design, **21**(4), pp. 417-423.

[80] Wu, X., and Mei, J., 2003, "Near Net Shape Manufacturing of Components Using Direct Laser Fabrication Technology," J. Mater. Process. Technol., **135**(2-3), pp. 266-270.

[81] Laeng, J., Stewart, J.G. and Liou, F.W., 2000. "Laser Metal Forming Processes for Rapid Prototyping - A Review," Int. J. Prod. Res., **38**(16), pp. 3973-3996.

[82] Hofmeister, W., Wert, M., Smugeresky, J., Philliber J.A., Griffith, M., and Ensz, M., "Investigating Solidification with the Laser-Engineered Net Shaping (LENS^{TM}) Process," J. Mater. (JOM-e), http://www.tms.org/pubs/journals/JOM/9907/Hofmeister/Hofmeister-9907.Html. Accessed in October, 2008.

[83] Banerjee, R., Collins, P.C., Genç, A., and Fraser, H.L., 2003, "Direct Laser Deposition of In Situ Ti6Al4V/TiB Composites," Mater. Sci. and Eng. A, **358**, pp. 343-349.

[84] Schwendner, K.I., Banerjee, R., Collins, P.C., Brice, C.A, and Fraser, H.L., 2001, "Direct Laser Deposition of Alloys from Elemental Powder Blends," Scripta Mater., **45**, pp. 1123-1129.

[85] Banerjee, R., Collins, P.C., and Fraser, H.L., 2002. "Laser Deposition of In Situ Ti–TiB Composites," Adv. Eng. Mater., **4**(11), pp. 847-851.

[86] Hofmeister, W., Griffith, M., Ensz, M., and Smugeresky, J., 2001. "Solidification in Direct Metal Deposition by LENS Processing," J. Mater., **53**(9), pp. 30-34.

[87] Wang, F., Mei, J., Jiang, H., and Wu, X, 2007, "Laser Fabrication of Ti6Al4V/TiC Composites Using Simultaneous Powder and Wire Feed," Mater. Sci. and Eng. A, **445-46**, pp. 461-466.

[88] Wang, F., Mei, J., Jiang, H., and Wu, X, 2008, "Direct Laser Fabrication of Ti6Al4V/TiB," J. Mater. Process. Technol., **195**(1-3), pp. 321-326.

[89] Griffith, M.L., Harwell, L.D., Romero, J.T., Schlienger, E., Atwood, C.L., and Smugeresky, J.E., 1997, "Multi-Material Processing by LENS," *Proceedings of the 8th International Solid Freeform Fabrication Symposium*, Austin, TX, USA, August 11-13.

[90] Liu, W., and DuPont, J.N., 2003, "Fabrication of Functionally Graded TiC/Ti Composites by Laser-Engineered Net Shaping," Scripta Mater., **48**(9), pp. 1337-1342.

[91] Domack, M.S., and Baughman, J.M., 2005, "Development of Nickel-Titanium Graded Composition Components," Rapid Protot. J., **11**(1), pp. 41-51.

[92] White, D.R., 2003, "Ultrasonic Consolidation of Aluminum Tooling," Adv. Mater. & Process., **161**(1), pp. 64-65.

[93] Kong, C.Y., Soar, R.C, and Dickens, P.M., 2004, "Ultrasonic Consolidation for Embedding SMA fibers Within Aluminium Matrices," Composite Structures, **66**(1-4), pp. 421-427.

[94] Kong, C.Y., Soar, R.C., and Dickens, P.M., 2004, "Optimum Process Parameters for Consolidation of 3003 Aluminum," J. Mater. Process. Technol., **146**, pp. 181-187.

[95] George J.L., 2006, "Utilization of Ultrasonic Consolidation in Fabricating Satellite Decking," Master's thesis, Utah State University, Logan, UT.

[96] Kong, C.Y., and Soar, R.C., 2005, "Fabrication of Metal–Matrix Composites and Adaptive Composites Using Ultrasonic Consolidation Process," Mater. Sci. Eng. A, **412**, pp. 12-18.

[97] Yang, Y., Janaki Ram, G.D., and Stucker, B.E., 2007, "An Experimental Determination of Optimum Processing Parameters for Al/SiC Metal Matrix Composites Made Using Ultrasonic Consolidation," J. Eng. Mater. Technol., **129**(4), pp. 538-549.

[98] Yang, Y., Janaki Ram, G.D., and Stucker, B.E., 2009, "Bond Formation and Fiber Embedment During Ultrasonic Consolidation," J. Mater. Process. Technol., **209**(10), pp. 4915-4924.

[99] Siggard, E.J., 2007, "Investigative Research into the Structural Embedding of Electrical and Mechanical Systems Using Ultrasonic Consolidation (UC)," Master's thesis, Utah State University, Logan, UT.

[100] Obielodan, J.O., and Stucker, B.E., 2009, "Effects of Post Processing Heat Treatments on the Bond Quality and Mechanical Strength of Ti/Al 3003 Dual Materials Fabricated using Ultrasonic Consolidation," *Proceedings of the 20th Solid Freeform fabrication Symposium*, Austin, TX, USA, August 3-5.

[101] Janaki Ram, G.D., Yang, Y., and Stucker, B.E., 2007, "Effects of Process Parameters on Bond Formation During Ultrasonic Consolidation of Aluminum Alloy 3003," J. Manuf. Syst., **25**(3), pp. 221-238.

[102] Kong, C.Y., Soars, R.C., and Dickens, P.M. 2003, "Characterization of Aluminium Alloy 6061 for the Ultrasonic Consolidation Process," Mater. Sci. and Eng. A, **363**(1-2), pp. 99-106.

[103] Johnson, K.E., 2008, "Interlaminar Sub-grain Refinement in Ultrasonic Consolidation," PhD thesis, Loughborough University, UK.

CHAPTER 2

MULTI-MATERIAL BONDING IN ULTRASONIC CONSOLIDATION

This chapter was published as an article in Rapid Prototyping Journal (Vol.16(3), pp.180-188, 2010). The permission to use it as a chapter in this dissertation is contained in the Appendix.

Abstract

Purpose - The increasing interest in engineering structures made from multiple materials has led to corresponding interest in technologies which can fabricate multi-material parts. This work is a further exploration of the multi-material fabrication capabilities of ultrasonic consolidation.

Design/Methodology/Approach - Various combinations of materials including titanium, silver, tantalum, aluminum, molybdenum, stainless steel, nickel, copper, and MetPreg® were ultrasonically consolidated. Some of the materials were found to be effective as an intermediate layer between difficult to join materials. Elemental boron particles were added *in situ* between selected materials to modify the bonding characteristics. Microstructures of deposits were studied to evaluate bond quality.

Findings - Results show evidence of good bonding between many combinations of materials, thus illustrating increasing potential for multi-material fabrication using ultrasonic consolidation.

Originality/Value – Multi-material fabrication capabilities using ultrasonic consolidation and other additive manufacturing processes is a critical step towards the realization of engineering designs which make use of functional material combinations and optimization.

2.1 Introduction

Ultrasonic consolidation (UC) is a solid-state fabrication process that combines ultrasonic metal welding and layered manufacturing techniques to produce three-dimensional freeform objects. The process uses the power of high frequency ultrasonic vibration at low amplitudes to bond thin foils of materials to form solid objects. It combines normal and oscillating shear forces on mating foils; and the resulting friction forces between materials to fracture and displace surface oxides. The exposed atomically clean surfaces are then brought into direct contact under modest pressure and temperatures that are less than half of the melting points of the materials. The materials are thus metallurgically bonded (White, 2003). Fractured oxides and surface impurities are distributed in the bond zone. The process combines the layer-by-layer addition of foils using ultrasonic seam welding with subtractive contour milling using an integrated 3-axis CNC milling head to produce desired component geometry.

Some notable advantages of the solid state UC process are as follows (White, 2003).

- No high-temperature process-associated safety hazards.
- No atmospheric control is required.
- As low temperature is involved and the volume of material affected is small, less energy is needed.
- Low temperature processing reduces embrittlement, residual stresses, distortion and dimensional changes compared to other metal additive manufacturing processes.

The welding horn, also known as a sonotrode, exerts normal force and oscillatory high-frequency vibration on the materials to be welded. Welding takes place on a substrate fixed on a heated plate. The UC machine is designed for automatic foil material feeding, but materials can also be fed manually. Figure 2.1 shows the schematic view of the ultrasonic consolidation process. The primary process parameters are vibration amplitude, temperature, welding speed, and normal force (Kong et al., 2004A). Other parameters that can affect weld qualities include sonotrode roughness, material surface finish (Janaki Ram et al., 2007A), and side-by-side foil positioning accuracy with respect to the automated material feed system (Obielodan et al., 2010).

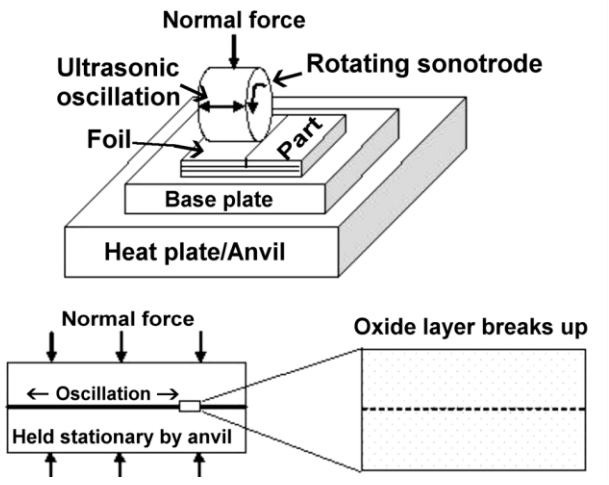

Figure 2.1: Schematic of UC process.

Ultrasonic consolidation is applicable for rapid tooling for injection molding, extrusion, vacuum forming tools and others. It is also used for fabricating tools with conformal cooling channels (White, 2003). Previous work has demonstrated other potential applications of UC, which include honeycomb structures (George, 2006), embedded shape memory alloy (SMA) fibers and silicon carbide fibers in aluminum

matrices (Kong and Soar, 2005, Kong et al., 2004B, Yang et al., 2007, Yang et al., 2009), embedded electronics (Siggard, 2007) and sensors Cheng et al.(2007). While the process has been widely used for single material fabrication with aluminum alloys, only a few researchers have demonstrated its capabilities for multiple material fabrications. The multi-materials capabilities of UC was demonstrated by (Janaki Ram et al., 2007B) in their work in which copper, brass, nickel, inconel 600, AISI 347 stainless steel, stainless steel AISI 304 wire mesh, MetPreg®, and aluminum alloy 2024 were individually welded to aluminum alloy 3003 H18. Fabrication of graded material structures with titanium and nickel alloys using UC have been demonstrated (Domack and Baughman, 2005). The capability of ultrasonic welding to weld metals to a polymer matrix composite has also been demonstrated (Kruger et al., 2004). In this present work, the capabilities of UC to fabricate multi-material structures are further explored. Suitable combinations of molybdenum, tantalum, nickel, stainless steel 316L, silver, MetPreg®, copper, and aluminum alloys 1100-O, 3003-H18, and 6061-O, were bonded using aluminum alloys 3003-H14 and 6061-T6 substrate materials. Boron powder was added *in situ* for some of the material combinations.

Engineers and designers desire to harness the benefits of combining a variety of function-specific materials where they are needed, and the geometrical complexities offered by the UC process to fabricate these structures. The applications of multi-material functional structures are diverse, including surface protection with corrosion or wear resistant materials, radiation shielding, and combining electrical insulators with highly conductive materials for use in aerospace, automobile, ship building, nuclear, electronics, industrial machinery and other industries.

2.2 Experimental Work

A Solidica Formation™ machine was used for the experimental work. Although the machine has an automatic foil feeding mechanism, all foils used except aluminum 3003-H18 material were manually fed. Materials of 40x20mm size of variable height, depending on the number of foils and their thicknesses, were deposited on the aluminum alloy 3003-H14 and 6061-T6 substrates. The two substrates were of 355 x 355 x 12 mm in size. For each deposited specimen, several layers of materials were welded to demonstrate their weldability within the current limits of the primary welding process parameters of the UC machine. Different orders of arrangements of foil stacking for the materials used were experimented. In each material combination, the welding parameters used for each layer was dependent on the material type to be welded at any instant, so for each material type, the most suitable welding parameters were used. The compositions and crystal structures of the materials used, valid at UC operating temperatures, are shown in Table 2.1.

All materials except aluminum alloy 1100-O and boron powder were welded directly using the appropriate process parameter values shown in Table 2.2. The optimum process parameters for aluminum alloy 3003 were obtained from previous work by (Kong et al., 2004B and Janaki Ram et al., 2007A). While work is still ongoing to determine the optimum parameters for most of the other materials in different combinations, the values used in the present work were found to work well for the respective materials. Aluminum alloy 1100 was generally used as an interlayer material between difficult to weld materials. The interlayer was manually placed between the difficult to weld materials and the sonotrode run on the topmost material to weld them together.

Table 2.1: Nominal Compositions and Crystal Structures of Materials Used

Material	Composition	Crystal Structure at UC Temperature	Thickness (μm)
Al alloy 1100-O	Al-0.12Cu	FCC	50
Al alloy 3003 H18	Al-1.2Mn-0.12Cu	FCC	150
Al alloy 6061-O	Al-1.2Mg-0.8Si	FCC	150
MetPreg®	Al2O3 Short Fiber Al matrix reinforced tape	-	200
Molybdenum	99.5%Mo	BCC	127
Tantalum	99.5%Ta	BCC	127
Titanium	Ti-0.59Fe-0.38Mn	HCP	70
Nickel	99.5%Ni	FCC	100
Silver	99.5%Ag	FCC	127
Copper	99.5%Cu	FCC	127
Stainless Steel 316L	Fe-18Cr-14Ni-0.08C	FCC	100
Elemental Boron diameter	B-1Mg	Rhombohedra	< 5 μm

The Al 1100-O interlayer material was found to bond well with most of the materials used in this study. In cases where boron powder was added at the interface of two materials, the powder was thoroughly mixed in water and a brush was used to apply the mixture onto the surface of the substrate or already welded foil. After moisture evaporation, the foil to be welded was manually placed for welding. Mixing the boron powder in water was found to make it adhere more effectively to the substrate before welding than applying loose, dry powder.

Small samples of the deposited materials were mounted and polished according to standard metallographic procedures and observed under an optical microscope. Some of the samples were etched with modified Keller's solution to further reveal the interfacial bonding at the grain size regime, especially for the aluminum alloys. The bonding qualities between the foils of different materials were qualitatively evaluated.

Table 2.2: Process Parameter Values Used for Each Material

Material	Amplitude (μm)	Speed (mm/s)	Normal Force (N)	Temperature (^{o}F)
Al 3003	16	23.70	1750	300
Al 6061	18	19.05	1750	300
Cu	28	15.24	1750	150
Ag	24	15.24	1750	150
Ni	28	12.70	2000	300
Ta	28	10.58	2000	300
Ti	28	10.58	2000	300
Mo	28	10.58	2000	300
MetPreg®	28	12.70	1750	300
SS 316L	28	10.58	2000	300

2.3 Results

Micrographs of bonded materials are shown in Figs. 2.2 to 2.8. The description of the welded foils in each figure is such that, the material that is welded directly on the substrate is the first, followed by the next material, and continuing to the topmost foil material. As an example, Fig. 2.2a shows the micrographs of two silver foils welded to an

Al 3003-H14 substrate, followed by Copper and nickel foils consolidated on each other, where the nickel foil is at the top.

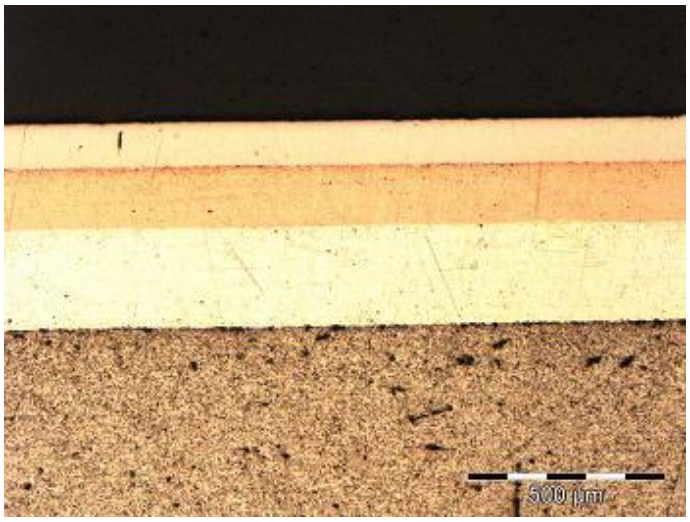

(a): 2Ag/Cu/Ni on Al 3003-H14 substrate.

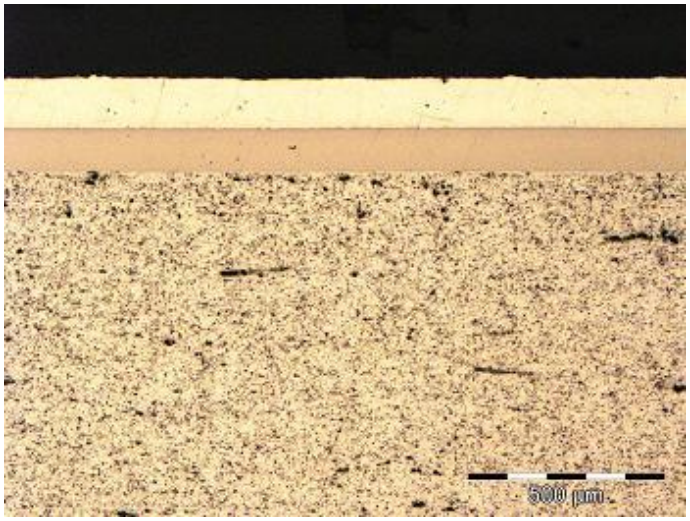

(b): Ni/Ag foils on Al 3003-H14 substrate.

Figure 2.2: Micrographs showing the bond qualities of FCC structured materials.

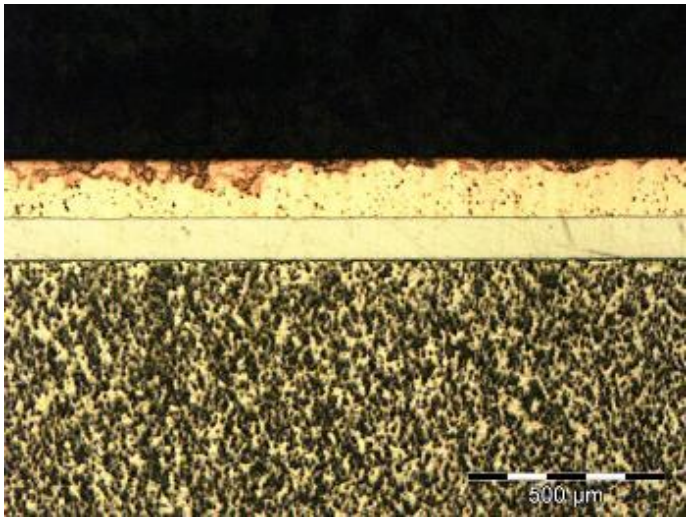

(c): Ni/Cu foils welded on Al 3003-H14 substrate.

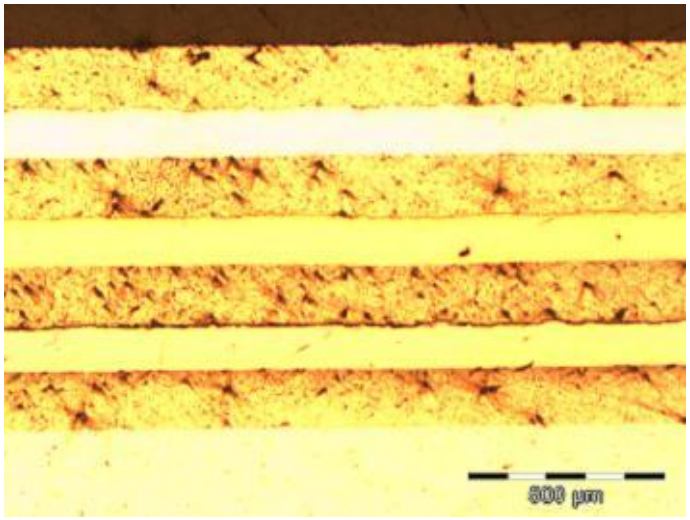

(d): Al 6061/Ni/Al 6061/Cu/Al 6061/Ag/Al 6061 on Al 6061-T6 substrate.

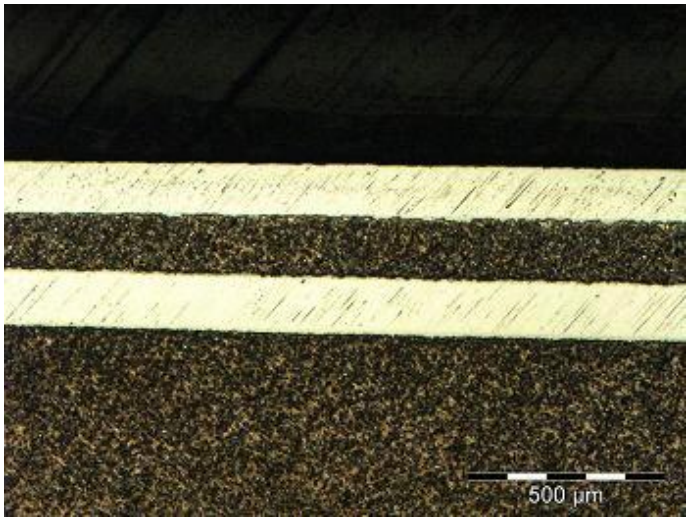

(a): Mo/Al 3003-H18/Mo on Al 3003-H14 substrate.

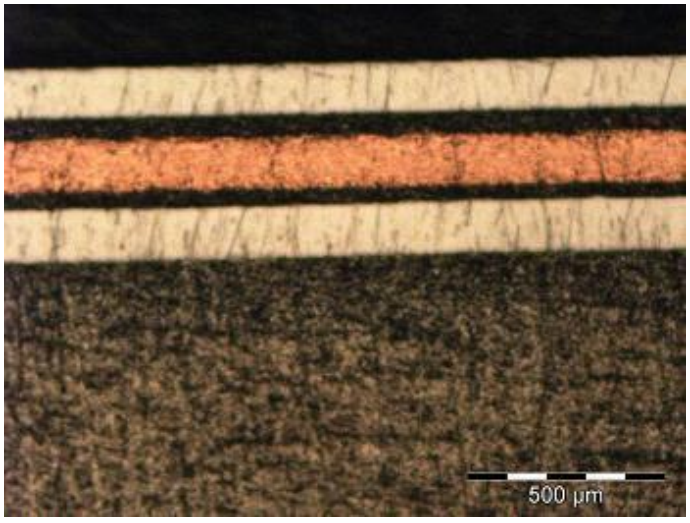

(b): Mo/Al 1100/Cu/Al 1100/Mo on Al 3003-H14 substrate.

Figure 2.3: Micrographs of molybdenum welded to different aluminum alloys.

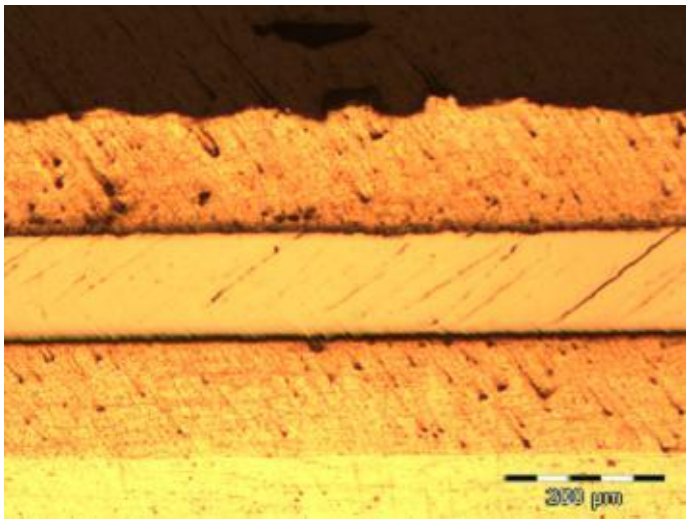

(c): Al 6061/Mo/Al 6061 on Al 6061-T6 substrate.

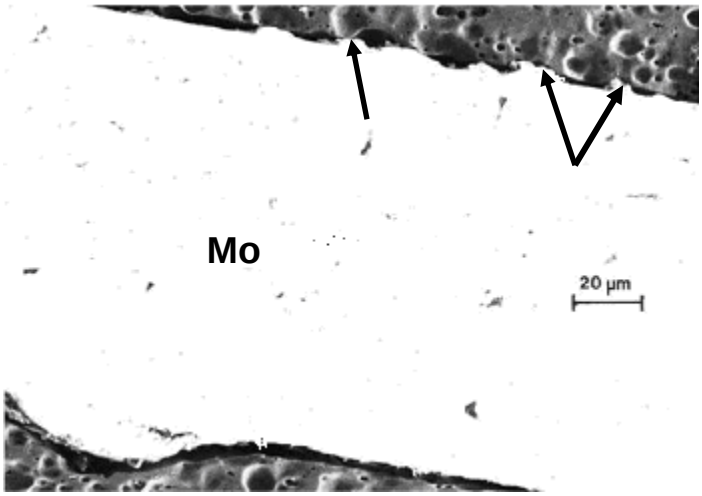

(d): SEM micrograph showing partially bonded regions between Mo and Al6061.

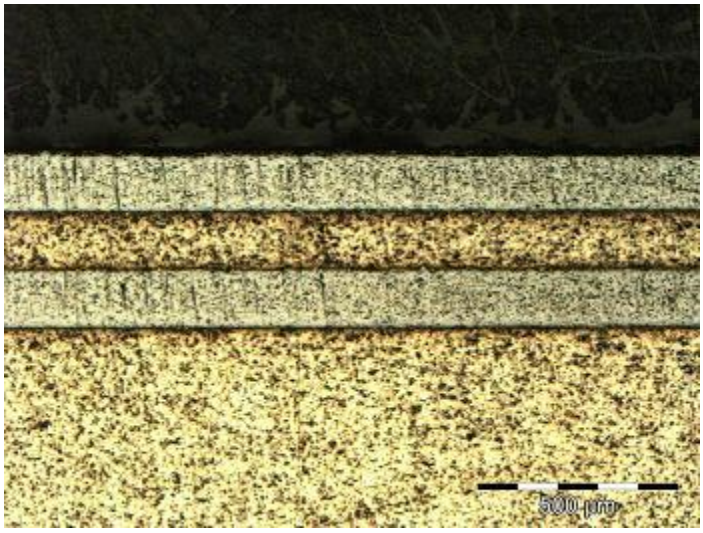

(a): Ta/Al 3003/Ta on Al 3003-H14 substrate.

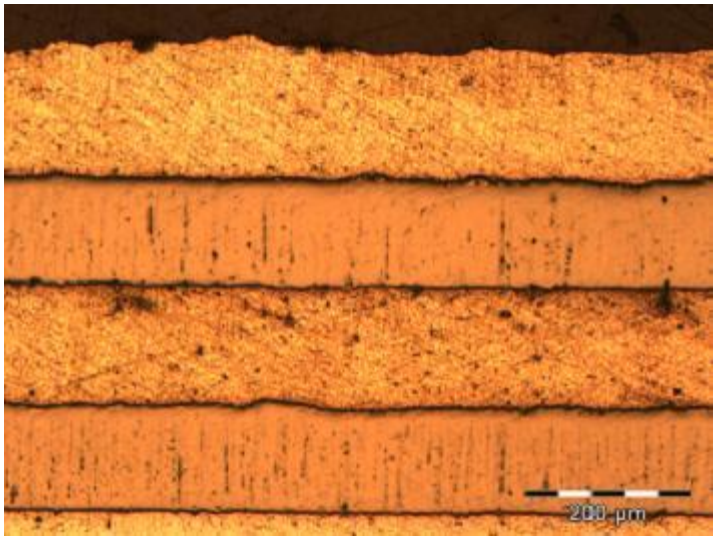

(b): Ta/Al6061/Ta/Al6061 on Al 6061-T6 substrate.

Figure 2.4: Micrographs of tantalum and Al 6061-O welded on Al 6061-T6 substrate.

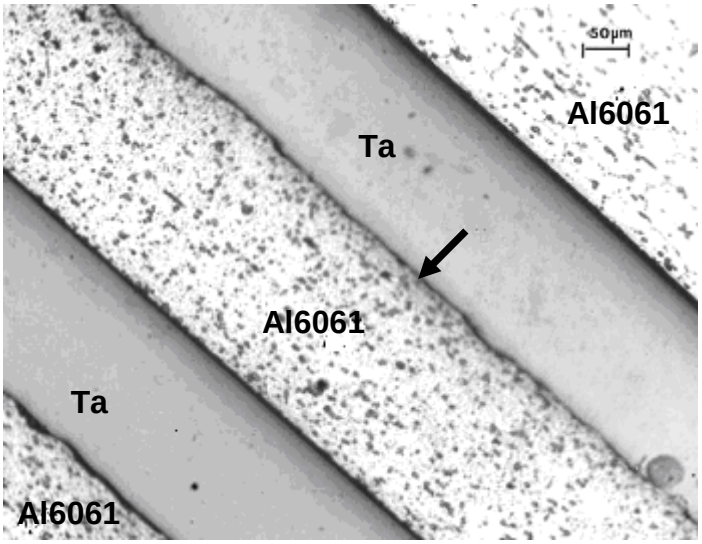

(c): Higher magnification of the Ta/Al6061/Ta/Al6061 showing some de-bonded regions.

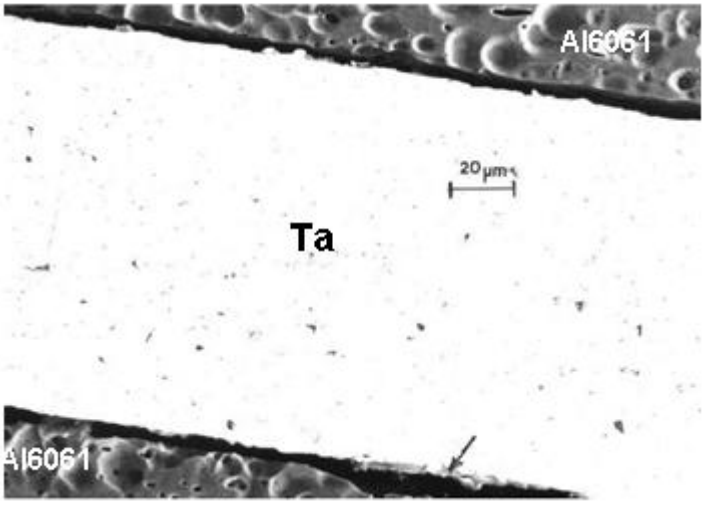

(d): SEM micrograph showing some de-bonded regions between Ta and Al6061.

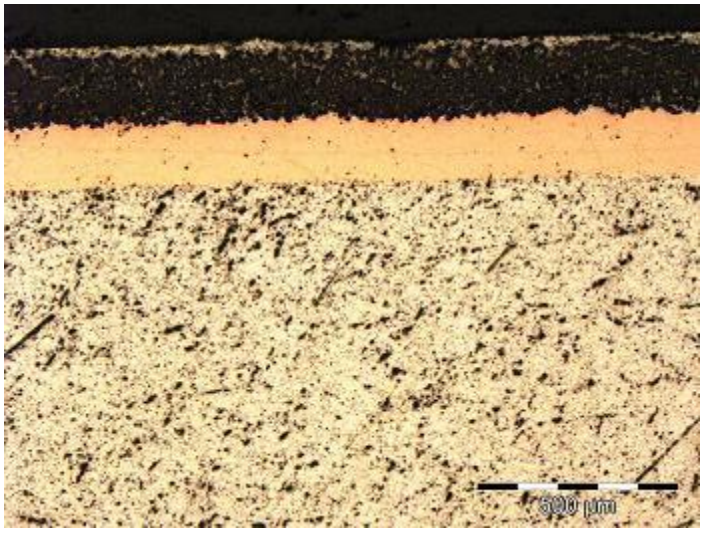

(a): Cu/MetPreg® on Al 3003-H14 substrate.

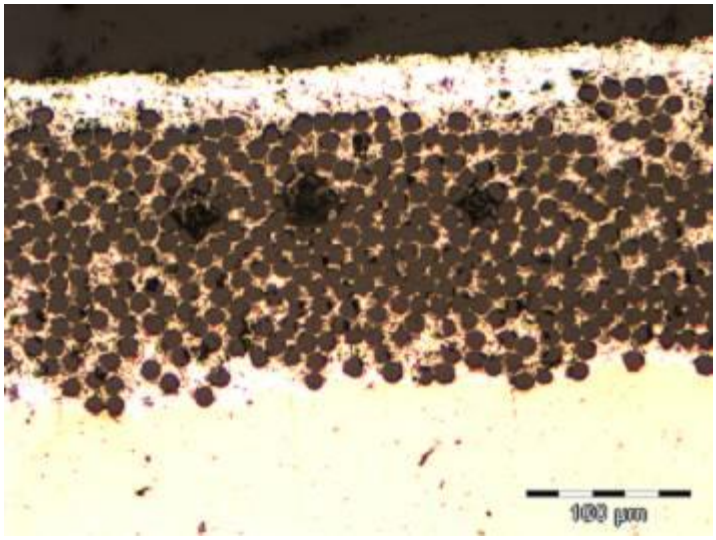

(b): Higher magnification of Cu/MetPreg® on Al 3003-H14 substrate.

Figure 2.5: Micrographs of MetPreg® welded to copper on Al 3003 H14 substrate.

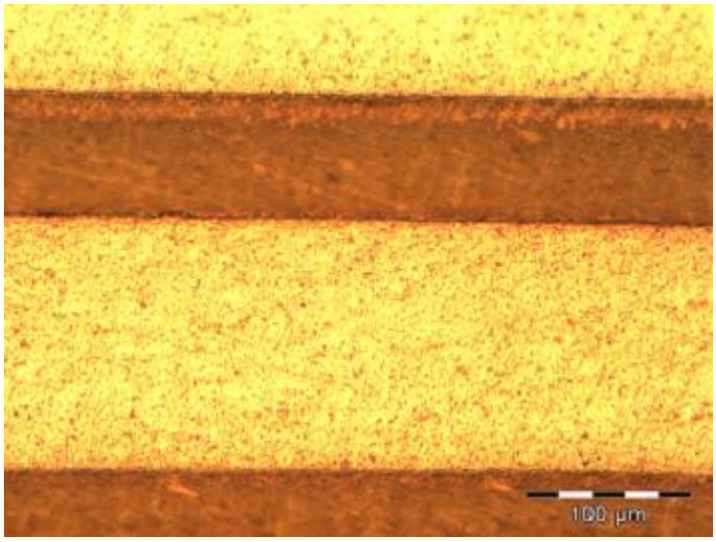

(a): Ti/Al 3003/Ti on Al 3003-H14 substrate.

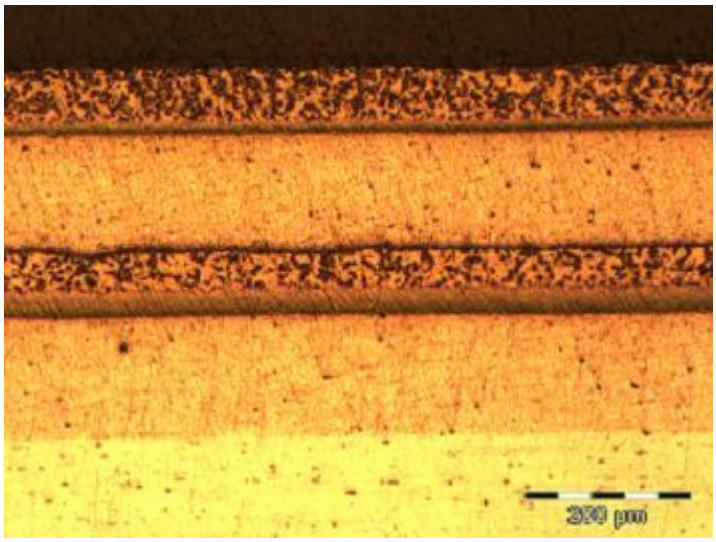

(b): Al 6061/Ti/Al 6061/Ti on Al 6061-T6 substrate.

Figure 2.6: Micrographs of titanium welded to Al 3003 and Al 6061.

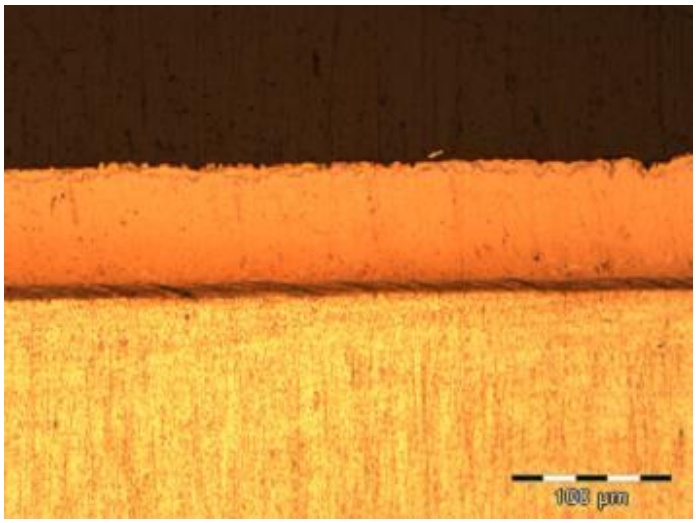

(a): Titanium/Al 3003 with elemental boron powder at the interface on Al 3003 substrate.

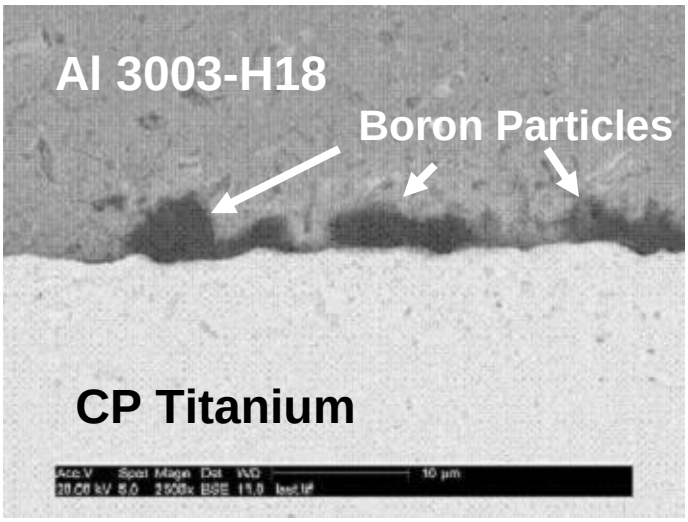

(b): 2500x magnification SEM micrograph of boron powder at the interface between Ti and Al 3003 foils.

Figure 2.7: Titanium/Al 3003 with elemental boron powder at the interface.

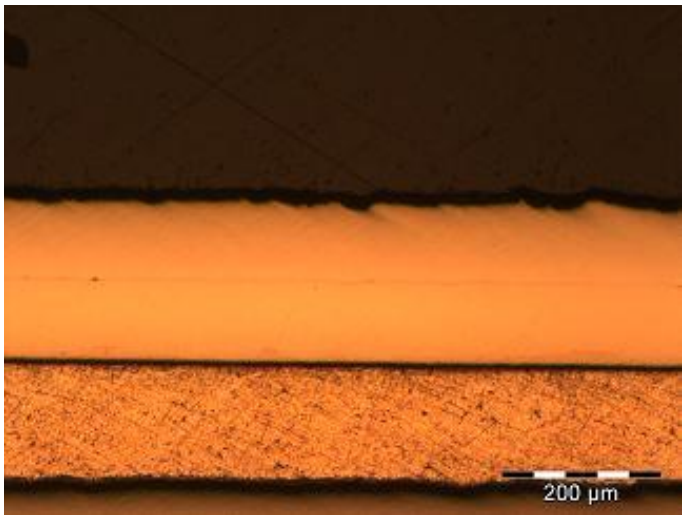

Figure 2.8: Nickel/stainless steel 316L welded on Al 6061-T6 substrate.

2.4 Discussion

The bonding mechanisms of ultrasonically consolidated foils were described by Janaki Ram et al. (2007B). The ability to plastically deform foil interfaces under the action of normal and oscillating shear forces acting at the interface of the mating foils is of paramount importance. These shear forces help break up the hard surface oxides; and repeated deformation of surface asperities exposes atomically clean surfaces to enable metallurgical bonding between the mating foils. Successful welding between two mating foils is a function of how well the surface oxides of the foil materials were removed as well as the ease of surface deformation. From the results presented, it can be observed that the relatively soft materials generally bonded well to each other. This is because their surface oxides were easily broken up and displaced along with the fact that they are more easily deformed under the influence of the operating forces. It is also worthy of note that most of these softer materials have face centered cubic (FCC) crystal structures while the harder ones have body centered cubic (BCC) and hexagonal close pack (HCP) structures at UC processing temperatures. So far, limited success has been achieved in bonding

softer materials to harder ones. All the aluminum alloy series used in this experiment bonded with all the hard materials, whereas none of silver, copper and nickel bonded with any of molybdenum, tantalum and titanium directly. Also, no two of the non-FCC materials, that is, molybdenum, tantalum and titanium, bonded well with each other. Thus, in addition to welding parameters; material composition, crystal structure and combinations thereof play important roles in determining good bonding. Observations from welded material combinations are discussed in the following subsections.

2.4.1 Silver/Copper/Nickel Welding

For these materials, two silver foils were successfully welded to each other on the Al3003 base plate as shown in Fig. 2.2. Copper foil also bonded well to both silver at the bottom and nickel at the top. From the micrograph it can be seen that the silver to silver weld has a very good linear weld density, a measure of bond quality (Janaki Ram *et al.*, 2007A), as there are no visible interfacial defects between the two layers. Silver welded well at 150^{o}F as well as at 300^{o}F, although it undergoes a high rate of oxidation at 300^{o}F. Except when bonding with materials that will significantly conceal the surface from atmospheric oxygen, it is better to weld silver at 150^{o}F. Copper to silver and copper to nickel foils also bonded very well to each other, as can be seen in Figs. .2a, 2.2b and 2.2c. From the micrographs, good welds were obtained between copper and nickel both at the top and bottom. In Fig. 2.2d, nickel, copper and silver are shown individually sandwiched between aluminum alloy 6061-O foils to demonstrate their good weldability to this aerospace grade material using UC. Al 6061-O foil bonded well with the Al 6061-T6 substrate material with no visible defects. All the materials welded in Fig. 2.2 shows good bond qualities.

2.4.2 Molybdenum/Aluminum/Copper Welding

Figure 2.3 shows the micrographs of well bonded and moderately bonded material combinations. Figure 2.3a shows good bonding between molybdenum and aluminum 3003 substrate and foils, with no visible defect. Molybdenum is a hard, wear and corrosion resistant refractory metal with high temperature strength, and resistance to plastic deformation. As can be seen in the micrograph, molybdenum bonded well with Al 3003 with either material at the top or bottom. A close look at the micrograph reveals that the sandwiched aluminum between the two molybdenum foils has higher surface roughness when compared with the molybdenum foils. This indicates that it underwent higher plastic deformation at the surfaces than the molybdenum foils. The top surface that had direct contact with the sonotrode is rougher than the bottom. In contrast, the surface of the molybdenum in contact with the substrate and the top surface of the topmost molybdenum foil shows much lower level of roughness. The level of surface roughness of the materials is a direct indication of their relative ease of plastic deformation.

In Fig. 2.3b copper is sandwiched indirectly between two molybdenum foils with aluminum alloy 1100 as intermediate layers. Within the limits of the welding parameters of the UC machine used, molybdenum could not be successfully welded to copper directly. The Al 1100 interlayer material of 50μm thickness bonded well with both materials. Ultrasonically consolidated molybdenum-copper multi-material structures with an interlayer material can be useful in applications requiring the properties of the principal materials if the interlayer materials are thin and do not compromise functionality. An example is an application requiring the wear and/or corrosion resistance properties of molybdenum and the electrical and/or thermal conductivity of copper.

Molybdenum-copper laminated materials have applications in thermal management for electronics packaging (Zweben, 1998). The bonding between molybdenum and aluminum 6061-O as shown in Fig. 2.3c is moderate, with evidence of bonding defects. The SEM micrograph in Fig. 2.3d reveals regions of partial bonding between the materials. The arrows in Fig. 2.3d show some localized bonds alternating with un-bonded areas. It suggests that there was insufficient surface plastic deformation of the two materials, which is necessary to achieve better bonding qualities. This is evidence that aluminum alloy 6061-O does not deform readily like aluminum alloy 3003, since a much lower ultrasonic energy was required to achieve better bond quality with Al 3003, as shown in Fig. 2.3a. However, with further welding parameter optimization, there is a possibility of better bonding with Al 6061.

2.4.3 Tantalum/Aluminum Welding

Micrographs of tantalum foils ultrasonically welded with aluminum alloys 3003-H18 and 6061-O are shown in Fig. 2.4. Tantalum is a refractory metal with good wear and corrosion resistance that can be ultrasonically welded to a material for surface protection against wear and corrosive environmental conditions. Tantalum is also used for radiation shielding in nuclear applications (Kublik, 1993). The tantalum foils used were in the as-rolled and tempered condition. The micrograph in Fig. 2.4a shows a good linear weld density between tantalum and aluminum alloy 3003, while Fig. 2.4b shows a moderately bonded tantalum and aluminum alloy 6061. Higher magnification of a section of the micrograph in Fig. 2.4b, shown in Fig. 2.4c, reveals de-bonded regions at some of the interfaces of the tantalum and Al alloy 6061. The arrowed interface shows fairly good bonding. The SEM micrograph in Fig. 2.4d clearly reveals the de-bonded regions.

2.4.4 MetPreg®/Copper Welding

MetPreg® was fully bonded with copper with 100% linear weld density on an aluminum 3003 substrate, as shown in the micrographs in Fig. 2.5. MetPreg® is a commercially available aluminum metal matrix composite made of aluminum reinforced with high strength, high stiffness Al_2O_3 fibers. As can be seen in Fig. 2.5b, the aluminum matrix has good bonding with the copper material. Also, some of the Al_2O_3 reinforcing fibers penetrated into the copper material, further strengthening bonding between the two materials. This multi-material deposit combines the hard, wear resistant properties of MetPreg® with the good heat and electrical conductivity of copper. The micro-hardness of the as-fabricated surface of the MetPreg® on copper is 600Hv.

2.4.5 Titanium/Aluminum Welding

Commercial pure titanium was successfully welded to aluminum alloys 3003-H18 and 6061-O ultrasonically as shown in the micrographs in Fig. 2.6. The micrographs show good bonding qualities between titanium foils and the aluminum alloys with either material at the top or bottom position. Titanium and aluminum have a wide range of applications in the aerospace industry. As such, ultrasonic consolidation provides a unique fabrication technique for their dual-material freeform fabrication for functional structures in the aerospace industry.

2.4.6 Titanium/Aluminum Welding with Embedded Boron Particles

Commercial pure titanium and aluminum alloy 3003-H18 welded well with embedded boron powder at the interface as shown in the micrographs in Fig. 2.7. The boron powder used has a particle size less than 5μm diameter. Plastic flow of aluminum

and titanium foils around the boron particles is crucial to obtaining good bonding. It can be seen in Fig. 2.7b that Al 3003-H18 plastically flowed around the boron particles to fully encapsulate them against titanium. The deformation of the titanium material is minimal. This is understandable since the Al 3003-H18 is a softer material than titanium. During welding, the oscillating motion of the vibrating sonotrode redistributes the particles at the interface of the welded foils; as such, uniform particle distribution is difficult to achieve. Embedding powder particles between ultrasonically consolidated foils can be used to alter composition for localized property control within a structure. It can also be used to fabricate particle reinforced composite materials, especially in cases where the UC particle embedment is an initial fabrication step before post consolidation heat treatments. The deposition shown in Fig. 2.7 was subjected to post process annealing at 480^{o}C for two hours and oven cooled. The result of Energy Dispersive X-ray (EDX) spot analysis, shown in Fig. 2.9 below at a 1μm point into the aluminum side from the boron powder, reveals that significant boron diffusion into the aluminum matrix took place.

2.4.7 Nickel/Stainless Steel 316L Welding

Figure 2.8 shows good bonding between stainless steel 316L and nickel on an Al 6061-T6 substrate. The austenitic stainless steel material with an FCC crystal structure demonstrates good weldability with nickel. The dual materials have applications in areas where strength and corrosion resistance is a major requirement.

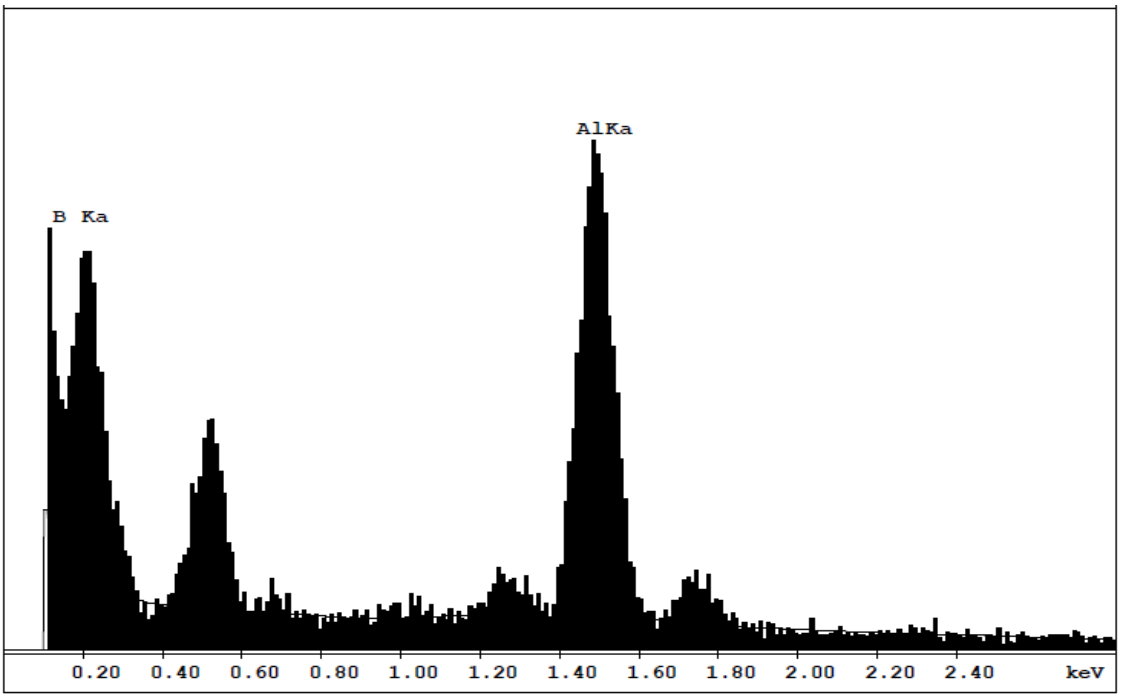

EDAX ZAF Quantification (Standardless)
Element Normalized
SEC Table : Default

Element	Wt %	At %	K-Ratio	Z	A	F
B K	75.38	88.43	0.4872	1.0172	0.6354	1.0000
AlK	24.62	11.57	0.2324	0.9435	1.0003	1.0000
Total	100.00	100.00				

Element	Net Inte.	Bkgd Inte.	Inte. Error	P/B
B K	34.54	14.40	3.26	2.40
AlK	71.38	6.36	1.82	11.22

Figure 2.9: Result of EDX spot analysis of a 1µm Point into the aluminum side of the titanium/aluminum material system with embedded boron powder.

2.5 Conclusions

The multi-material capabilities of ultrasonic consolidation have been further demonstrated in this work. All FCC crystal structure materials used welded well with each other. Among the materials used, only aluminum alloys 1100 and 3003 welded very well with molybdenum, tantalum and titanium. Aluminum alloy 6061 bonded moderately with the three non-FCC materials. With further optimization of the welding parameters

for most of the material combinations, multi-material structures with function specific members can be fabricated using ultrasonic consolidation.

References

Cheng, X., Datt,a A., Choi, H., Zhang, X. and Li, X. (2007), "Study on embedding and integration of microsensors into metallic structures for manufacturing applications", *Journal of Manufacturing Science and Engineering*, Vol. 129, pp. 416-424.

Domack, M.S. and Baughman, J.M. (2005), "Development of nickel-titanium graded composition components", *Rapid Prototyping Journal*, Vol. 11, No. 1, pp. 41-51.

George, J.L. (2006), "Utilization of ultrasonic consolidation in fabricating satellite decking", Master's thesis, Utah State University, Logan, UT.

Janaki Ram, G.D., Yang, Y. and Stucker, B.E. (2007A), "Effects of process parameters on bond formation during ultrasonic consolidation of aluminum alloy 3003", *Journal of Manufacturing Systems*, Vol. 25, No. 3, pp. 221-238.

Janaki Ram, G.D., Robinson, C., Yang, Y. and Stucker, B.E. (2007B), "Use of ultrasonic consolidation for multi-material structures", *Rapid Prototyping Journal*, Vol. 13, No. 4, pp. 226-235.

Kong, C.Y., and Soar, R.C. (2005), "Fabrication of metal–matrix composites and adaptive composites using ultrasonic consolidation process", *Materials Science and Engineering A*, Vol. 412, pp. 12-18.

Kong, C.Y., Soar, R.C., and Dickens, P.M. (2004A), "Optimum process parameters for consolidation of 3003 aluminum", *Journal of Materials Processing Technology*, Vol. 146, pp. 181-187.

Kong, C.Y., Soar, R.C, and Dickens, P.M. (2004B), "Ultrasonic consolidation for embedding sma fibers within aluminum matrices", *Composite Structures*, Vol. 66, No. 1-4, pp. 421-427.

Kublik, T.J. (1993), "A radiation shield for use in a radiotherapy machine", European Patent No: EP0555919, August, p. A1.

Kruger, S., Wagner, G. and Eifler, D. (2004), "Ultrasonic welding of metal/composite joints", *Advanced Engineering Materials*, Vol. 6, No. 3.

Siggard, E.J. (2007), "Investigative research into the structural embedding of electrical and mechanical systems using ultrasonic consolidation (UC)", Master's thesis, Utah State University, Logan, UT.

White D.R. (2003), "Ultrasonic consolidation of aluminum tooling", *Advanced Materials & Processes,* Vol. 161, No. 1, pp. 64-65.

Yang, Y., Janaki Ram, G.D., and Stucker, B.E. (2007), "An experimental determination of optimum processing parameters for Al/SiC metal matrix composites made using ultrasonic consolidation", *Journal of Engineering Materials and Technology,* Vol. 129, pp. 538-549.

Yang, Y., Janaki Ram, G.D., and Stucker, B.E. (2009), "Bond formation and fiber embedment during ultrasonic consolidation", *Journal of Materials Processing Technology,* Vol. 209, No. 10, pp. 4915-4924.

Zweben, C. (1998), "Advances in composite materials for thermal management in electronic packaging", *JOM Journal of the Minerals, Metals and Materials Society,* Vol. 50, No. 6, pp. 47-51.

CHAPTER 3

OPTIMIZATION OF THE SHEAR STRENGTHS OF ULTRASONICALLY CONSOLIDATED TI/AL 3003 DUAL-MATERIAL STRUCTURES

This chapter was submitted for publication in the Journal of Materials Processing Technology.

Abstract

The interfacial bonding between layers in ultrasonically consolidated structures is poor for some material combinations, resulting in relatively low bond strength. This makes resultant parts unsuitable for structural applications. This work discusses a study of the effects of post process heat treatment of ultrasonically consolidated commercially pure titanium and aluminum alloy 3003 dual-material systems. The lap shear strengths of as-consolidated specimens as well as heat treated ones were tested. The results show that there is significant improvement of the strengths of post processed specimens over the as-consolidated ones. The improvement is as a result of stress relieving of the strain hardened interface between the two materials and some interactions of the base materials across the interfacial boundaries at elevated temperatures, leading to stronger bonds. The study highlights the role of post process heat treatments for improving the mechanical properties of ultrasonically consolidated structures.

3.1 Introduction

Ultrasonic consolidation (UC) is a solid-state fabrication process that combines ultrasonic metal welding and layered manufacturing techniques to produce three-dimensional objects. The process uses the power of high frequency ultrasonic vibration at low amplitude to bond thin foils of materials to form solid objects. It combines normal and oscillating shear forces on mating foils and the resulting frictional forces between the materials to fracture and displace surface oxides from the materials. The exposed atomically cleaned surfaces are then brought into direct contact under modest pressure and temperatures that are less than half of the melting point of the materials. The materials are thus metallurgically bonded (White, 2003). Fractured oxides and surface impurities in the materials are distributed in the bond zone. The process combines the layer-by-layer addition of foils with contour milling using an integrated 3-axis CNC machining facility to produce desired component geometry. It is therefore both an additive and subtractive process.

The Solidica Formation^{TM} UC machine consists of a welding horn, also known as a sonotrode that exerts a normal force and the oscillatory high-frequency vibration on the materials to be welded. Welding takes plate on a substrate fixed on a heated plate or anvil. Figure 3.1 shows a schematic view of the ultrasonic consolidation process. The UC primary process parameters determined in earlier work by Kong et al. (2004A) include vibration amplitude, temperature, welding speed, and normal force. These process parameters determine to a great extent, the bonding quality of consolidated materials. Janaki Ram et al. (2007A) in their experimental work determined that in addition to the primary process parameters, the sonotrode roughness and material surface finish affect

the bonding between two materials. Obielodan et al. (see chapter 4) also in their work determined that the accuracy of foil side-by-side placement in automatic material feed systems have direct influence on gap defect incidence rates between adjacent foils in a layer.

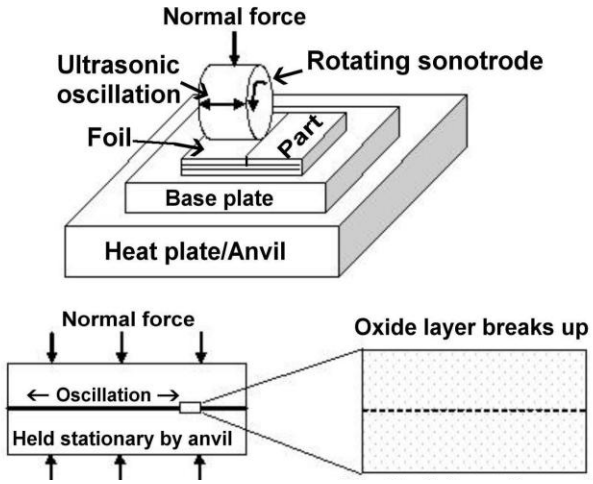

Figure 3.1: Schematic of the UC process.

The potential applications of UC have been demonstrated in previous work. Its capability for the fabrication of honeycomb structures for panel stiffening was demonstrated by George (2006). Various levels of success have been achieved when using UC for embedding fibers for different applications. Kong et al. (2004B) used UC to successfully embed shape memory alloy (SMA) and optical fibers; other demonstrated fiber embedment include SiC fibers for metal matrix composites by Yang et al. (2007, 2009); and active and passive fibers for making adaptive composites by Kong and Soar (2005). Electrical and mechanical devices were also embedded by Siggard (2007). Aluminum alloy 3003 matrix materials were used for all the embedded fibers and structures mentioned, principally because of its good weldability, relatively low cost and wide spread applications.

While UC has been widely used for single material fabrications, especially using aluminum alloys, a few researchers have demonstrated its capabilities for multiple material fabrications. The multi-material capabilities of UC were demonstrated by Janaki Ram et al. (2007B) in their work in which copper, brass, nickel, inconel 600, AISI 347 stainless steel, stainless steel AISI 304 wire mesh, MetPreg, and aluminum alloy 2024 were individually welded to aluminum 3003 H18 materials. Domack and Baughman (2005) demonstrated the potentials of UC for graded materials composition fabrications using titanium and nickel alloys. Obielodan et al. (see chapter 2) have also demonstrated UC multi-material capabilities by welding different combinations of molybdenum, tantalum, titanium, copper, silver, nickel, aluminum alloys 1100, 3003, 6061 and boron powder.

The bond strengths of UC fabricated structures is a major concern in attempts to use them for mechanically stressed structural applications. Some inter-layer and intra-layer bond related mechanical properties of ultrasonically consolidated structures have been investigated in earlier work. Kong et al. (2003) determined the important process parameters and the process window for achieving optimum peel strength for Al alloy 6061. In their work, welding speed and normal pressure were reported to have the major effects on the peeling strength (resistance to peel) between two welded foils. Amplitude was found not to have significant effect when compared to those two factors; this is opposed to findings on aluminum alloy 3003 in other work by Kong et al. (2004A) in which increase in amplitude was reported to result in increase in peel strength. Tuttle (2007) determined the peel strength between stainless steel 316L foils welded on a stainless steel plate. He reported an increase of peel strength with reduction in weld speed

and increase in sonotrode vibration amplitude. Also, Yang et al. (2007) in their work determined that significant plastic deformation at the interface aided the bonding of embedded SiC fibers to the aluminum 3003 matrices. Amplitude, normal force, welding speed, and substrate temperature were found to significantly influence the bond strength between fibers and matrix. Obielodan et al. (see chapter 4) determined the conditions for optimum transverse tensile strength of ultrasonically consolidated structures made with automatically fed aluminum alloy 3003-H18 foils.

While most of the previous work used similar materials, there is a growing interest in multi-material structures fabrication by ultrasonic consolidation. A major limiting factor is that many materials are not easily joined at the current limits of operating parameters of available UC machines. Some material combinations will require much higher values of parameters that are beyond the upper bounds of commercially available machines. The present work seeks to apply post process heat treatment as a way to improve the bond strength between ultrasonically consolidated titanium and aluminum alloy 3003. Although the low temperature operating conditions of UC is a major advantage as stated earlier, it is postulated that by applying post processing treatments such as heat and pressure at optimized levels, significant inter-layer material diffusion across the consolidated foil interface will be achieved resulting in better bonding strengths. It is a well known fact that high temperature treatment of some dual materials lead to the formation of brittle intermetallic phases; this study seeks to avoid or minimize their formation.

The UC post process treatment in this work is limited to elevating consolidated specimens to higher temperatures without pressure application. The improved strength

advantages derivable from post process heat treatments will offset the additional costs incurred. This study seeks to create synergy by combining the freeform fabrication capabilities of UC additive manufacturing with the inherent advantages of diffusion bonding. Improved diffusion based interlayer bonding strengths and achievable complex geometries will expand the scope of applications for ultrasonically consolidated structures.

Kong et al. (2004A) used peel tests to characterize the bond strength between consolidated aluminum alloy 3003 rather than lap shear tests because, in attempts to use the latter, the two foils bonded failed in tension rather than shear. In this work, lap shear specimens will be used to characterize the bond strength between commercially pure (CP) titanium and aluminum alloy 3003. Rather than use lap shear specimens made of two ultrasonically consolidated foils, which did not work as reported by Kong et al. (2004A), several layers of foils will be consolidated on the substrate to ensure failure by shear is obtained. The success of this work with titanium and aluminum 3003 will lay the ground work for further investigations and eventual applications in different industries including aerospace.

3.2 Experimental Work

3.2.1 Material Preparation

A Solidica Formation^{TM} machine was used for all the UC fabrications in this work. The materials used were CP Titanium foils of 75 microns thickness and Aluminum alloy 3003-H18 of 150 microns thickness with chemical compositions shown in Table 3.1. Deposits were made on Aluminum 3003-H14 substrates. Aluminum substrates and

foils were procured from Solidica. The titanium and aluminum foils were welded on the substrate in alternate layers for the first four layers, with titanium foils being the first to be welded onto the substrate. Different welding parameters were applied for the two materials as listed in Table 3.2. The welding temperature was maintained at 300^{o}F (150^{o}C) for the two materials.

Table 3.1: Chemical Compositions, Mechanical Properties and Size of the Materials Used

Material	Nominal Composition	Tensile Strength (MPa)	Shear Strength (MPa)	Shear Modulus (GPa)	Thickness (μm)
CP Titanium	Ti-0.6Fe-0.38Mn	430	380	45	75
Al 3003-H18	Al-1.2Mn-0.12Cu	200	110	25	150

Table 3.2: Ultrasonic Welding Parameters Used for the Different Materials

Material	Amplitude (μm)	Speed (mm/s)	Normal Force (N)	Temperature (^{o}F)
CP Titanium	28	10.58	2000	300
Al 3003-H18	16	23.70	1750	300

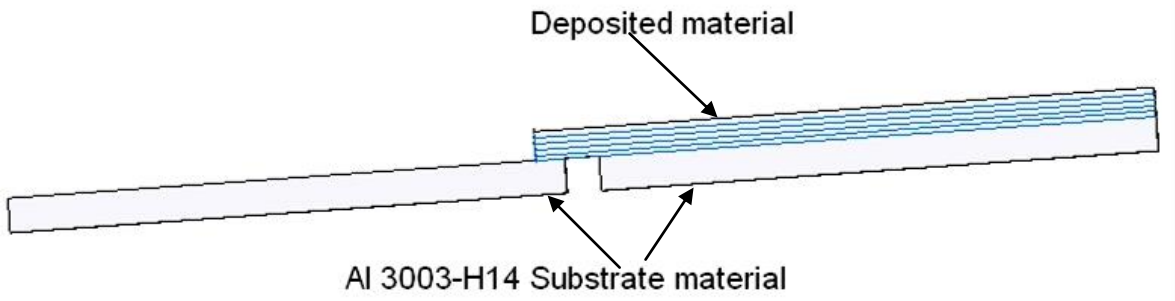

Figure 3.2: Lap shear strength specimen design.

Titanium foils were manually placed on the substrate for welding while the aluminum foils were automatically fed. Additional layers of aluminum were welded on

top of the first four layers in order to strengthen the welded foils and avoid tensile failure outside the joints as reported for two single aluminum 3003 foils tested for lap shear tests by Kong et al. (2003). The shear test specimens described in Fig. 3.2 were designed to fail in shear along the lapping surface between the first titanium foil and the aluminum 3003-H14 substrate material.

During initial specimen trials, slots of 3.2mm width and 3mm depth were machined into the Al 3003 substrate with the integrated CNC milling head in the UC machine, before the first titanium foil deposit was made. The initial slot was to provide a precise separation between the ends of the tensile shear specimens at predetermined location. It was found that the foils deposited above the slots were not bonded to each other as there was no support material underneath to resist the normal force of the sonotrode for proper welding. The titanium foils exposed by the slots were thus highly oxidized during heating in the oven. These specimens failed prematurely because the tensile loads applied were not evenly distributed, and the exposed titanium foils were weakened by oxidation. With subsequent specimen trials, the slots were not cut into the substrate before the foil welding. They were cut using a milling machine after material deposition and post process heat treatment were completed.

Eighteen specimens were fabricated and randomly grouped into six groups of three specimens each. Each group was then randomly assigned to a post process annealing at 480^{o}C for the following lengths of time: 0 (control), 30, 60, 120, 180 and 270 minutes, after which they were oven cooled to room temperature. The treatments are respectively labeled A, B, C, D, E and F for the purpose of analysis. Those assigned to zero minutes (treatment A) were not heat treated, and served as the control specimens for

the purpose of comparison with the groups that were subjected to post process annealing. A Lindberg BlueM laboratory table top oven without atmospheric control was used for the post process heat treatments. The foil lapping surfaces were not exposed to the oven atmospheric conditions, only the edges (which are very small compared to the total surface area of the titanium foils) were exposed, and as such, minimal lapped surface oxidation occured. The samples were loaded into the oven for annealing without machining the substrates off, in order to avoid heat induced distortion in the specimens. After removal from the oven, the substrate materials were machined down to 3mm after which the slot was cut to separate the two ends of the tensile shear specimens, which were then only joined at the overlapping surface of the welded foils as illustrated in Fig. 3.2. Because the preparations for the slot machining were manually done, the slot cuts resulted in different overlap lengths for the specimens. These overlap lengths ranged from 2.32 to 3.3mm. It is assumed that the differences do not significantly affect the lap shear strength measurements obtained, since the shear strength is obtained by normalizing the load at failure with respect to the surface area of each specimen. A 50KN capacity Tinius Olson tensile testing machine was used for the lap shear test. The specimens were held in the flat grips of the testing machine and pulled in tension at a speed of 1mm/min until fracture.

3.2.2 Metallography and Microhardness Testing

Small samples cut from the unstrained grip ends of the tensile shear strength specimens were mounted and polished according to standard metallographic procedures. Some of them were etched with Flick's reagent (10ml HF, 15ml HCL, 90ml H_2O) for 5 seconds at 0^oC followed by a special solution (25ml HNO_3, 75ml H_2O). The later solution

was applied because of the difficulty in etching Al 3003. This produced irregular etching and chemical attack on the aluminum regions but excellent rendering of the titanium grain structure. Kellers reagent (150ml H_2O, 3ml HNO_3, 6ml HCl and 6ml HF) was applied at 0^oC for 5 minutes to reduce pitting and surface corrosion. Line scan Energy Dispersive X-ray Spectroscopy (EDS) analysis across the interface of the titanium and Al 3003-H18 deposits were undertaken for one representative specimen randomly selected from each of the five specimen groups that were annealed. This was done to verify if post process heat treatment-induced diffusion took place (and the distribution of diffusing elements, if it occurred) across the interface of the consolidated materials. The lack of atomic diffusion across the interface of ultrasonically consolidated dual material foils in previous experiments (Yang et al., 2009) indicated that it was unnecessary to carry out EDS analysis on any of the control specimens. It is assumed that detectable diffusion will not occur at the UC operating parameters in any of the control samples.

Micro-hardness testing was carried out for samples from the specimen groups using a Struer's Doramin-A300 micro-indentation tester with a 100 gf load. Hardness signatures were obtained across five consolidated foils covering the cores and the interfaces.

3.3 Results and Discussion

The optical and SEM micrographs of the specimens are shown in Figs. 3.3-3.9. Figures 3.3 to 3.8 show that the bondings between consolidated titanium/Al3003 layers were generally good. There are no visible bond defects between the layers. Figure 3.9 shows the fracture features of some of the specimens. The fracture morphology at the lapped surfaces is shown in Fig. 3.9a. Figure 3.9b shows how in some of the specimens,

the first consolidated titanium layer that bridge the two halves of the lap shear specimens failed in tension during application of loads. The tensile failure of the first consolidated titanium layer is most probably due to the delamination of that layer occuring as a result of induced bending moment about the center of the lapping surface as the applied tensile shear load reaches a particular level.

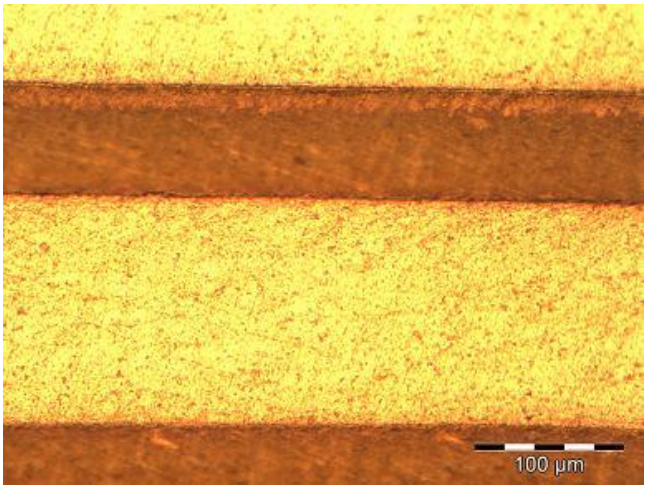

Figure 3.3: Optical micrograph of a specimen without post processing.

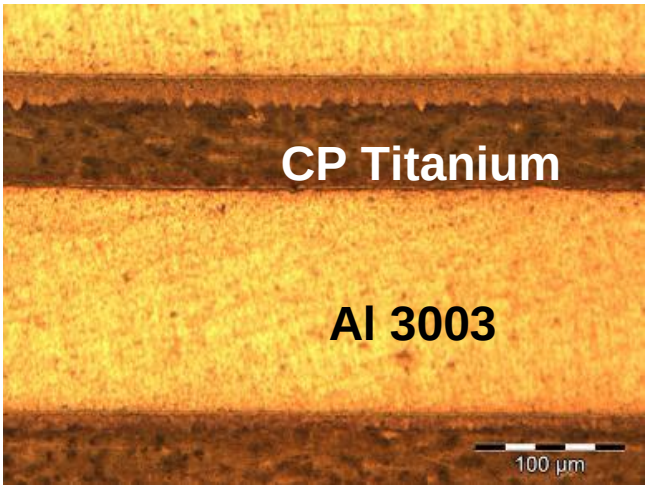

a: Optical micrograph of a 30-minute annealed specimen.

Figure 3.4: Optical and SEM micrographs of 30 minutes annealed specimens.

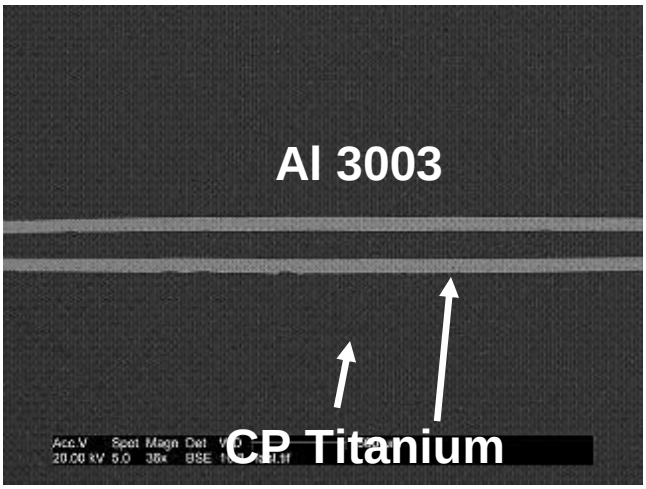

b: SEM micrograph of a 30-minute annealed specimen.

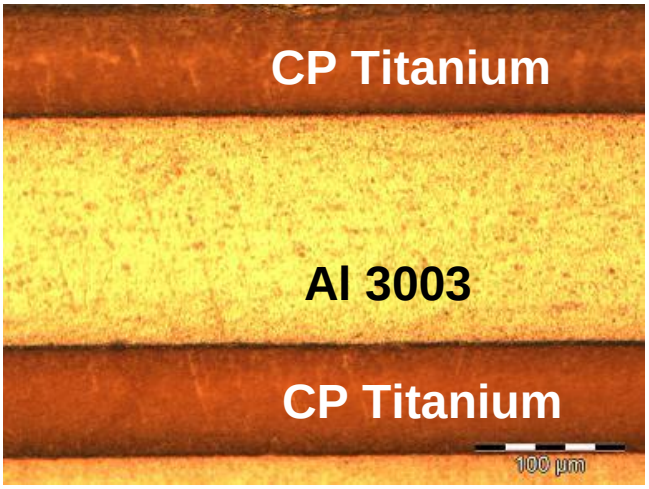

(a): Optical micrograph of a 60-minute annealed specimen.

Figure 3.5: Microstructures of 60-minute heat treated Ti/Al 3003 material system.

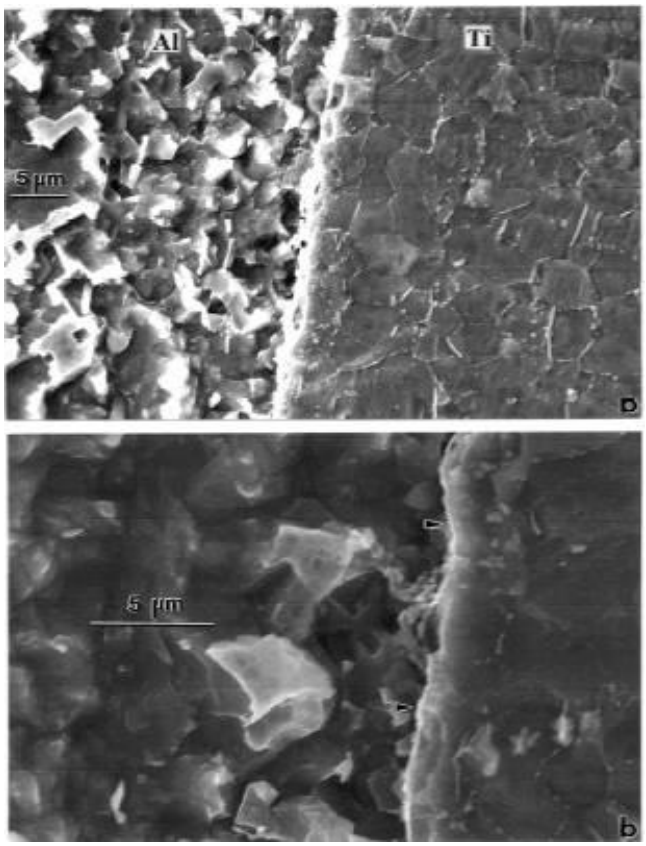

(b): Magnified SEM view of the 60-minute heat treated Ti/Al 3003 material system showing grain structures and the weld interface.

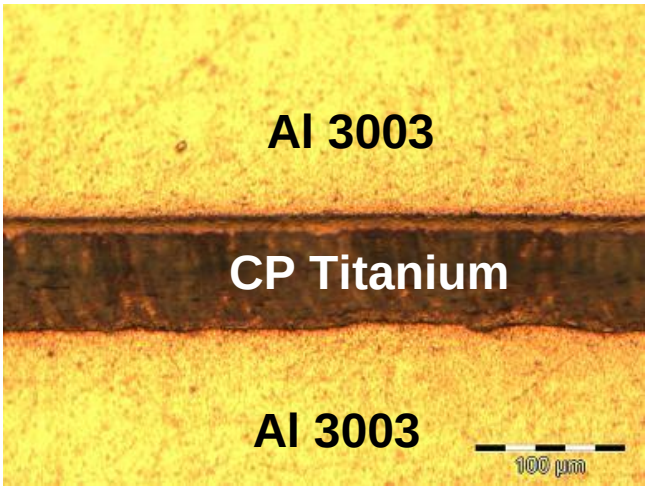

Figure 3.6: Optical micrograph of a 120-minute annealed specimen.

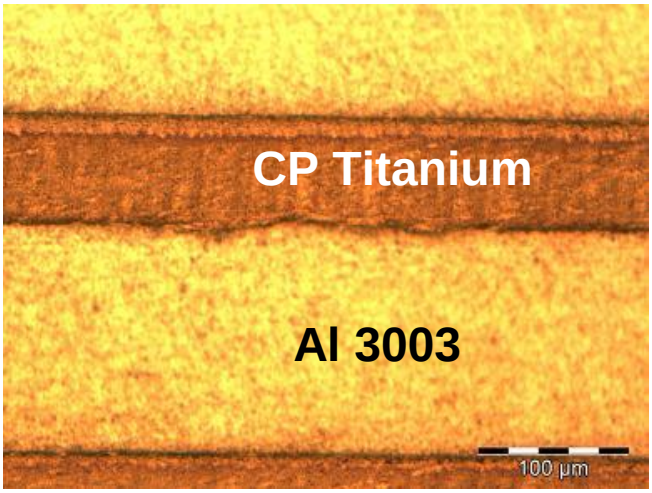

Figure 3.7: Optical micrograph of a 180-minute annealed specimen.

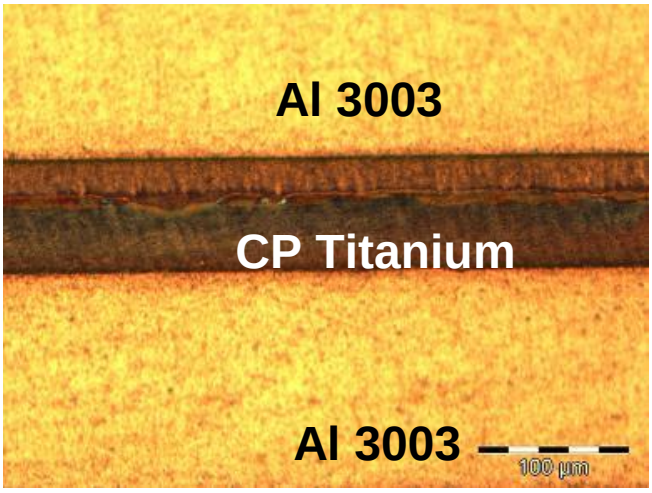

Figure 3.8: Optical micrograph of a 270-minute annealed specimen.

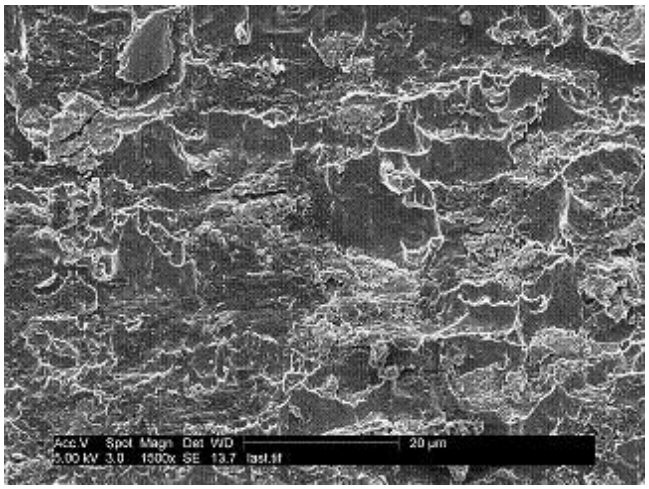

a: SEM showing the fracture morphology of a 30 minute annealed specimen.

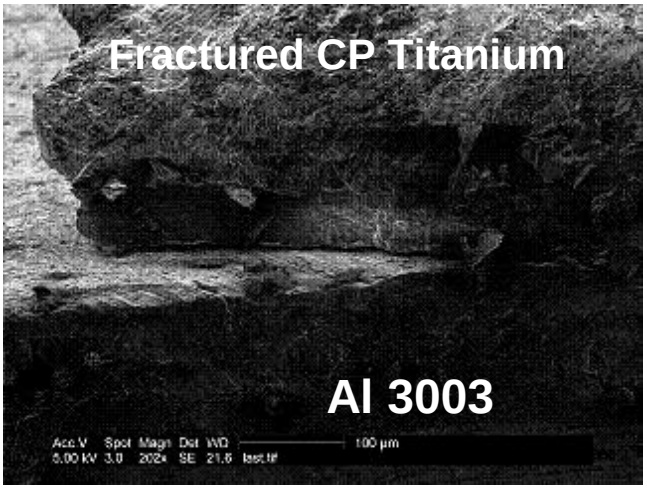

b: SEM show the fracture mode of a 30-minute annealed specimen.

Figure 3.9: SEM of the fracture features of the specimens.

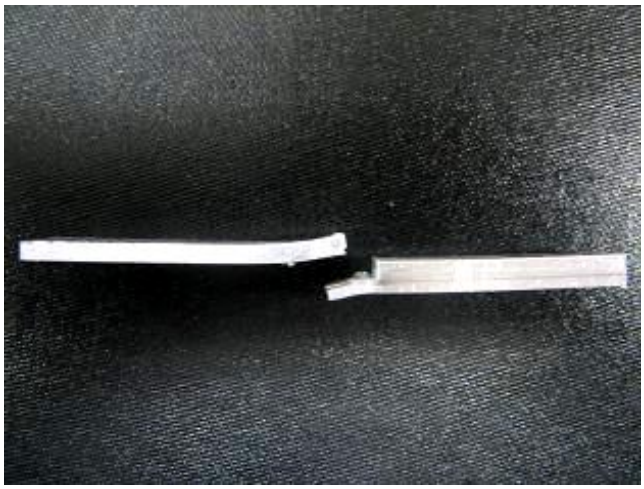

Figure 3.10: A lap specimen with bent lapped section.

Table 3.3: Lap Shear Strength (MPa) Data

Annealing Time (minutes)	Samples 1	2	3	Average
0	44.30	31.48	37.56	37.78
30	69.34	62.73	86.82	72.96
60	51.17	43.06	70.73	54.99
120	53.81	33.53	41.96	43.10
180	46.25	32.26	53.84	44.12
270	53.61	69.96	50.87	58.15

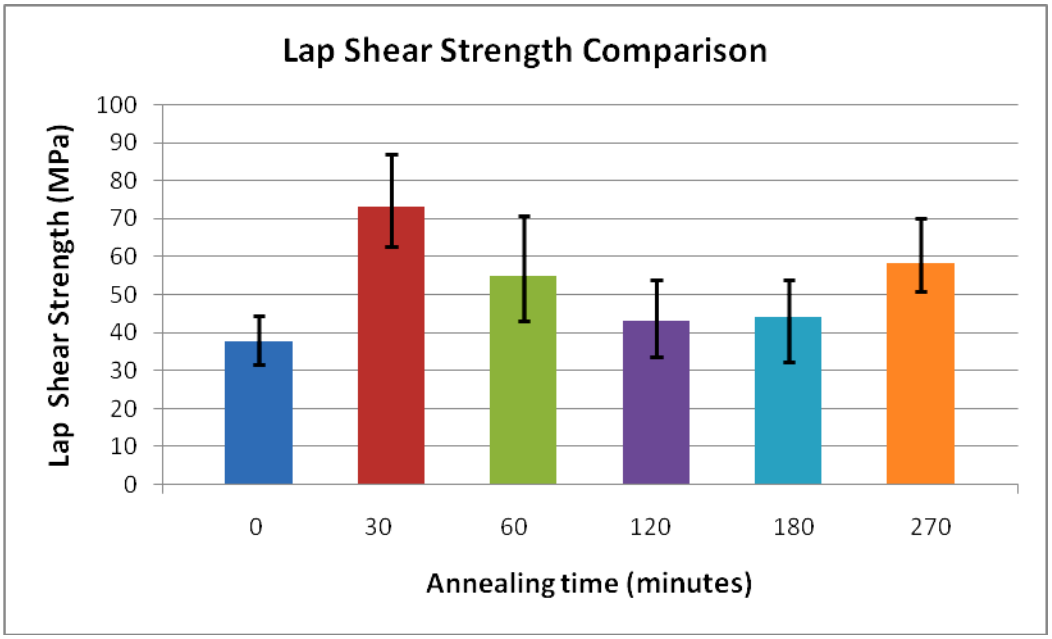

Figure 3.11: Bar chart of the lap shear strengths of the different groups of specimens.

Fig. 3.10 shows the picture of the bent profile of a 30-minute annealed specimen. The delamination causes differential strain between the separated foil and the un-delaminated ones. This leads to early failure of the delaminated foil because the developing stresses soon exceed its tensile strength as a result of the small foil thickness. In those cases, the lapping foil fraction is completely severed from the longer side causing the immediate consolidated aluminum foil to fracture by shear as the applied load increases. The output data obtained from the lap shear strength tests are shown in Table 3.3 and Figure 3.11.

SAS 9.1 software was used for the statistical analysis of the data to verify the effects of post process annealing as a single factor with six treatment levels on the shear strength of the specimens. The boxplot from the analyses did not show any outliers and the normal quantile plot is close to a straight line. Also, all the tests for normality have

high P-values, so the assumption of approximate normality of the data is satisfied. The results of the analysis also show that there is a uniform spread of the errors, which means the data satisfies the homoscedasticity assumption. The analysis of variance (ANOVA) in Table 3.4 with a P-value of 0.0210 shows that post process annealing has a significant effect on the lap shear strengths for the different groups of specimens. A post hoc mean comparison using the Ryan-Einot-Gabriel-Welsch multiple range test (REGWQ) method is shown in Table 3.5. The REGWQ controls the maximum experiment-wise error rate under any complete or partial null hypothesis. The table shows that the specimens with 30 minutes post process annealing (treatment B) have the highest mean shear strength of 72.963MPa. Since treatment B shares the same REGWQ group A with specimens that were annealed for 270 minutes (treatment F) with mean shear strength of 58.147MPa and also, with those annealed for 60 minutes (treatment C) with mean shear strength of 54.987MPa, it shows that its differences in result with those two treatments groups are not statistically significant. It (treatment group B) however, has statistically significant higher mean shear strength than specimens that were annealed for 120 minutes (treatment D), 180 minutes (treatment E), and the control specimens (treatment A).

Table 3.4: Analysis of Variance (ANOVA) for the Data

Source	DF	Sum of Squares	Mean Square	F Value	Pr > F
Model	5	2488.774111	497.754822	4.10	0.0210
Error	12	1457.120067	121.426672		
Corrected Total	17	3945.894178			

Table 3.5: REGWQ Post Hoc Means Comparison

Means with the same letter are not significantly different.				
REGWQ Grouping		**Mean**	**N**	**treatment**
	A	72.963	3	B
	A			
B	A	58.147	3	F
B	A			
B	A	54.987	3	C
B				
B		44.117	3	E
B				
B		43.100	3	D
B				
B		37.780	3	A

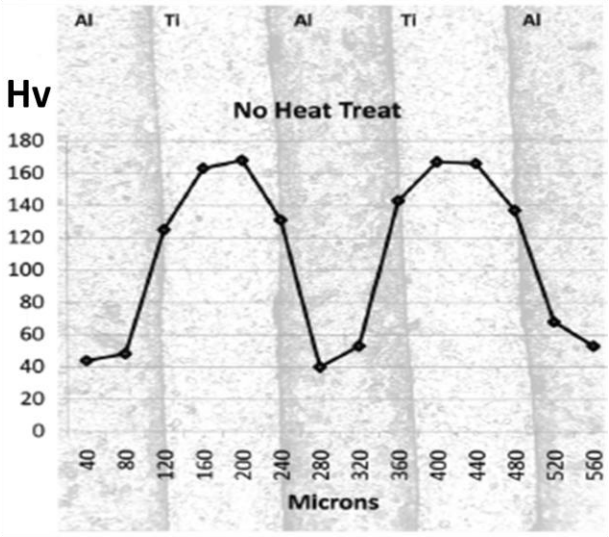

(a) Ti/Al3003 control specimen.

Figure 3.12: Vickers microhardness measurements across the Ti/Al3003 material systems.

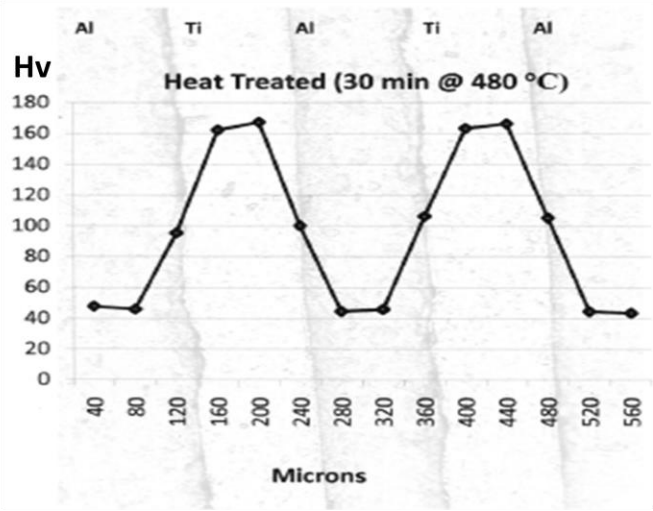

(b) Ti/Al3003 30-minute heat treated sample.

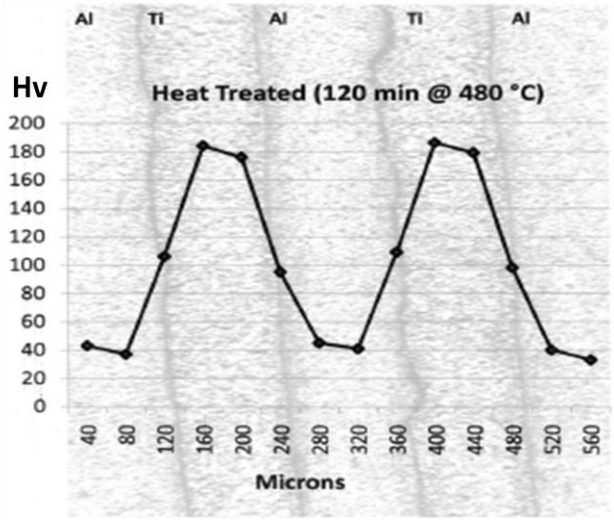

(c) Ti/Al3003 120-minute heat treated sample.

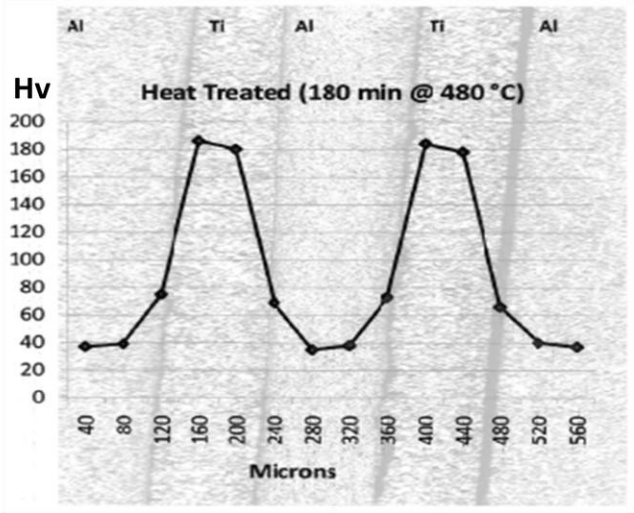

(d) Ti/Al3003 180-minute heat treated sample.

Figure 3.12 shows the microhardness signatures across consolidated foils for the Ti/Al 3003 material systems. The control (as-consolidated, without treatment) sample in Fig. 3.12a yielded an average microhardness of 130Hv at the Al 3003 side of the interface. This value is much higher than the 50Hv average value at the core of the material. This is an indication of significant work hardening of the surface during the ultrasonic consolidation process. The microhardness values for all the samples shown are generally symmetrical, an indication that there is little or no difference in the level of work hardening in all the interfaces. So there is no difference whether any of the surfaces had direct contact with the welding sonotrode or not. Also, the high hardness values at the interface of the control samples must have contributed to the low shear strengths recorded as shown in Table 3.3 and Fig. 3.11 for those samples because of the embrittlement of the interface.

The sample subjected to 30-minute heat treatment time shown in Fig. 3.12b yielded an average microhardness value of 100Hv on the Al 3003 side of the interface;

this is less than the average value recorded for the control sample in Fig. 3.12a. The reduction in hardness is due to stress relieving that took place as a result of the 30-minute oven annealing. The 60 and 120 minutes heat treated samples yielded about the same microhardness values as the 30-minute heat treated sample, but the 180-minute sample yielded a much less average value of 70Hv. 59Hv was obtained for the 270-minute sample measured. The trend shows that there is continuous softening of the work hardened Al 3003 interface as the heat treating time increases because of stress relieving and recrystalization of the grains. The longer the materials are heated, the more ductile they become. The 30-minute samples recorded the highest shear strength because of the toughness gained in the relatively short time in the oven. Longer heating time resulted in softening due to recrystalization and grain growth leading to the drop in shear strength.

A combination of factors must have been responsible for the general increase in shear strength for all the heat treated sample groups over the control samples. Stronger bonding must have occurred as a result of heat treatment induced element diffusion across the Ti/Al3003 material interface. This mass transport phenomena results in solution strengthening at the interface of the materials over a range of soaking temperature durations. The shear strength values obtained from the samples are therefore determined by the equilibrium of the effects of the active hardening and softening mechanisms. The 73MPa optimum shear strength, which is 66 percent of the value for one of the base materials, Al 3003 (as shown in Table 3.1) is comparable to the range of strength properties obtained for some dissimilar material systems bonded using other methods like diffussion bonding (Ghosh et al, 2003) and friction stir welding (Cavaliere and Cerri, 2005; and Shigematsu et al., 2003). Although lower than the value for Al 3003,

the optimum shear strength obtained by post consolidation annealing is a significant improvement over the 37.78MPa average shear strength obtained for the as-consolidated specimens without heat treatment. It is assumed that if heat treatable aluminum alloys are used, better shear strength values can be obtained.

Figure 3.13 shows the results of line scan EDS analysis sampled at 0.87 micron intervals across the Ti/Al3003 material interface indicating that some diffusion took place across the materials. The extent of the diffusion may be difficult to deduce accurately from the line scan results because of interference of electromagnetic waves released from adjacent elements in the materials during the scanning process. However, Fig. 3.13 shows that the extent of diffusion increases with increase in soaking time. Materials soaked for 30 minutes show less diffusion while those soaked for 270 minutes recorded the highest depth. Undersirable hard intermetallic materials are expected to form at high weight percent diffusion as shown in Fig. 3.14.

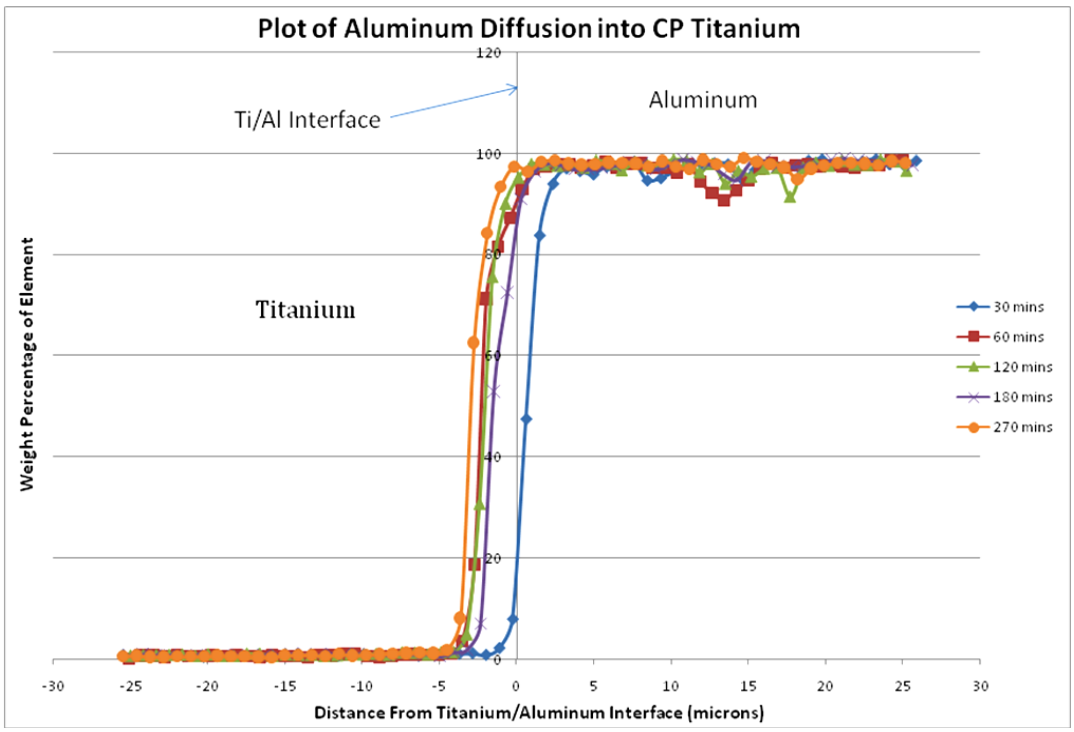

Figure 3.13: A plot of line scan EDX analysis result showing diffusion trend of aluminum into titanium at the interface at different annealing times.

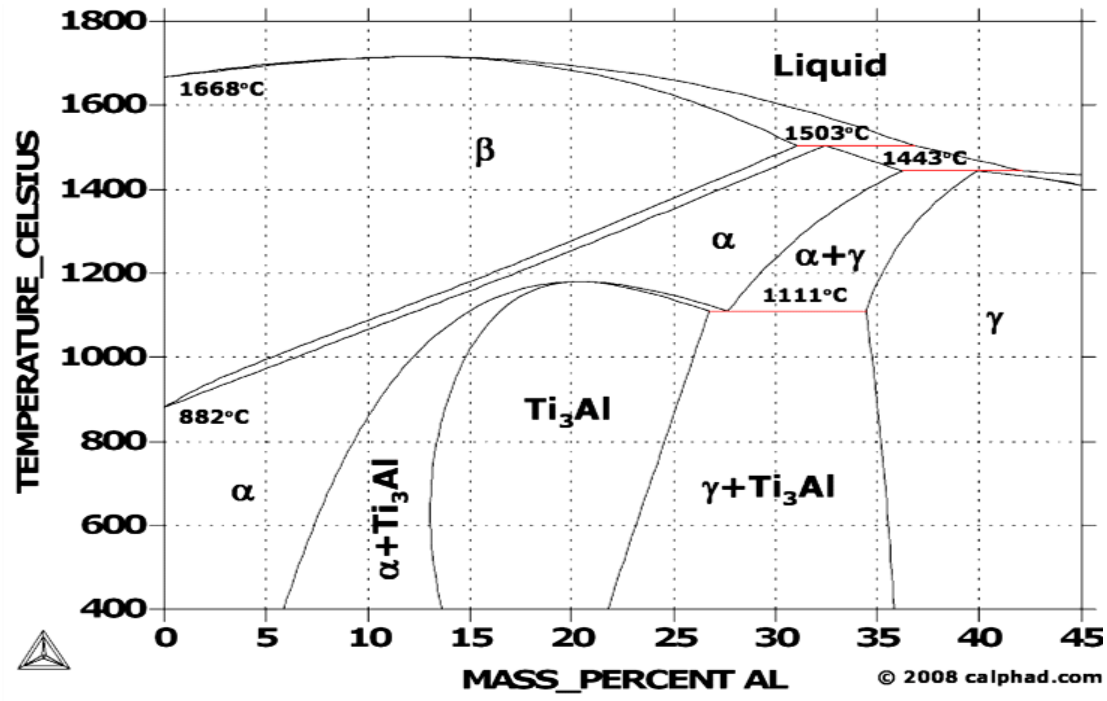

Figure 3.14: Titanium-aluminum (Ti-Al) phase diagram (Computational Thermodynamics, www.calphad.com/titanium-aluminum.html).

3.4 Conclusions

This experiment has shown that post consolidation heat treatment by annealing at 480^{o}C has significant effects on the lap shear strengths of UC specimens. The best average lap shear strength of 73MPa was obtained for specimens heat treated for 30 minutes compared to 38MPa for as-consolidated ones. Higher heat treatment times resulted in recrystalization and grain growth, making the specimens softer with reducing shear strength. Heat treated samples generally have higher average shear strengths than the as-consolidated samples. For optimum strength, a 30-minute post consolidation soaking at 480^{o}C and oven cooling yield the best shear strength.

References

Cavaliere, P., Cerri, E., 2005. Mechanical response of 2024-7075 aluminum alloys joined by friction stir welding. J. Mater. Sci. 40, 3669-3676.

Computational Thermodynamics Inc., at http://www.calphad.com/titanium-aluminum.html. Accessed July 2009.

Domack, M.S., Baughman, J.M., 2005. Development of nickel-titanium graded composition components. Rapid Protot J. 11, 41-51.

George, J.L., 2006. Utilization of ultrasonic consolidation in fabricating satellite decking. Master's thesis, Utah State University, Logan, UT.

Ghosh, M., Bhanumurthy, K., Kale, G.B., Krishnan, J., Chatterjee, S., 2003. Diffusion bonding of titanium to 304 stainless steel, J. Nucl. Mater. 322, 235-241.

Janaki Ram, G.D., Yang, Y., Stucker, B.E., 2007A. Effects of process parameters on bond formation during ultrasonic consolidation of aluminum alloy 3003. J. Manuf. Syst. 25, 221-238.

Janaki Ram, G.D., Robinson, C., Yang, Y., Stucker, B.E., 2007B. Use of ultrasonic consolidation for multi-material structures. Rapid Protot. J. 13, 226-235.

Kong, C.Y., Soar, R.C., Dickens, P.M., 2003. Characterization of aluminium alloy 6061 for the ultrasonic consolidation process. Mater. Sci. Eng. A 363, 96-106.

Kong, C.Y., Soar, R.C., Dickens, P.M., 2004A. Optimum process parameters for consolidation of 3003 aluminum. J. Mater. Process. Technol. 146, 81-187.

Kong, C.Y., Soar, R.C, Dickens, P.M., 2004B. Ultrasonic consolidation for embedding SMA fibers within aluminum matrices. Comp. Struct. 66, 421-427.

Kong, C.Y., Soar, R.C., 2005. Fabrication of metal–matrix composites and adaptive composites using ultrasonic consolidation process. Mater. Sci. Eng. A 412, 12-18.

Shigematsu, I., Kwon, Y.J., Suzuki, K., Imai, T., Saito, N., 2003. Joining of 5083 and 6061 aluminum alloys by friction stir welding. J. Mater. Sci. Lett. 22, 353-356.

Siggard, E.J., 2007. Investigative research into the structural embedding of electrical and mechanical systems using ultrasonic consolidation (UC). Master's thesis, Utah State University, Logan, UT.

Tuttle, R.B., 2007. Feasibility study of 316L stainless steel for the ultrasonic consolidation process. J. Manuf. Process. 9, 87-93.

Yang, Y., Janaki Ram, G.D., Stucker, B.E., 2007. An experimental determination of optimum processing parameters for Al/Sic metal matrix composites made using ultrasonic consolidation. J. Eng. Mater. Technol. 129, 538-549.

Yang, Y., Janaki Ram, G.D., Stucker, B.E., 2009. Bond formation and fiber embedment during ultrasonic consolidation. J. Mater. Process. Technol. 209, 4915-4924.

White D.R., 2003. Ultrasonic consolidation of aluminum tooling. Adv. Materials & Process. 161, 64-65.

CHAPTER 4

MINIMIZING DEFECTS BETWEEN ADJACENT FOILS IN ULTRASONICALLY CONSOLIDATED PARTS

This chapter was published as an article in the Journal of Engineering Materials and Technology (**132**(1), pp. 011006-1 - 011006-8, 2010). The permission to use it as a chapter in this dissertation is contained in the Appendix.

Abstract

Background: Two types of defects normally occur in ultrasonically consolidated parts: (i) defects that occur between mating foils in successive layers ("Type 1" defects), and (ii) defects that occur within a layer between two foils laid side-by-side ("Type 2" defects). While some success has been achieved in minimizing Type 1 defects, Type 2 defects, however, have been given very little attention. Both types of defects are undesirable and should be minimized if ultrasonically consolidated parts are to be used in structural applications.

Method of Approach: This work describes an investigation of how to minimize Type 2 defects in ultrasonically consolidated parts. According to our hypothesis, a foil being deposited must overlap the adjacent deposited foil by an optimum amount to ensure a defect-free joint between the two foils. Transverse tensile specimens were fabricated with various amounts of foil overlap (by changing the foil width setting) to test this hypothesis. Metallographic and fractographic studies showed a clear correlation between foil overlap, defect incidence, and tensile strength. It was found that a foil width setting

of 23.81mm helps minimize Type 2 defects in ultrasonically consolidated Al 3003 parts using standard foils of 23.88mm (equivalent to 0.94") nominal width.

4.1 Introduction

Ultrasonic consolidation (UC) is an innovative solid-state fabrication process that combines ultrasonic welding of metal foils and layered manufacturing methodologies to produce complex three-dimensional objects [1]. The UC process developed by Solidica Inc., USA, employs an ultrasonic frequency vibration combined with normal force to generate static and oscillating shear forces between metal foils to produce solid-state bonds. A layer consists of as many horizontally adjacent foils as the width of the fabricated part requires. Layers are welded one on top of the other to fabricate a part. A subtractive process is integrated in UC via a 3-dimensional computer numerical control (CNC) milling head for generating the layer by layer geometrical profile of the solid object. The geometry of each layer in the CAD file is replicated on the fabricated part. This additive and subtractive process fabricates near net shape parts, as only the substrate or base plate need to be removed by milling to form the complete part. In the case where the base plate is integrated into the design, the process is a net shape process.

Previous work has shown the viability of this novel additive process for fabricating various multi material solid objects including metal matrix composites [2]. Some of the applications of the UC process include fabrication of tools with conformal cooling channels, embedded electronic structures, embedded fiber optics, honeycomb structures and structures with arbitrary cavities [3-6]. Also, as UC is a low temperature solid freeform process, this offers a major distinction for the process when compared with other additive manufacturing processes for metals. It operates below 50% of the melting

temperatures of the metals being processed. As such, thermal stresses and related problems like distortion and embrittlement in fabricated parts are minimized.

How well the layers are bonded to each other determines the quality of UC fabricated parts. Lack of good bonds between foils results in low-strength parts that are unsuitable for structural applications (due to the presence of defects or unbonded regions along the layer interfaces). Also, leakage can result in cases where flow channels are incorporated in the part. Use of optimum process parameters (determined for each material combination) is beneficial to achieve metallurgically sound parts. Optimum process parameters have been established for the fabrication of some materials in previous studies, especially Aluminum 3003-H18. Other materials for which process parameters have been established are aerospace grade aluminum such as 6061, aluminum-silicon carbide metal matrix composites, and 316L stainless steel [1,6,7]. The important process parameters in UC are vibration amplitude, normal force, welding speed, temperature, and layer surface roughness. All of these parameters have direct influence on the bond quality between layers, and hence the strength of the structure. It has been established that linear weld density can be greatly improved by surface machining each deposited layer. Almost 100% linear weld density has been achieved by surface machining [2].

Previous efforts largely focused on improving interlayer bonds between foils, thereby reducing defects that occur between mating foils in successive layers (“Type 1” defects). In a typical UC fabricated part with less than 100% linear weld density, a number of interlayer bond defects will be present. Figure 4.1 shows a number of Type 1

defects in a UC fabricated Al 3003 sample. The process parameters mentioned above are generally optimized to eliminate or reduce those defects.

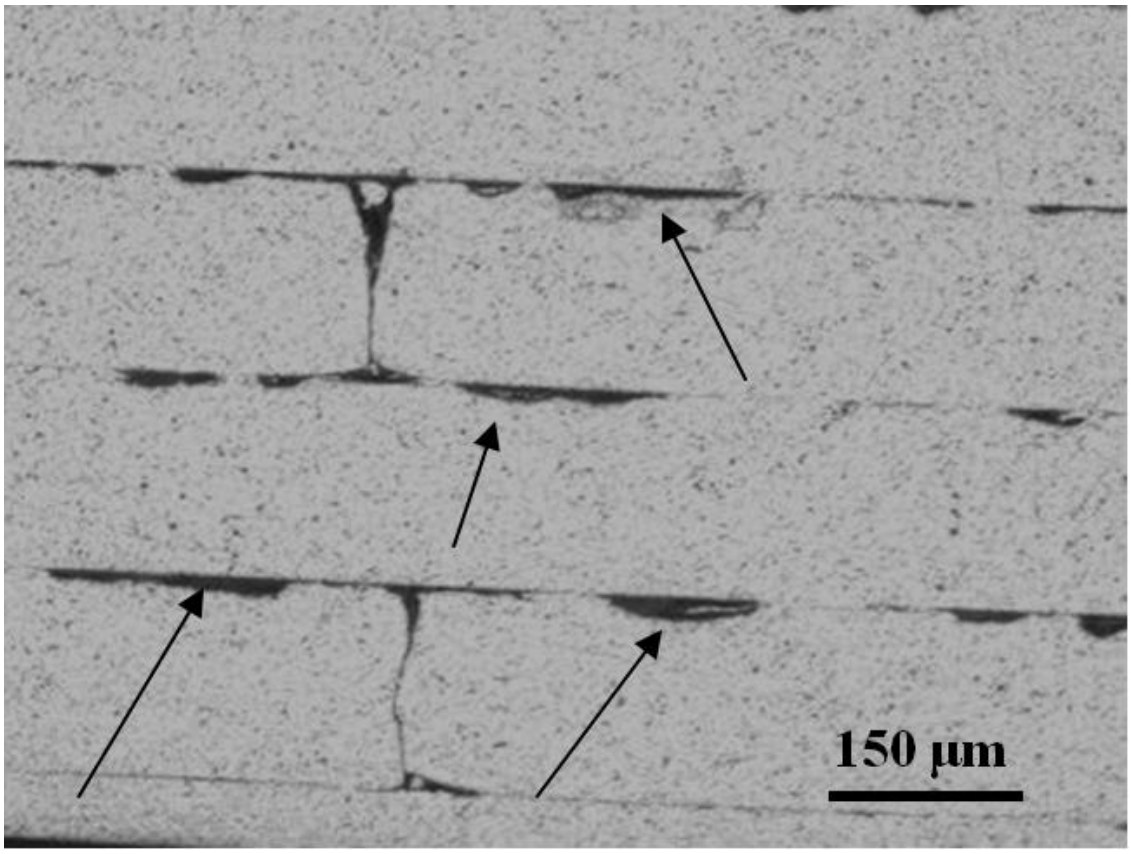

Figure 4.1: Micrograph showing Type 1 interlayer bonding defects (arrowed).

Another area of concern, which has been given very little attention so far, is the edge-to-edge joint between adjacent foils within a layer ("Type 2" defects). For parts with more than 23.88mm width (the nominal width of a typical foil); more than one foil laid side-by-side are required to cover the entire part width for fabrication. The foil joint condition, that is, whether an overlap or a gap exists between adjacent foils, is a critical consideration. Gaps between adjacent foils are very common defects in UC deposited parts. The optimized process parameters mentioned above have not offered any solution to this problem, thereby limiting the suitability of UC fabricated parts for certain

structural applications. These defects create potential stress risers that affect the load carrying capability of structures fabricated by UC. An example of such foil joint defects in an Al 3003 fabricated part is shown in the micrograph in Fig. 4.2. It reveals gaps between adjacent foils in a typical UC fabricated part. The topmost gap is about 150μm, almost the same as the thickness of the foil. This work focuses on investigating the effects of Type 2 defects on the mechanical strength of UC fabricated structures and establishing optimum conditions for minimizing or eliminating them.

If UC fabricated parts are to be used in load-bearing structural applications, especially in situations involving dynamic loads, it is necessary to minimize or eliminate Type 2 defects. The weakening effects of these defects is more pronounced in complex structures that have features like ribs with transverse foil orientation to the direction of loading. Those features are more likely to fail early in comparison with other parts that have foils in the longitudinal direction to the applied load in the presence of these defects. A default foil width of 23.90mm in the machine code for part fabrication is generally maintained in the UC machine. This width automatically sets the foil edge-to-edge joint condition for a standard Al 3003 UC foil. In this work, tensile test specimens fabricated using different intra-layer foil joint conditions with varied tape width settings were tested for strength. The tensile test specimens were machined from larger rectangular blocks in a transverse orientation to the foil direction. The fractured specimens were subjected to metallographic and fractographic studies to establish possible correlations between Type 2 defects, the mode of fracture and the strength of the specimens.

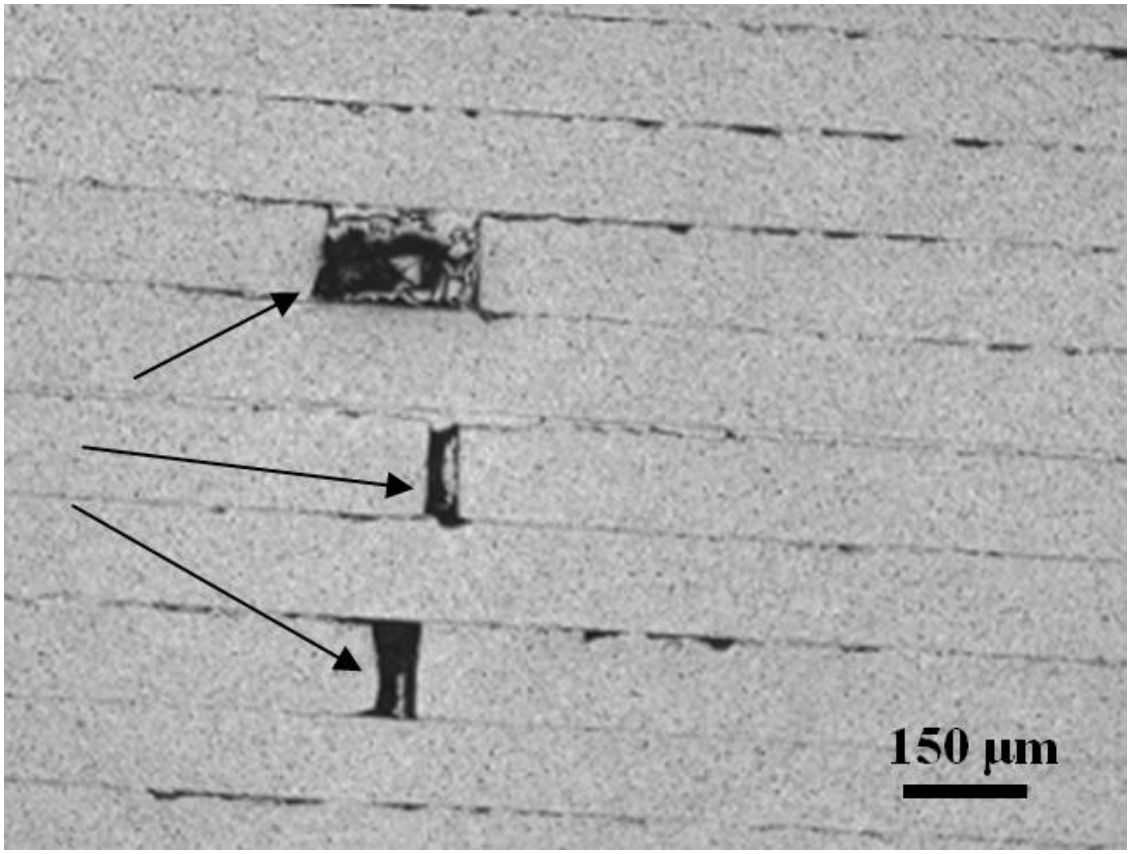

Figure 4.2: A micrograph with arrows showing Type 2 defects between adjacent foils.

4.2 Experimental Work

4.2.1 Material Fabrication

The UC experiments were carried out on a Solidica Formation^{TM} ultrasonic consolidation machine shown in Fig. 4.3. Foil feed and positioning, welding and contour milling operations on the machine are computer numerically controlled. A machine code is generated for the 3D CAD model of the part to be fabricated. This code incorporates the fabrication process parameters and directs the sequential operations of the UC machine. The foil positioning is generally randomized across the layers in the machine code automatically. This random arrangement almost always requires adjustments for

good interlayer bonds and ease of fabrication. The machine has a heat plate, by which the substrate is regulated at the desired fabrication temperature. Al 3003 base plate or substrates (dimensions: 355mm x 355mm x 12mm) bolted to the heat plate were used for the deposition of the foils. A rotating ultrasonic sonotrode of 150mm diameter vibrating at 20 kHz frequency travels on the automatically fed foil to weld it to the substrate. It runs twice on the foils in a layer. On its first run, it performs a tacking operation, which in this experiment was set at the following parameters: tack force 300N, tack rate 42mm/s, and tack amplitude of 8μm. On the second run, it welds the foil to the substrate. The sonotrode along with the foil feed mechanism is integrated into the x-axis gantry as shown in Fig. 4.3. During build, the gantry moves a horizontal distance equal to the specified foil width in the machine code to deposit adjacent foils in the layers through the sonotrode. The following optimum process parameters already established in previous work for Al 3003 fabrications [2] were applied in the machine code for all the specimens fabricated in this work: temperature 300^{o}F; normal force 1750N; amplitude16μm; and welding speed 16mm/s. Aluminum 3003H-18 foil (nominal composition by wt%: Al-1.2Mn-0.12Cu, 23.88mm nominal width and 150μm thickness) sourced from Solidica Inc., USA was used.

The default tape width setting in the machine code is 23.90mm with the standard Al 3003-H18 foil supplied by Solidica. Since the foils are of the same nominal width, the distance the sonotrode is moved to weld determines the nominal gap or overlap between adjacent foils. If the sonotrode displacement exceeds the actual foil width, adjacent foils do not touch each other and a gap is created between them within the layer. However, if the displacement is less than the actual foil width, an edge-to-edge overlap of adjacent

foils results in a layer (See Fig. 4.4 for illustration). The extent of the gap or overlap created at the joint is dependent upon the difference between the actual foil width and the sonotrode displacement or foil width specified in the machine code. In this work, each block of material fabricated have distinct foil width setting, and is maintained throughout its build.

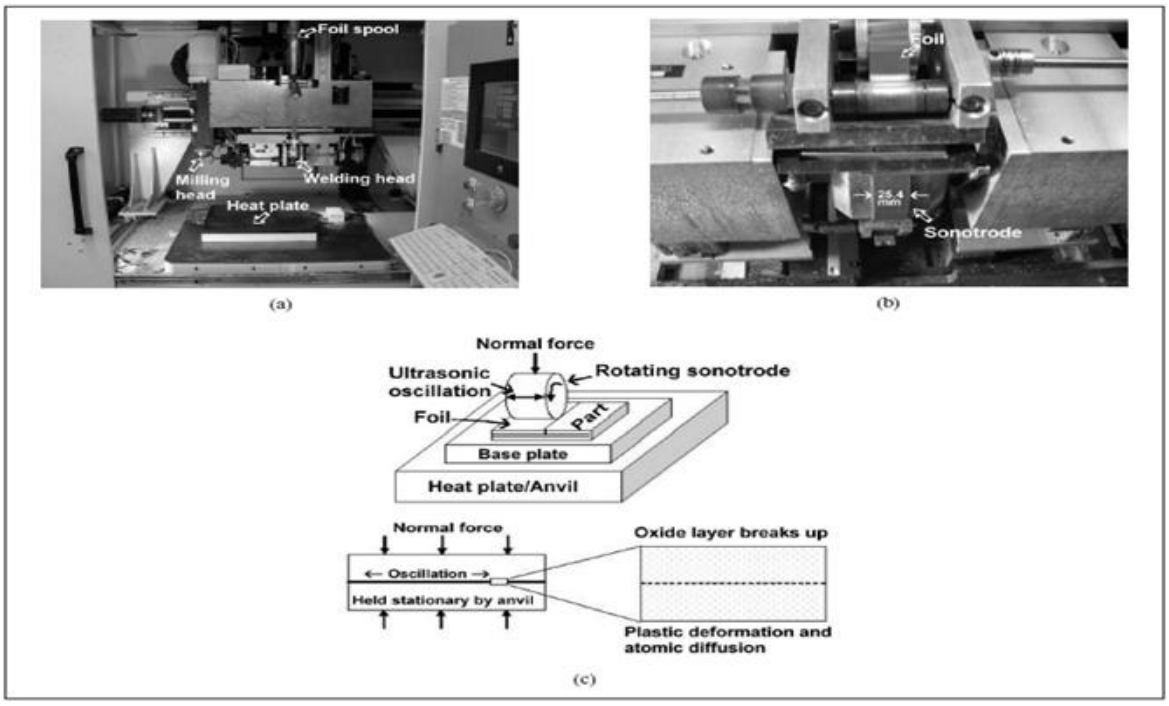

Figure 4.3: (a) Solidica Formation™ UC machine, (b) Close-up view of ultrasonic sonotrode from below, (c) Schematic of UC process.

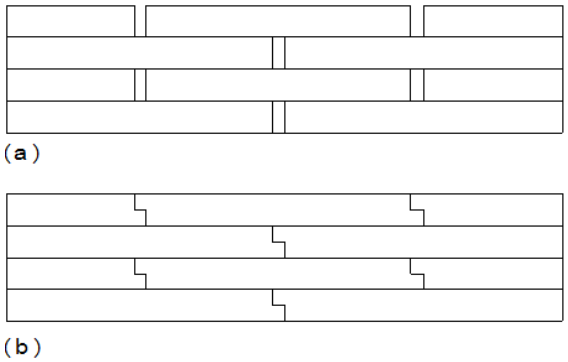

Figure 4.4: End view of (a) gap and (b) overlap between two adjacent foils.

A solid block of material with dimensions 210mm x 75mm x 7.2mm was deposited for each set of parameters, each modeling a specific foil edge-to-edge joint condition. The foils were arranged with either a 50% overlap across adjacent layers or a random arrangement of overlaps, as illustrated in Fig. 4.5. The 50% overlap brick wall arrangement is such that the edge-to-edge joints are located at the middle of joints in the immediate adjacent layers. It was chosen to ensure that deposited foils have equal amount of surface overlap in contact with the two previously welded foils under them. The joints are equally spaced to avoid strength degradation due to close packing of weak areas and to inhibit fracture propagation from layer to layer. It is also easy to assess the quality of the foil edge-to-edge joints in alternate layers in micrographs. Seven blocks of material were fabricated with differing tape width settings, ranging from 23.78mm to 23.96mm with an increment of 0.03mm. These seven sets utilized 50% foil overlap between two adjoining layers, as shown in Fig. 4.5a. The 23.93mm and 23.96mm foil width settings were expected to produce poor results, as they were larger than the default width setting of 23.90mm (which was known to produce gaps). Another two blocks were fabricated to model tape width settings of 23.96mm and 23.81mm with random overlap. An example of the random overlap is illustrated in Fig. 4.5b. These were fabricated to provide a comparison of the strengths of specimens with random overlap and 50% overlap settings.

For the purpose of identification and comparison in this work, the materials have been labeled according to their width specifications in the machine code without the “mm” and decimal notations. The 50% overlap materials are labeled without any prefix while the randomly overlapped materials are prefixed with an “R”. As an example, the

50% overlap 23.78mm width material is labeled “2378” while the random overlapped 23.96mm material is labeled “R2396.” The longitudinal sample set is labeled “Long”.

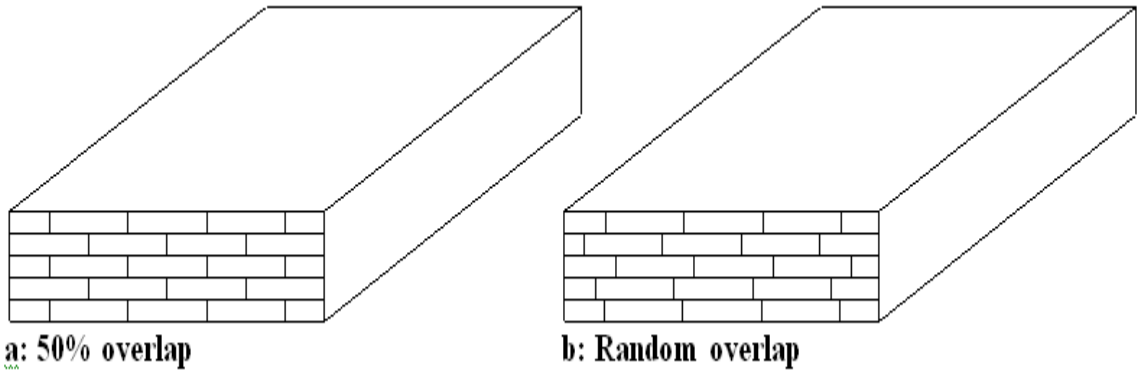

Fig.5a: 50% overlap. **Fig.5b: Random overlap.**

Figure 4.5: End view patterns of (a) 50% and (b) random overlap foil arrangements.

4.2.2 Problems Encountered

There were problems encountered during the deposition of some of the rectangular blocks for the tensile specimens. The depositions with foil width settings of 23.78mm, 23.81mm, 23.84mm and 23.96mm were the most problematic. The level of difficulty increased as the width difference between the default 23.90mm width and the desired width setting increased. This difficulty is due to the design of the tape-feeding mechanism, which has more allowance more than required. Although the tape-feeding mechanism can be moved a precise amount along with the sonotrode, the tape can wander a small amount within the mechanism from its nominal position between foil deposits. Excessive ability to wander (larger width settings) and too much foil overlap (smaller width settings) can both experience fabrication problems. In either case, however, these problems could be rectified. Figure 4.6 shows a picture of one of the

deposition problems that was encountered a number of times during the fabrication of the blocks. Some foils popped up without bonding to the previously deposited layer as a result of the new width settings. This problem was typically corrected by rewelding the affected foil(s). However, in some cases the entire layer was removed by a milling recovery operation. The deposition process was then continued from the recovered layer.

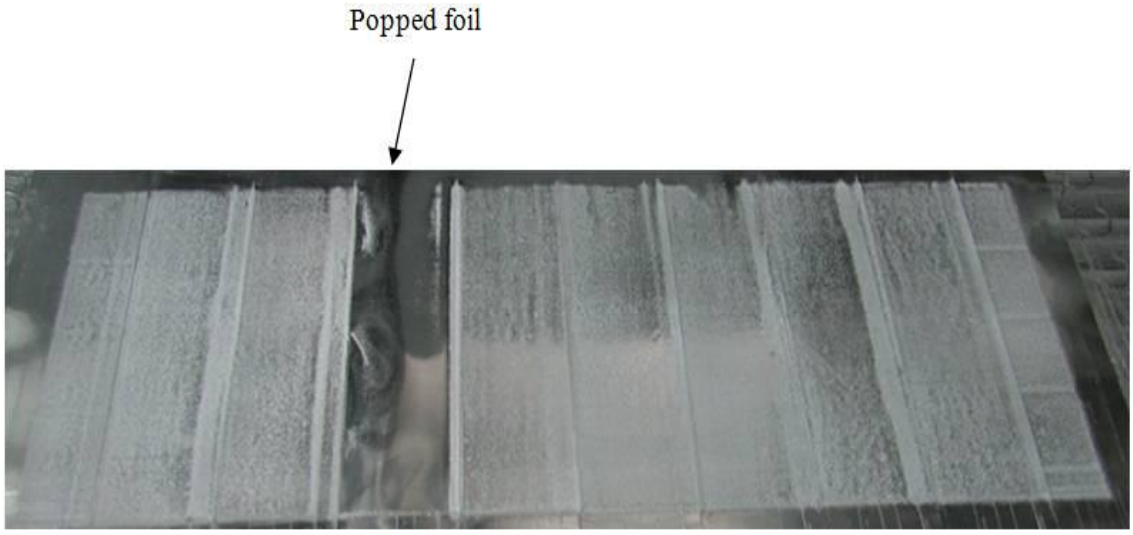

Figure 4.6: Picture showing a layer with a popped foil. This was corrected by repeating the weld.

4.2.3 Tensile Testing

Standard tensile testing bars conforming to ASTM standard test method E8 were fabricated with the following dimensions (Figure 4.7): gage length – 50.0mm; width – 12.5mm; thickness – 7.0mm; radius of fillet – 12.5mm; overall length – 200.0mm; reduced section – 57.0mm; length of grip section – 50.0mm; and width of grip section – 20.0mm. Three tensile bars were fabricated for each foil joint model from the fabricated solid blocks of materials described in section 2.1. Transverse orientation specimens were machined from the blocks fabricated using the 50% overlap layup and the tape width

settings ranging from 23.78mm to 23.96mm and from the random overlap arrangement for tape width settings of 23.96mm and 23.81mm.

One set of tensile specimens was machined in the longitudinal orientation such that the axis of the tensile bar was parallel to the foil direction. The default foil width setting of 23.90mm in the machine code and the 50% overlap arrangement was used for these specimens. Tension tests were performed on an Instron tensile testing machine (model 3367) with a load cell capacity of 30KN according to ASTM E8M. An Instron 2630-100 Series clip-on extensometer was used for strain measurements.

Figure 4.7: Ultrasonically consolidated tensile test specimens.

4.2.4 Metallographic Studies

Small samples cut from the undistorted tensile specimens' grip ends were mounted and polished according to standard metallographic procedures. They were then etched with Kellers reagent (90ml H_2O, 5ml HNO_3, 3ml HCl and 2ml HF) and observed under an optical microscope. Also, fractographic studies were carried out on tensile fractured samples using a Scanning Electron Microscope (SEM).

4.3 Results and Discussion

4.3.1 Microstructures

Optical micrographs reveal distinctive microstructures for each set of specimens, as shown in Fig. 4.8(a-i).

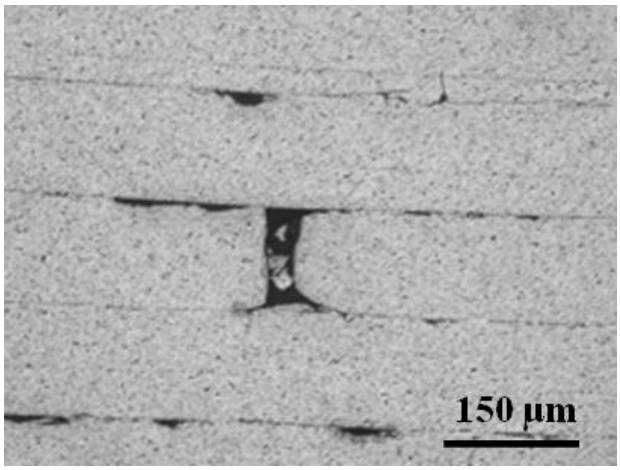

(a): Longitudinal sample.

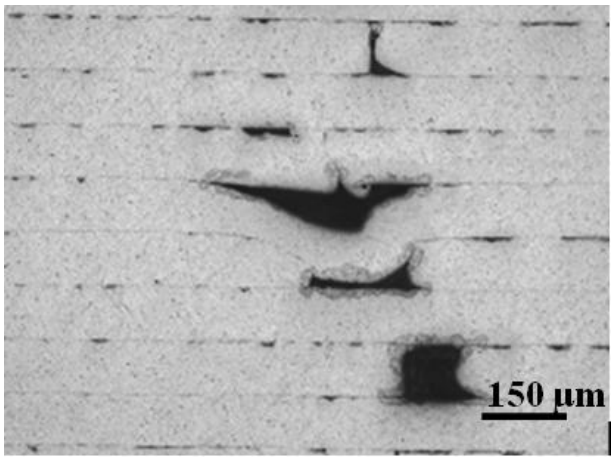

(b): 2396 sample.

Figure 4.8: Representative micrographs for each set of tensile specimens.

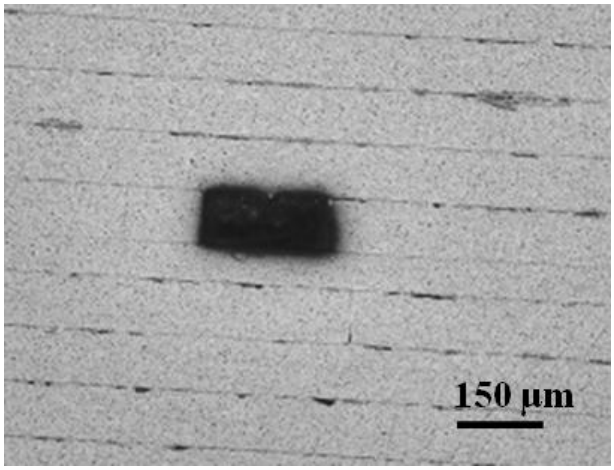

(c): R2396 sample.

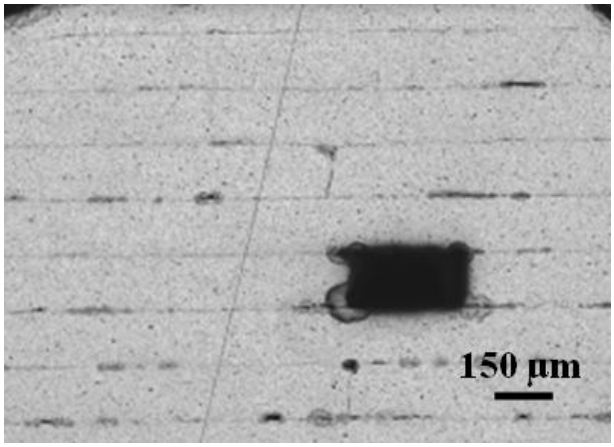

(d): 2393 sample.

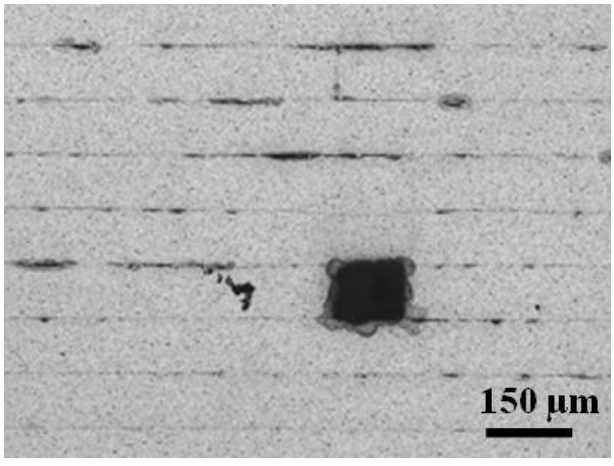

(e): 2390 sample.

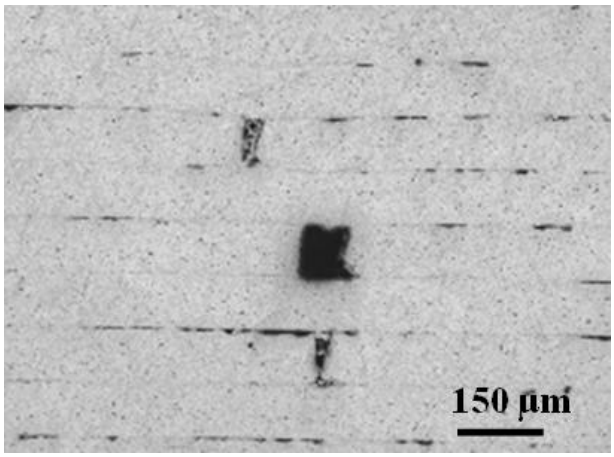

(f): 2387 sample.

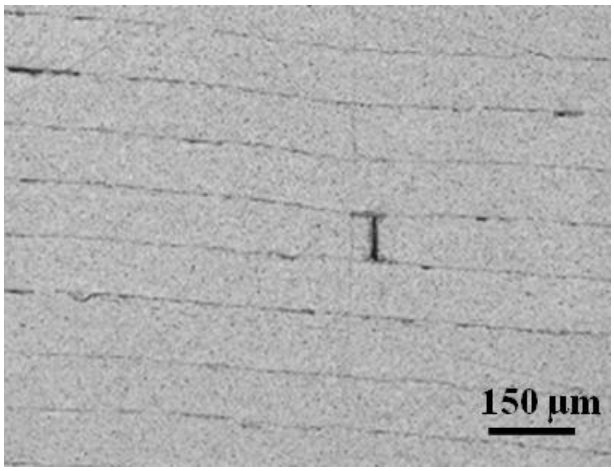

(g): 2384 sample.

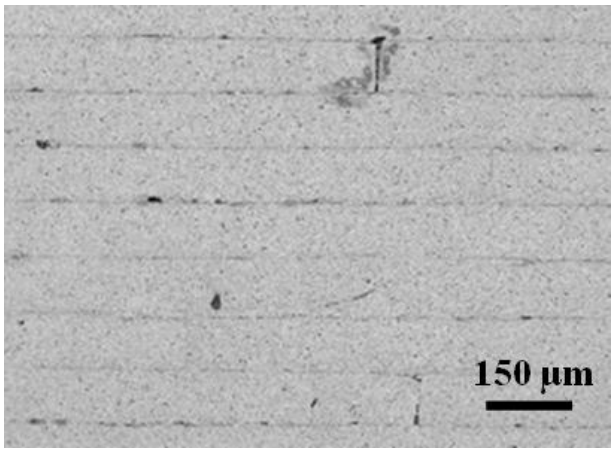

(h): 2381 sample.

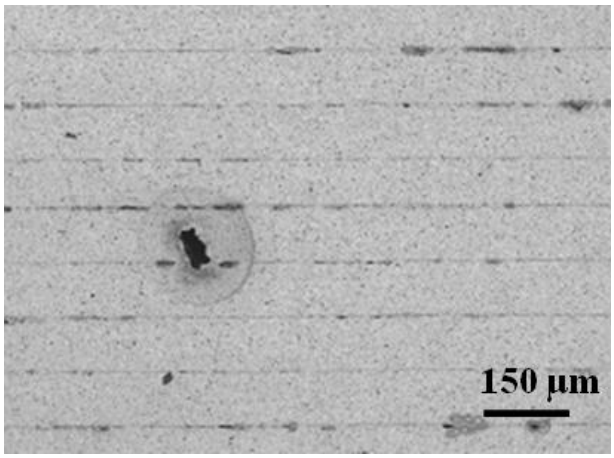

(i): 2378 sample.

The micrographs in Fig. 4.8 reveal the condition of bonds between the edges of adjacent foils. It is evident that the size of defects at the joints and their frequency is directly related to the foil width specified in the machine code for each set of specimens. The 2396 sample in Fig. 4.8b, representing the largest foil width setting, exhibits the largest and the most numerous gaps between the foils when compared with other specimens of smaller width specification. Virtually all alternate layers have sizable gaps in the 50% overlap samples because of the "brick-wall" arrangements. A trend can be observed in the size reduction and frequency of defects from Figures 4.8b to 4.8i, representing a decrease in the foil width from 23.96mm to 23.78mm. Foil edge-to-edge defects progressively decrease down to the 2381 sample, where we see the smallest defect size. There is a slight increase in defect size in the 2378 sample (due to problems with foil placement at higher levels of overlap). It is noteworthy that the 2390 sample representing the default setting for most UC fabrication experiments with Al 3003 alloys, has a relatively large prevalence of edge-to-edge foil joint defects. This can also be confirmed in the longitudinal sample shown in Fig. 4.8a, built at the default 23.90mm

setting. This suggests that the default foil width setting of 23.90mm for Al 3003 may not provide an optimized, defect-free microstructure using the current UC foil feeding mechanism. Since the default setting is 20μm more than the nominal width, it is not surprising that defects are observed with the default setting. The micrographs also reveal that the foil joints are not in perfect alignment at every other layer, as was intended for the 50% overlap condition. In some cases, there is up to 150μm displacement between foil joint locations. This further illustrates that the UC machine does not precisely deposit foils in the location prescribed by the machine code. The precision of the machine is thus a limitation since a 150μm error is relatively high for a process that is sensitive to gap widths. From observations made on the feeding and guiding mechanism of the machine, there is more clearance than required to precisely locate the foils in the tacking positions on the substrate. Also, when the foils are not properly tacked, sometimes they "walk" out of alignment during the welding operation, thereby creating gaps between adjacent foils. In addition to these effects, the translation precision of the gantry on the axes of the machine may also contribute, to a lesser extent, to positioning errors.

4.3.2 Tensile Strengths

Table 4.1 shows the tensile strength data obtained from the specimens. The table contains the average strength and standard deviation. Figure 4.9 shows the same data in the form of a bar chart for visual comparison. Each of the bars in the Figure represent the average tensile strength of each set of specimens, while the error bars show the range of tensile strengths in the respective set. The stiffness data for the specimens are shown in table 4.2. There are no significant variations between the stiffness of the samples sets.

Apart from the R2396 samples with an average stiffness of 62.2GPa, all others have close values.

Tensile strength results are consistent with the defect trends seen in the microstructural studies in section 3.1. As expected, the longitudinal specimens, which contain no transverse joints exhibit the highest strength. The 2396 samples have the lowest strength among the 50% overlap transversely oriented tensile specimens. It can be seen that strength increases as foil width setting decreases. This means that as the size of defects between adjacent foils decreases, the strength increases. Therefore, it can be reasonably stated that the foil width specified determines the foil edge-to-edge joint integrity and hence, the strength of a UC fabricated part. The tensile strengths peaked for the width setting of 23.81mm at an average strength of 201.3 MPa. The lower width value of 23.78mm resulted in a slightly smaller average strength of 197MPa. It should be noted that difficulties encountered in welding the 2378 samples as a result of the reduced foil width could also have contributed to this reduction in strength. Thus, from this study, it appears that the 23.81mm width setting is the optimum width, beyond which the part begins to degrade in strength due to an accumulation of fabrication errors. This optimum width setting, however, presents fabrication difficulties, such as described in section 2.2, when compared to the default 23.90mm setting. Nevertheless, if strength is an important factor in the application of the fabricated part, it would be best to apply this optimum value.

Table 4.1 shows that specimens with random foil arrangements (i.e. R2396 and R2381) did not yield a consistent strength trend when compared to their 50% overlap counterparts (i.e. 2396 and 2381 respectively). While the R2396 yielded a 22.3% average

strength improvement over 2396 specimens, the R2381 samples have 7.5% lower average strength than the 2381 specimens. Tensile strength values of 208MPa and 206MPa obtained for samples 2 and 3 of the R2381 respectively are comparable to those obtained for the 2381 specimens. However, the sample 1 of the R2381 yielded a much lower strength of 145MPa when compared to the other two specimens. This low strength may be a result of several Type 2 defects that are close to one another in that particular sample because of the random foil placement. These data shows that it is possible to obtain comparable strength values from both random and 50% overlap fabricated parts. The 50% overlap specimens however, offer a more reliable data compared to ones with randomly arranged foils.

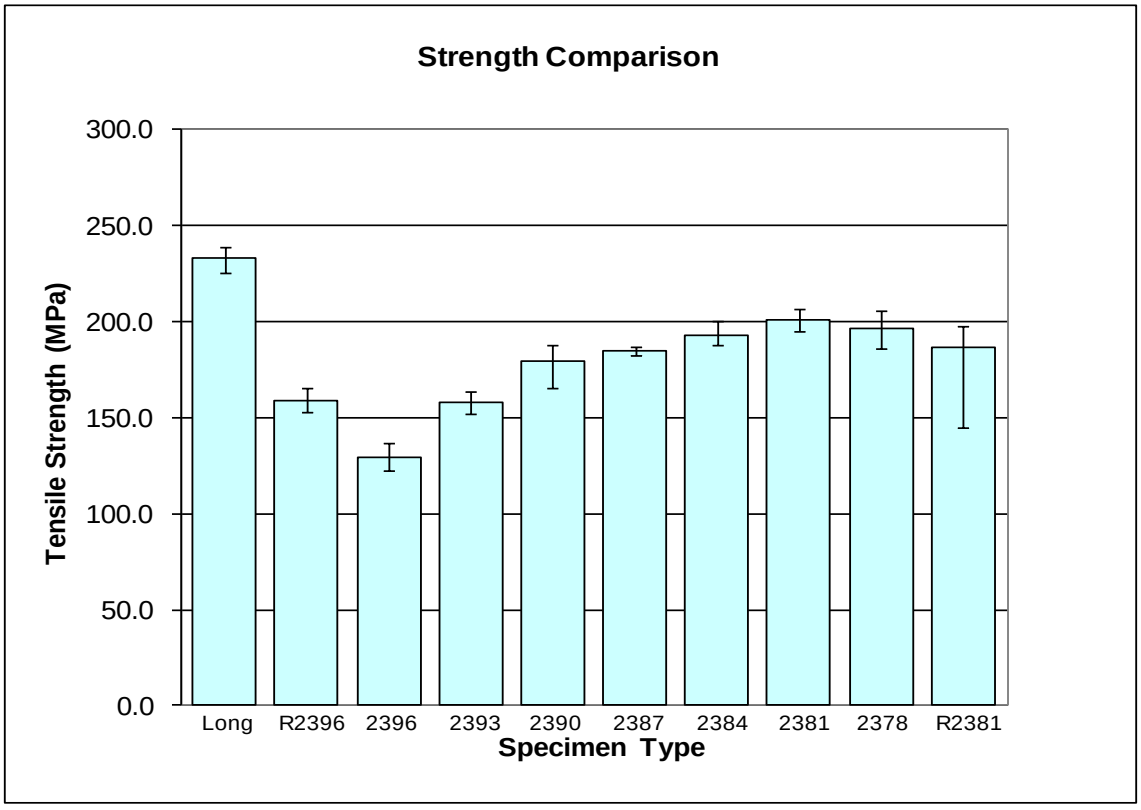

Figure 4.9: Bar chart with error bars showing strength comparison for samples fabricated with different width settings.

Table 4.1: Tensile Strength (MPa) Data

Sample	1	2	3	Average	St. Dev.	St. Dev.(%)
2396	137	123	129	130	7.0	5.42
R2396	166	153	157	159	6.7	4.20
2393	152	159	164	158	6.0	3.81
2390	166	185	188	180	11.9	6.64
2387	185	187	183	185	2.0	1.08
2384	189	188	201	193	7.2	3.75
2381	202	195	207	201	6.0	2.99
R2381	145	208	206	186	35.8	19.2
2378	186	199	206	197	10.1	5.15
Long	234	239	226	233	6.6	2.81

4.3.3 Fracture features

Some of the distinctive features of the fracture surfaces and fracture paths of the specimens are revealed by examination of the SEM images shown in Figures 4.10(a-f) and 4.11(a-d).

The SEM pictures for R2396 and 2390 samples in Figures 4.10c and 4.10d, respectively, show the mode of fracture propagation for cases where the width settings are above the optimum value. The fracture surfaces exhibit some regions of original foil edges and some regions of dimpled rupture. The original foil edges were evident at alternate layers for the 50% overlap settings and at random locations for the random overlap samples. The original foil edges correspond to fracture paths through gaps created by Type 2 defects, where no apparent bonding between adjacent foils occurred.

At those locations, there were no fractures in the material. The regions of dimpled rupture are evidence of fracture at locations within continuous foils or at locations where good bonding occurred between adjacent foils.

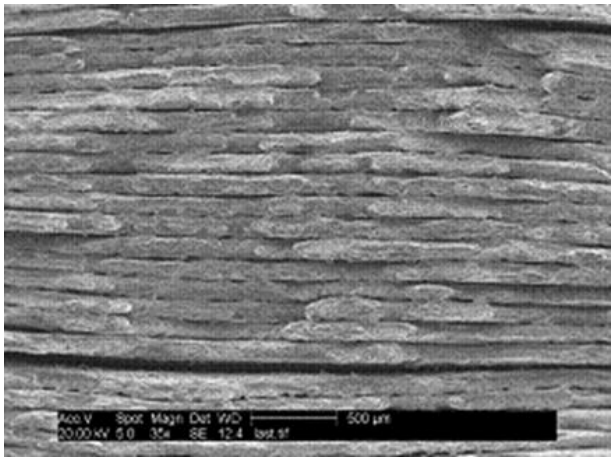

(a): A view of the fractured surface of a longitudinal sample.

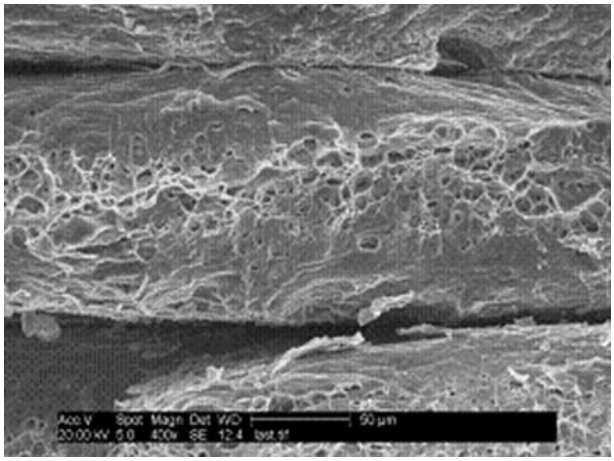

(b): Higher magnification view of the longitudinal sample.

Figure 4.10: Fractured surfaces of selected sample specimens.

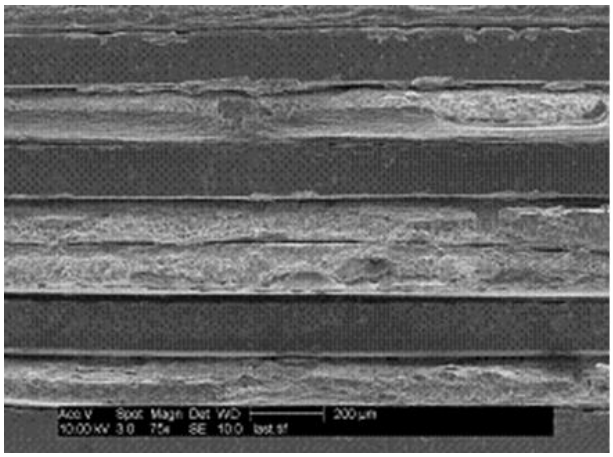

(c): A view of the fractured surface of an R2396 sample.

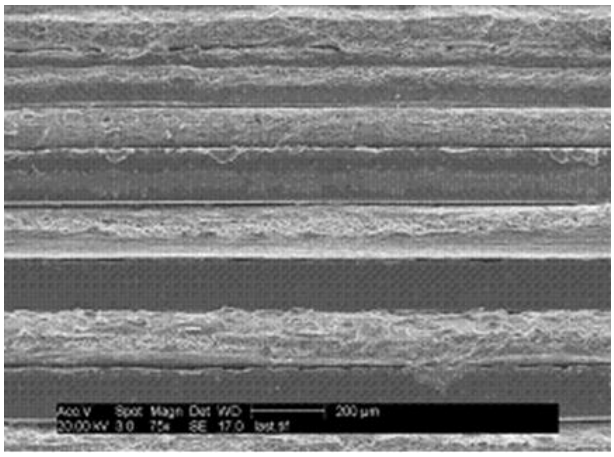

(d): A view of the fractured surface of a 2390 sample.

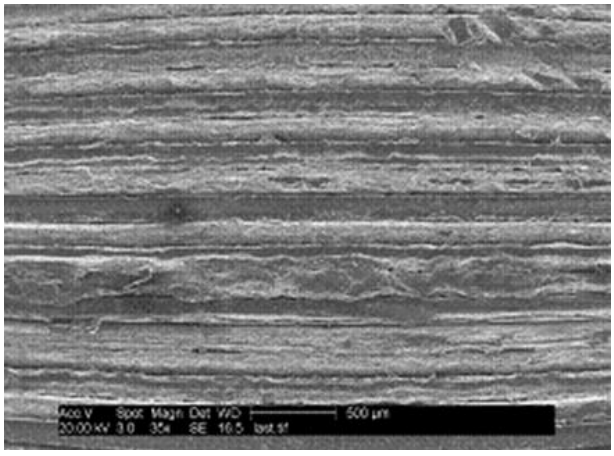

(e): A view of the fractured surface of a 2384 sample.

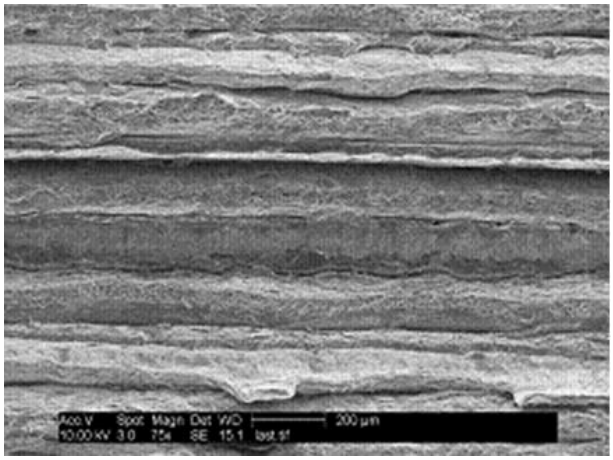

(f): A view of the fractured surface of a 2381 sample.

Figure 4.11 shows side views of fracture paths of some of the samples. Figure 4.11a shows evidence of necking before final fracture in the longitudinal samples, a characteristic of ductile failure. This is understandable since all the foils run through the length of the samples, and all of them were fractured. The measured properties of the longitudinal specimens are dominated by the foil properties rather than bond strength. In contrast, all the 50% overlap transversely oriented samples exhibit a somewhat flat fracture surface, which is characteristic of less ductile materials. The flatness is associated with the transverse orientation of the tensile samples, where measured properties, failure mode and fracture path are influenced by a combination of foil properties, bond quality, and the occurrence of Type 2 defects. For the brick type specimens, the Type 2 defects are found almost directly above one another in alternate layers. Also, since perfect bonding was not achieved in all the joints, the weakest points in the specimens will be at those un-bonded and partially bonded joints. The fracture lines therefore pass through them, this resulted in a near straight fracture line through the samples, as illustrated with arrows in Fig. 4.11c. In the case of random overlap samples,

represented by an R2396 sample in Fig. 4.11d, the fracture path can be seen to pass through un-bonded and partially bonded foil joints. The arrows in Fig. 4.11d point to some of the un-bonded foils in alternate layers where the fracture path follows the random pattern of the foil arrangements.

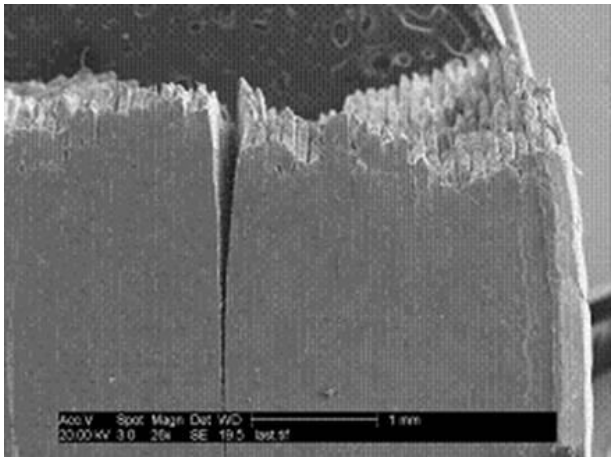

(a): Side view of the fracture surface of a longitudinal sample.

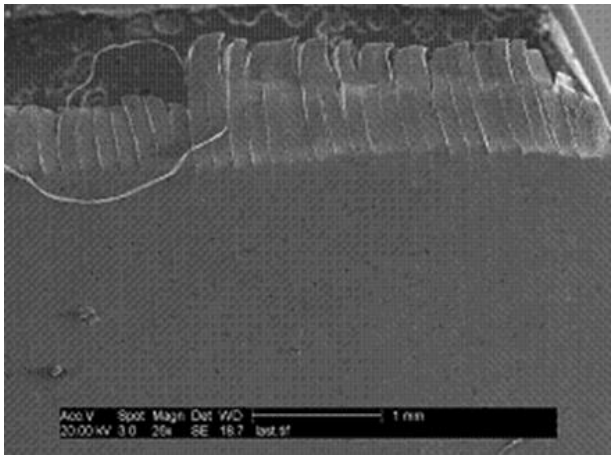

(b): Side view of the fracture surface a 2390 sample.

Figure 4.11: Fracture paths of some of the specimens.

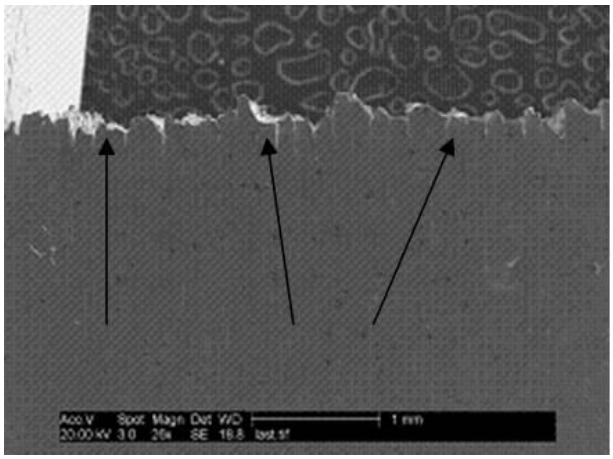

(c): Side view of the fracture surface a 2384 sample.

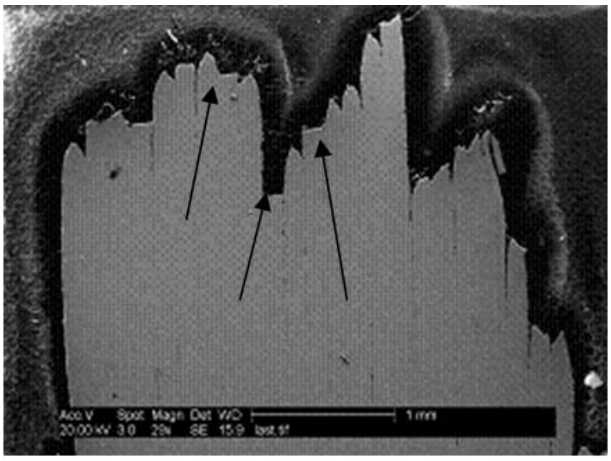

(d): Fracture line of a polished R2396 sample.

4.4 Conclusions

In this work it has been shown that the default foil width setting of 23.90mm for UC fabrication does not produce structures free of Type 2 defects. The quality of bonding at foil edge-to-edge joints is directly correlated to the foil width settings used in the UC process, and is found to directly influence part strength. Higher width settings lead to larger Type 2 defects and lower strengths within the fabricated part. The effects of the feeding and guiding mechanism on the foil positioning with respect to edge-to-edge joint

defects have been highlighted. Improved feeding and guiding mechanisms are needed to repeatably place foils, thus reducing the presence of defects and increasing the strength of UC fabricated structures.

Foil edge-to-edge joint defects were found to strongly influence the strength of fabricated structures. Data generated through tensile tests and microstructural studies show that a width setting of 23.81mm for Al 3003 standard foils of 23.88mm nominal width yields an optimal strength for UC fabricated structures with foils oriented transversely to the direction of loading. Smaller width settings create bonding problems described in section 2.2 during the fabrication of the specimens and are not recommended.

The longitudinal samples exhibited higher strength values as compared to the transverse samples. This is due, in part, to the fact that the foil used was manufactured by rolling, which inherently introduces anisotropic properties. However, the presence of Type 2 defects significantly degraded the strength of transverse specimens. In all cases, the strength measured in the transverse orientation exceeded 50% of that measured in the longitudinal orientation in spite of the fact that, for the larger width settings, all of the defects were aligned every other layer. Cross sectional micrographs of the non-optimum samples show that some of the layers have well bonded foil edge-to-edge joints, clearly indicating that the frequency of Type 2 defects is less than the number of joints in those specimens. The fraction of well bonded joints supports the observed transverse strengths.

The 50% overlap specimens offer more consistent strength data than the specimens fabricated with randomly overlapped foils. Based on the result of the data obtained, the 50% foil overlapped fabrications are recommended for structural parts.

References

[1] Kong, C.Y., Soar, R.C., and Dickens, P.M., 2004, "Optimum Process Parameters for Ultrasonic Consolidation of 3003 Aluminium," J. Mater. Process. Technol. **146**(2), pp. 181-187.

[2] Janaki Ram, G.D, Yang, Y., and Stucker, B.E., 2006, "Effect of Process Parameters on Bond Formation During Ultrasonic Consolidation of Aluminum Alloy 3003," J. Manuf. Syst., **25**(3), pp. 221-238.

[3] White, D.R., 2003, "Ultrasonic Consolidation of Aluminum Tooling," Advanced Materials and Processes, **161**(1), pp. 64-65.

[4] Kong, C. Y., 2005, "Investigation of Ultrasonic Consolidation for Embedding Active/Passive Fibers in Aluminum Matrices," Doctoral thesis, Loughborough University, Loughborough, UK.

[5] Siggard, E.J., Madhusoodanan, A.S., Stucker, B., and Eames, B., 2006, "Structurally Embedded Electrical Systems Using Ultrasonic Consolidation (UC)," *Proceedings. of 17th Solid Freeform Fabrication Symposium,* Austin, TX, USA, August 14-16.

[6] Yang, Y., Janaki Ram, G.D., and Stucker, B.E., 2007, "An Experimental Determination of Optimum Processing Parameters for Al/SiC Metal Matrix Composite Made Using Ultrasonic Consolidation," J. Eng. Mater. Technol., **129**(4), pp. 538-549.

[7] Tuttle, R.B., 2007, "Feasibility Study of 316L Stainless Steel for the Ultrasonic Consolidation Process," J. Manuf. Process., **9**(2), pp. 87-93.

CHAPTER 5

MULTI-MATERIAL MINIMUM WEIGHT STRUCTURES FABRICATION USING ULTRASONIC CONSOLIDATION

This chapter has been prepared for publication in the Journal of Materials Processing Technology

Abstract

The multi-material capability of additive manufacturing (AM) processes has created opportunities for structural designs that would otherwise be impossible. This work involves the development of a methodology for fabricating dual-material minimum-weight structures using ultrasonic consolidation (UC). Sample structures were designed, fabricated and tested for load carrying capabilities. Analyses of results show that dual-material minimum weight structures made of Al3003/MetPreg® and Al3003/Ti composite material members can withstand significantly higher loads than similar structures made of the matrix Al 3003 material. This is an indication that UC can be effectively used to fabricate multi-material structures for real life applications.

5.1 Introduction

Research on the fabrication of multi-material structures using different additive manufacturing (AM) processes has accelerated in recent years. AM processes have the potential for flexible variation of materials and microstructures, both in continuous and discrete fashion in addition to their capabilities for complex geometry structures. New uses of some advanced materials are being discovered because of the ability to combine them with other materials in AM fabricated structures. Also, some of the materials that would otherwise be difficult to combine in conventional processes are being processed (Cohen et al., 2006; Malone et al., 2004; Liu and DuPont 2003; Griffith et al., 1997; Arcaute et al., 2009; Janaki Ram et al., 2007; chapter 2). This ability to deposit function specific materials where they are needed in a structure further revolutionizes engineering structure design and material usage. One of the driving forces is the economic use of costly advanced materials that are prescribed to be deposited just where they are functionally required in a structure. The application of these capabilities is diverse, ranging from medical to aerospace, automobile, nuclear and others.

Potential applications of multi-material structures fabricated using AM processes have been demonstrated. Arcaute et al. (2009) used stereolithography (SL) for the fabrication of multi-material scaffolds with spatially controlled characteristics for tissue engineering applications. Also, Wicker et al. (2004) fabricated complex multi-material hydrogel constructs for nerve regeneration and guided angiogenesis applications. Meso and macro scale multi-material structures have also been fabricated using SL (Jae-Won Choi et al. 2009 and Inamdar et al. 2006).

Objet Geometries Limited commercialized the 3D printing of dissimilar material end use products using polymer materials (www.growit3d.com/services/multi-material-polyjet). Objet's Connex™ machines jet multiple materials simultaneously to fabricate multi-material structures.

Different laser powder metal deposition processes have been used to deposit multi-material structures. Examples include gradient structures (Griffith et al., 1997; Liu and DuPont, 2003), surface cladding with corrosion and wear resistant materials for machinery (Foroozmehr et al., 2009) and medical implants applications (Janaki Ram and Stucker, 2008). Both 3D printing and laser powder deposition processes have capabilities for continuous material variation as well as discrete material domains in fabricated multi-material structures.

Ultrasonic consolidation has been demonstrated to have the capabilities for multi-material structures fabrication. This capability was demonstrated by Janaki Ram et al., 2007B, in their work in which copper, brass, nickel, inconel 600, AISI 347 stainless steel, stainless steel AISI 304 wire mesh, MetPreg®, and aluminum alloy 2024 were each welded to aluminum alloy 3003-H18. Domack and Baughman (2005) investigated the capability of UC to fabricate graded titanium and nickel alloy multi-material structures. Additionally, ultrasonic welding has been successfully used to weld metals to a polymer matrix composite (Kruger et al., 2004). Obielodan et al. (chapter 2), further demonstrated UC multi-material capabilities by welding different combinations of molybdenum, tantalum, titanium, copper, silver, nickel, MetPreg®, aluminum alloys 1100, 3003, 6061 and boron powder. Also, the shear strengths of titanium/aluminum ultrasonically bonded foils were characterized by Obielodan and Stucker (2009).

Ultrasonic consolidation, described more fully elsewhere (White, 2003 and chapter 4), is a low temperature process that combines ultrasonic welding and additive manufacturing technology. Multi-material structures fabricated using UC characteristically have discrete material domains as opposed to the continuous material variation that is obtainable with laser powder deposition processes and 3D printing. The process has the potential for fabricating structures for applications in systems subjected to mechanical loading. In this study, a methodology for fabricating multi-material structures using UC was developed. UC structures made of single materials are relatively easy to fabricate when compared to multi-material fabrications, as foils can be automatically fed.

Multi-material minimum weight Michell structures (Dewhurst, 2001; Dewhurst, 2005; Selyugin 2004; Michell, 1904) represent one of the categories of structures that can be geometrically and materially complex to fabricate using conventional processes. They are made of multiple, thin members that are preferably made from light weight materials with high specific strength and stiffness. Such structures are readily applicable to aerospace and automotive industries, where there is continuous emphasis on higher strength and lower weight structures for improved fuel efficiency and performance. Figure 5.1 shows an example of a complex minimum weight structure with members that could be made of different materials based upon Michell theory (Michell, 1904). In the illustration, if the structure is pinned at points A and B and a load is placed at C, parallel to a line between A&B, as shown with the arrow, the outer member labeled D will be in pure compression, as well as all the inner members that join D tangentially. Those inner members that are perpendicular to D, and the member between A and C will be in pure tension. In order to optimize a structure to its fullest extent, the members in tension can

be made of materials different from those in compression. In this case, the intersection between the tensile and compressive members and the design and strength of these joints is of critical importance for the structure's reliability and performance.

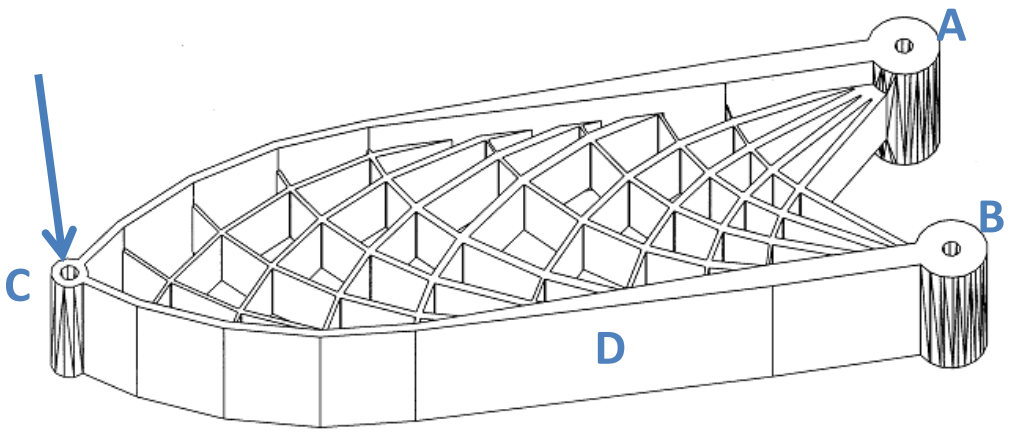

Figure 5.1: A minimum weight structure design (Dewhurst, 2001).

Simplified minimum weight structures based on maximum strength and maximum stiffness criteria (Dewhurst, 2005) were designed and fabricated. Figure 5.2 shows a free body diagram of the structure with *oa, ob* and *oc* as compression members and *ab* and *ac* as tension members when subjected to compressive load *F* with simple supports at *b* and *c*. Given a simplified minimum weight structure shown in Fig. 5.2 with

span = L,

applied force = F,

$F = f\sqrt{2}$,

where f is the stress acting on the tension members at any point during loading. Table 5.1 shows the load relationships existing in the structure members. Structures designed based on maximum stiffness criterion must satisfy the following strain ratio (Dewhurst, 2005)

$$\frac{\varepsilon_T}{\varepsilon_C} = \left[\frac{\left(\rho_T / E_T\right)}{\left(\rho_C / E_C\right)}\right]^{\frac{1}{2}} = \left(\frac{E_C \rho_T}{E_T \rho_C}\right)^{\frac{1}{2}} \quad \text{(i)}$$

In this work, simple dual-material minimum weight structures consisting of MetPreg®/aluminum alloy 3003 composite as tension members and aluminum alloy 3003 as compression members were fabricated. Samples with titanium/aluminum alloy 3003 and aluminum alloy 3003 as separate structural members were also fabricated. Both maximum strength and maximum stiffness design criteria were used for the design of the fabricated structures

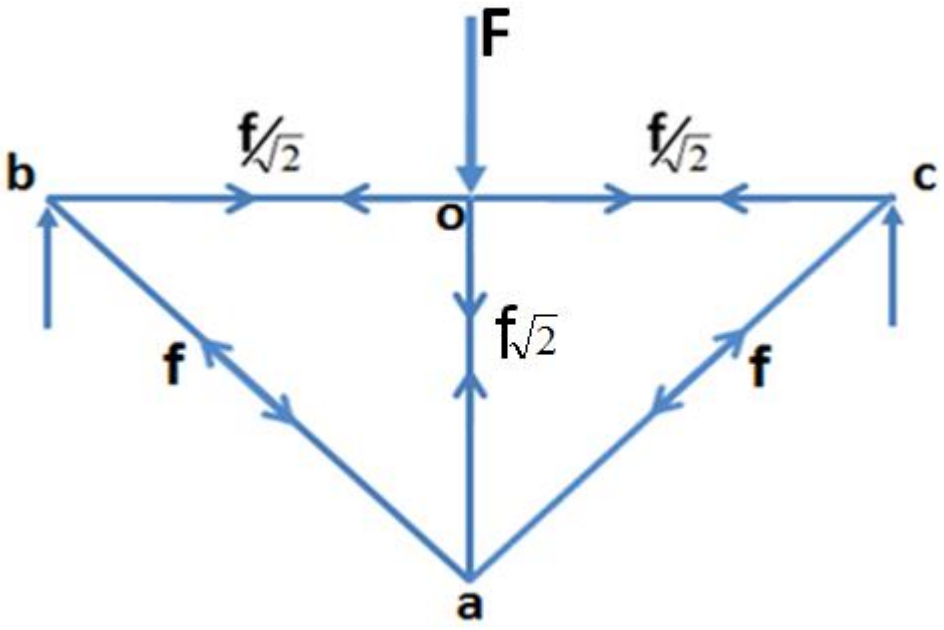

Figure 5.2: Free body diagram of the dual-material minimum weight structure.

Table 5.1: Load and Size Relationship for the Minimum Weight Structure

Element	Length	Force	Cross-sectional area
oc	$L/2$	$F/2 = f/\sqrt{2}$	$F/(2\sigma_C)$
oa	$L/2$	$F = f\sqrt{2}$	$F/(\sigma_C)$
ac	$L/\sqrt{2}$	$F/\sqrt{2} = f$	$F/(\sqrt{2}\sigma_T)$

5.2 Experimental Work

A Solidica Formation™ ultrasonic consolidation machine was used for all the fabrications in this work. During typical operation, the machine uses an automatic foil feeding mechanism, but foil materials can be fed manually when it is necessary. The parts were made on aluminum alloy 3003-H18 substrate materials of 355 x 355 x 12 mm size, mounted on a heat plate. Foil materials of aluminum alloy 3003-H18, MetPreg® and CP titanium were used for the fabricated structures. The structures are composed of tension and compression members. The tension members carry simple tensile loads while the compression members carry simple compressive loads when a three-point load is applied as illustrated in Fig. 5.2. One set of the structures consist of MetPreg®/Al3003 composite tension members and Al3003 compression members. The other set was made of titanium/Al3003 composite tension members and Al3003 compression members. Both maximum stiffness and maximum strength minimum weight structure design criteria were used for each material combination. Thus, for MetPreg®/Al3003 composite and Al3003 material combination, the two criteria were used to design structures having different member sizes. The same criteria were applied for the titanium/Al3003 and

Al3003 material combination. Three structure replicates were fabricated using each criteria and material combination.

A third set of structures were ultrasonically consolidated exclusively with Al 3003-H18 foil material using exact dimensions of the MetPreg®/Al 3003 material minimum weight structures. Another set of structures were fabricated using wrought Al 3003 H-18, having the same base material as the Al 3003 foil used. These last sets of structures were fabricated as single material copies of the shape and sizes of the MetPreg® and titanium reinforced dual-material structures described above. All the single material structures were fabricated for the sole purpose of comparing their load carrying capabilities with those of the dual-material structures. The major comparison factor is the strain energy densities of the structures at failure.

For the purpose of analysis and discussion in this work, the structures have been named as follows. All structures designed based upon maximum strength design criterion or single material copies of such designs have their labels hyphenated with "STR". Similarly, those designed based upon maximum stiffness criterion or their single material copies have their labels hyphenated with "STF". Thus, MetPreg®/Al 3003 dual-material structures designed based on maximum strength criterion are labeled Met-STR, while structures of the same materials designed based on maximum stiffness criterion are labeled Met-STF. Corresponding structures designed based on Ti/Al 3003 materials are labeled Ti-STR and Ti-STF. The single material direct copies of Met-STR and Met-STF structures ultrasonically consolidated using Al 3003 foils are correspondingly labeled Al-STR and Al-STF. Also, those machined out directly from Al 3003-H18 plate as single material structure copies of Met-STR and Met-STF are correspondingly labeled W-Al-

Table 5.2: Member Sizes for Fabricated Structures

Structure	Sample	Member widths (mm)			Thickness (mm)
		oa	***oc***	***ac***	
Met-STR	1	12.00	6.00	3.05	3.85
	2	12.00	6.00	3.05	3.57
	3	12.00	6.00	3.05	3.00
Met-STF	1	10.00	5.00	4.91	3.22
	2	10.00	5.00	4.91	3.63
	3	10.00	5.00	4.91	3.45
Ti-STR	1	8.00	4.00	6.00	3.00
	2	8.00	4.00	6.00	3.15
	3	8.00	4.00	6.00	3.00
Ti-STF	1	8.00	4.00	5.16	2.87
	2	8.00	4.00	5.16	3.57
	3	8.00	4.00	5.16	3.23
Al-STR	1	12.00	6.00	3.05	4.10
	2	12.00	6.00	3.05	4.13
	3	12.00	6.00	3.05	3.70
Al-STF	1	10.00	5.00	4.91	4.00
	2	10.00	5.00	4.91	3.86
	3	10.00	5.00	4.91	3.89
W-Al-MSTR	1	12.00	6.00	3.05	3.30
	2	12.00	6.00	3.05	3.30
	3	12.00	6.00	3.05	3.18
W-Al-MSTF	1	10.00	5.00	4.91	3.14
	2	10.00	5.00	4.91	3.30
	3	10.00	5.00	4.91	3.46
W-Al-TSTR	1	8.00	4.00	6.00	3.46
	2	8.00	4.00	6.00	3.24
	3	8.00	4.00	6.00	3.03
W-Al-TSTF	1	8.00	4.00	5.16	3.34
	2	8.00	4.00	5.16	3.05
	3	8.00	4.00	5.16	3.00

MSTR and W-Al-MSTF, while copies of Ti-STR and Ti-STF are respectively labeled W-Al-TSTR and W-Al-TSTF. The sizes of the members of the fabricated structures are shown in Table 5.2. The maximum strength and maximum stiffness design criteria structures are respectively designated as 1 and 2 in the analysis of results.

Four different machine codes were developed using Initial Graphics Exchange Specification (IGES) 3-D model files for each of the dual material structures. This became necessary as the UC machine needed to operate in an unconventional sequence characterized by interruptions while changing from one file to the other because of the different materials used. The first code was for consolidating the Al 3003 matrix material of 100 x 105 x 0.3mm consisting of two layers of foils. After the consolidation, the integrated 3-axis CNC milling facility was used to machine out the channels for accommodating the embedded reinforcing materials. This was used to accommodate the reinforcing materials for the respective tension members in the fabricated structures. The MetPreg® foil was embedded in 9.5mm wide cavities while that for the titanium foils was 12 mm. This first step is illustrated in Fig. 5.3a.

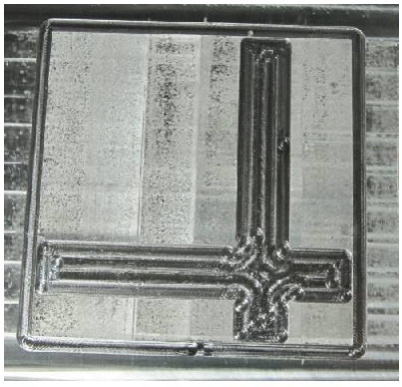

(a): Cavity machined into deposited Al 3003 matrix.

Figure 5.3: Structure fabrication sequence.

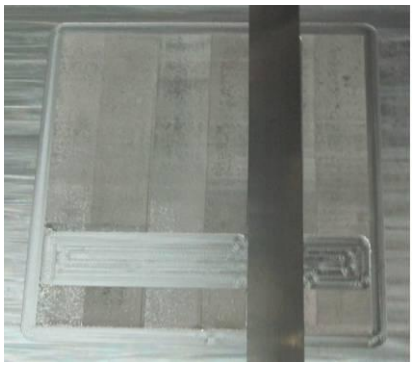

(b): Reinforcing foil placed in position.

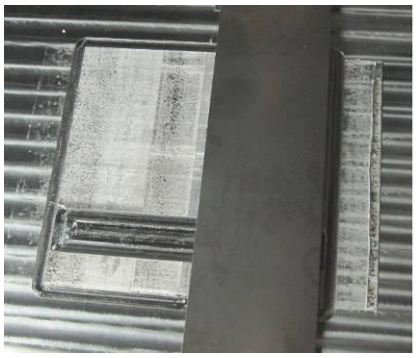

(c): Titanium foil of equal width with the sonotrode placed on top of reinforcing foil preparatory to indirect welding.

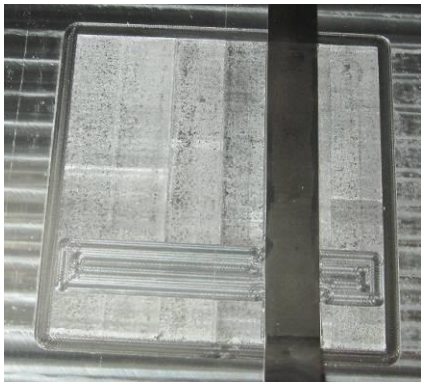

(d): The first reinforcing foil fully welded into the Al 3003 matrix.

(e): The second reinforcing foil fully welded into the Al 3003 matrix.

(f): The structure profile machined using UC integrated CNC milling.

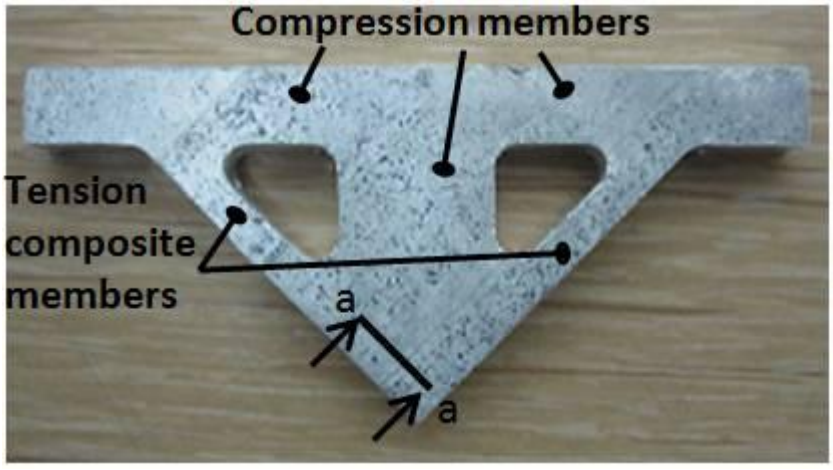

(g): The structure removed from the substrate using conventional millling.

The second and third machine codes were used to weld the reinforcing material that is sandwiched with Al 3003 foils in alternate layers to make the composite tension members in each of the structures. In the respective structures, the reinforcing materials serve to reinforce the Al 3003 matrix foils in the tension members. The composite reinforcing foils in the affected layer cavity were put in place one at a time and welded indirectly by placing a 25mm width titanium foil between it and the welding sonotrode as shown in Figs. 5.3b to 5.3e. The indirect welding was to prevent the sonotrode from having direct contact with the softer Al 3003 matrix material because of the required high welding amplitude applied for the reinforcing materials. Direct welding can destroy the Al 3003 matrix material at the high welding amplitude. The structures' constituent materials were welded using different sonotrode vibration amplitudes as determined in earlier work by Obielodan et al. (chapter 2). Table 5.3 shows the compositional, hardness and dimensional details of the materials used while Table 5.4 shows the welding parameters applied for their consolidation. The mechanical and physical properties of the materials are shown in Table 5.5.

Table 5.3: Nominal Compositions, Crystal Structures and Hardness of Materials Used

Material	Composition	Crystal Structure at UC Temperature	Micro-Hardness (Hv)	Thickness (μm)
Al alloy 3003 H18	Al-1.2Mn-0.12Cu	FCC	80	150
Titanium	Ti-0.59Fe-0.38Mn	HCP	185	70
MetPreg® Al matrix reinforced tape	$Al2O_3$ Short Fiber	-	600	200

Table 5.4: UC Process Parameter Values Used for Each Material

Material	Amplitude (μm)	Speed (mm/s)	Normal Force (N)	Temperature (^{o}F)
Al 3003	16	23.70	1750	300
Ti	28	10.58	2000	300
MetPreg®	28	12.70	1750	300

Table 5.5: Some Mechanical/Physical Properties of the Materials

Material	Reinf. Material Vol. Fraction (%)	Stiffness (GPa)	Tensile strength (MPa)	Density (Kg/m^3)
MetPreg® /Al3003 Composite	66	129	500	3020
Ti/Al3003 Composite	25	77.1	232	2934
Al3003	-	68	200	2730

The cycle of operations described above were repeated until the desired final thickness of the structure was attained. Thereafter, the fourth machine code file was used to cut out the profile of the structure as shown in Fig. 5.3f in reverse order from top to the bottom using the integrated CNC milling head. The completed structure is shown in Fig. 5.3g. The fabricated structures were subjected to three-point loading using a short beam shear test fixture (ASTM D 2344) as illustrated in Fig. 5.4. A 50kN capacity Tinius Olsen tension testing machine was used to apply a compressive load at 0.5mm/min speed until the structure failed.

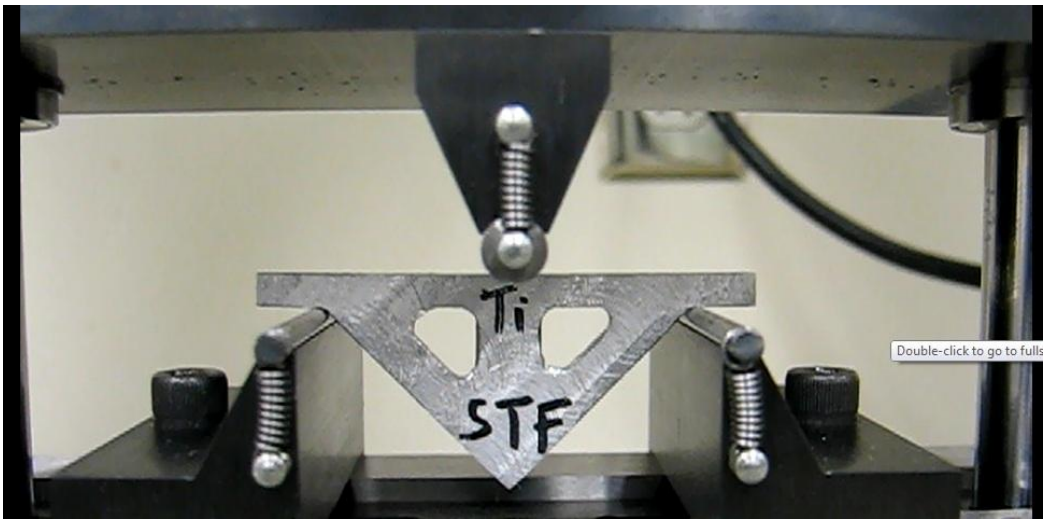

Figure 5.4: Structure under test using a 3-point bend test fixture.

Small samples cut from the intersecting joints of the composite members were mounted and polished according to standard metallographic procedures. They were observed under optical microscope. Fractographic studies were also carried out on fractured surfaces of the structures.

5.3 Results and Discussion

5.3.1 Microstructures

Micrographs of section a-a in Fig. 5.3g at the intersection joints of representative structures are shown in Fig. 5.5 below. Figure 5.5a shows the side and end views of reinforcing MetPreg® foils for the left and right hand side tension members respectively of the structure shown in Fig. 5.3g. MetPreg® foils for the left hand side tension member have their foils (with fibers as shown) stretching through the length of the member in alternate layers. At the other layers, shorter reinforcing foils are seen with abutting joints with those of the right hand side tension member (that is, those with their end views shown in darker color). Each of the reinforcing foil layers are alternated with the Al 3003

matrix material. The abutting reinforcing foil joints have gaps of varying sizes, because, they were manually laid without any tacking operation by the sonotrode. There is some measure of foil displacement of un-tacked foils during the welding operation resulting in the shift of positions. For structures reinforced with titanium foils, Fig. 5.5b shows corresponding foil arrangement at the intersection joint between the two tension members.

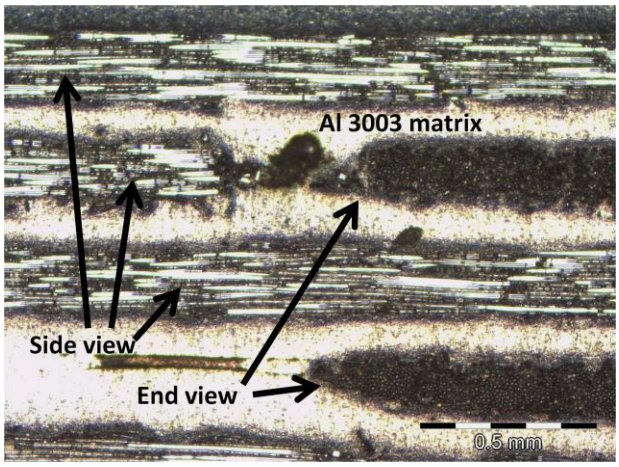

(a): A view of interlocking MetPreg® foils in Al 3003 matrix at the intersection joints.

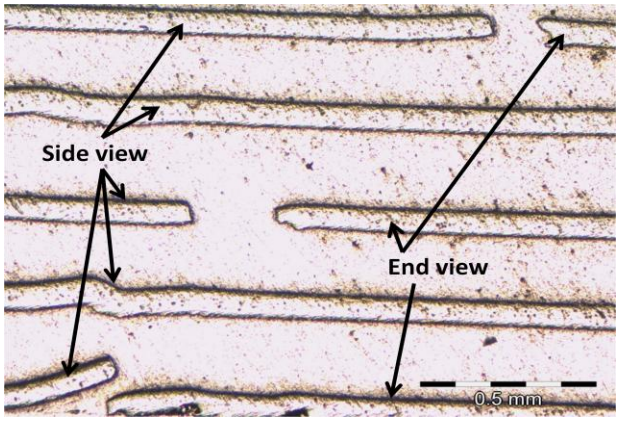

(b): A view of interlocking titanium foils in Al 3003 matrix at the intersection joints

Figure 5.5: Micrographs of the interlocking foils at the intersection joints of reinforced structures. The side viewed and end viewed foils belong to the left and right tension members of Fig. 5.3g respectively.

5.3.1 Failure Strengths

For the purpose of analysis, alphabetical letters are assigned to groups of experimental units based on the material used as follows: A = Met-STR and Met-STF; B = Ti-STR and Ti-STF; C = Al-STR and Al-STF; D = W-Al-MSTR and W-Al-MSTF; and E = W-Al-TSTR and W-Al-TSTF. Thus, material as a factor comprise five levels while the structure design criteria as a factor comprise two levels 1 and 2 corresponding to structures designed based upon maximum strength and maximum stiffness, respectively.

Tables 5.6 and 5.7 show the failure loads for each of the fabricated structures. It can be observed that the structures designed using maximum strength criterion failed at higher loads when compared to those fabricated using maximum stiffness criterion. The failure load data can, however, not be used for direct comparison since the structures were not exactly of the same thickness. The more useful data based on calculated strain energy densities at the point of failure are presented graphically in Fig. 5.6 to Fig. 5.8. They were calculated by dividing the area under the load-displacement curve by the volume of respective specimens. The area was obtained by numerical integration using the load and displacement data generated during testing. The load-displacement curve pattern for representative specimen types is illustrated in Fig. 5.9.

Although MetPreg®/Al 3003 structures generally failed at much higher loads when compared to Ti/Al 3003 structures, the later structures yielded higher average strain energy densities than the former. This is because, MetPreg® reinforced structures generally failed before undergoing significant plastic deformation in contrast to Ti reinforced structures that undergo much higher deformation before failure as shown in Fig. 5.9. This make the absorbed energy (area under the load-displacement curve) higher

for titanium reinforced structures than MetPreg® reinforced structures. Failures in MetPreg® reinforced structures occurred at the edge-to-edge foil joints, both for the matrix material and the reinforcing materials at the tension members as will be further discussed under failure modes in sub-section 5.3.4. Because titanium is a much more ductile reinforcing material, none of the Ti/Al 3003 structures failed at the edge-to-edge foil joints of the tension members, rather, failure occurred at the flanges.

Unreinforced UC fabricated Al 3003 structures (C material structures) failed at the foil-edge-to-edge foil joints on the tension members before undergoing plastic deformation in a similar fashion as the MetPreg/Al 3003 structures. The strain energy densities for the unreinforced ultrasonically consolidated structures are much lower than those for the reinforced structures. Unconsolidated Al 3003 structures (D and E material structures) machined out of wrought plates exhibited higher strain densities than ultrasonically consolidated C structures as shown in Figs. 5.6 and 5.7.

The distribution of the mean stiffness of the tested structures is shown in Fig. 10. Stiffness values were obtained by calculating the slope within the linear regime of the load-displacement curve for each specimen. It can be seen from the Figure that stiffness is more material dependent than design criteria. The structures that exhibited less plastic deformation before failure yielded the highest stiffness values. Ultrasonically consolidated Al 3003 (C material) structures with the least plastic deformation before failure yielded the highest stiffness followed by MetPreg reinforced (A material) structures. Titanium reinforced ultrasonically consolidated structures (B material) and those fabricated from wrought materials (D and E) yielded about the same stiffness values. These structures deformed plastically more than others as seen in Fig. 9.

Table 5.6: Failure Load (N) Data for MetPreg®/Al 3003 Based Structures

Sample	1	2	3
Met-STR	5190	4760	4140
Met-STF	4060	5020	4720
Al-STR	3120	3060	2530
Al-STF	4010	3840	3760
W-Al-MSTR	3020	2880	2780
W-Al-MSTR	3060	3150	3270

Table 5.7: Failure Load (N) Data for Ti/Al 3003 Based Structures

Sample	1	2	3
Ti-STR	3890	3760	4120
Ti-STF	3210	3360	3500
W-Al-TSTR	3200	3000	2730
W-Al-TSTR	2340	2230	2320

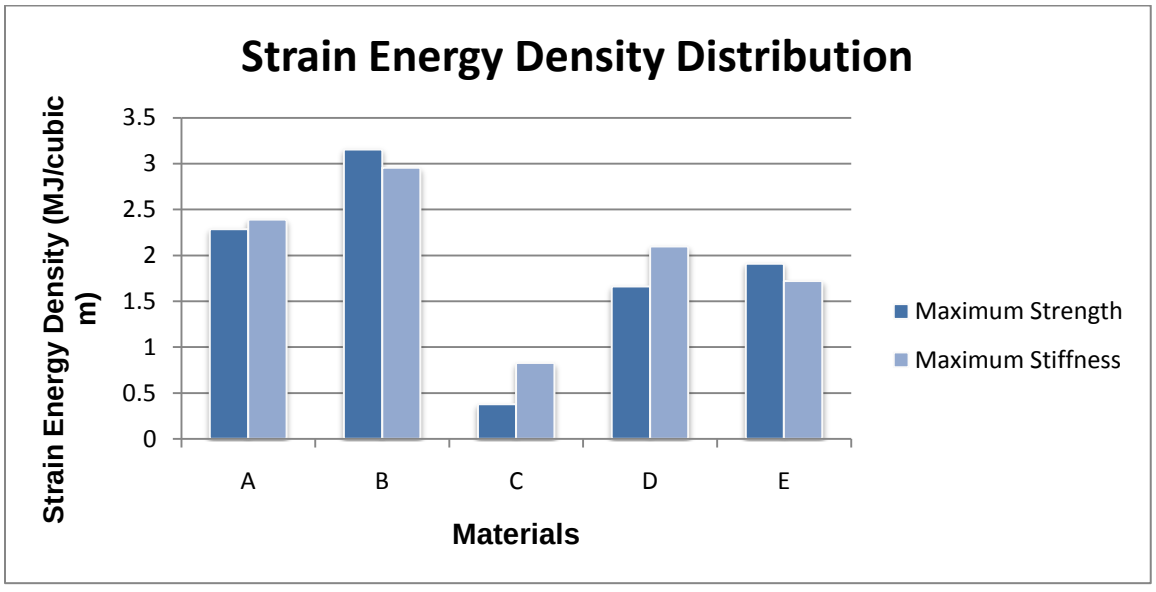

Figure 5.6: Strain energy density distribution for structures based upon material type and design criteria.

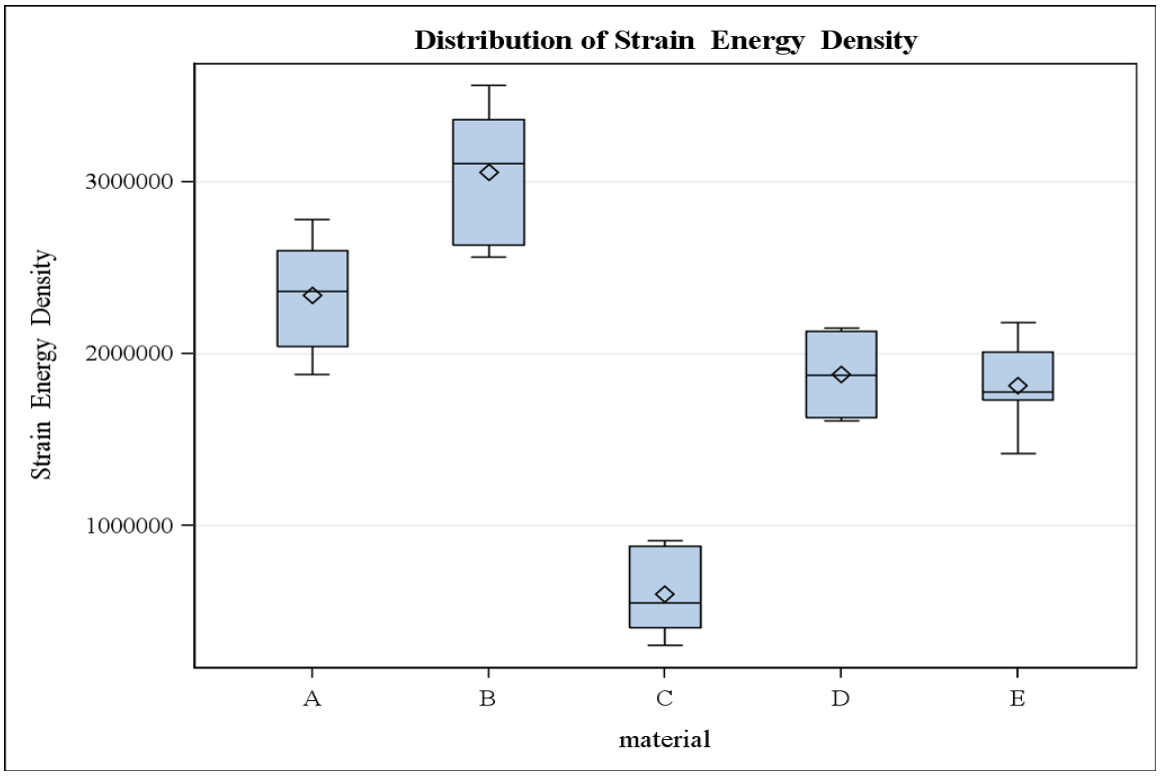

Figure 5.7: Strain energy density distribution based upon material type.

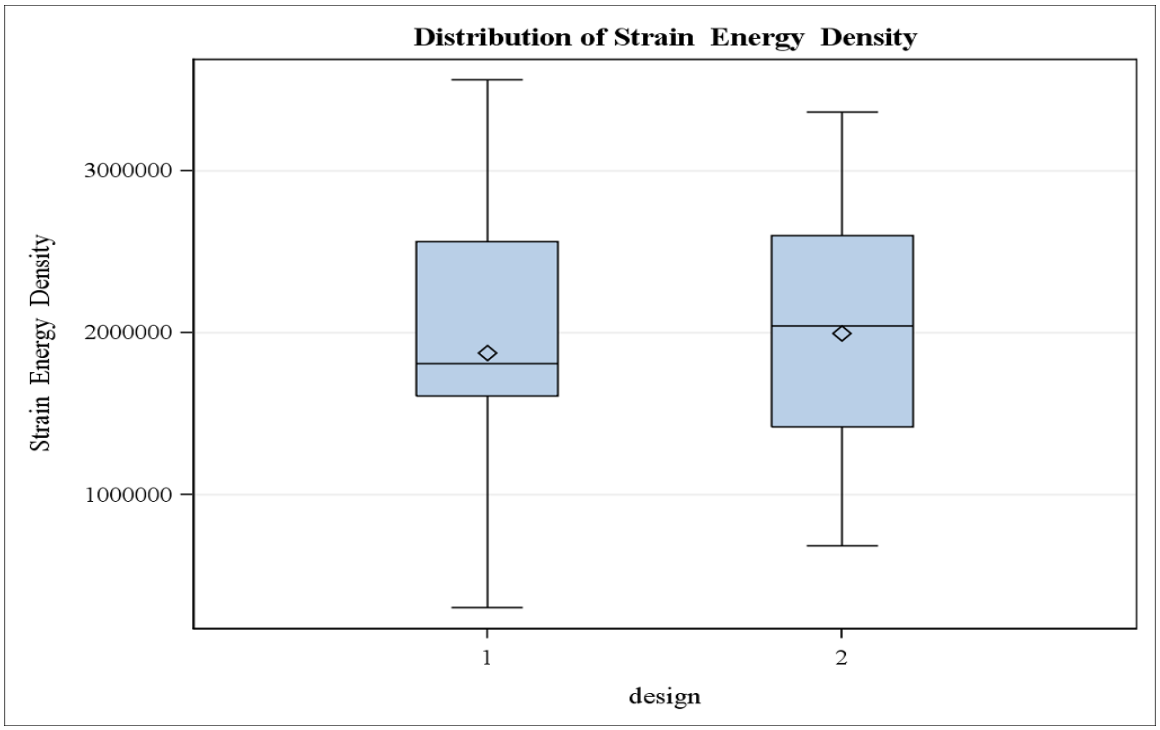

Figure 5.8: Strain energy density distribution based upon design criteria.

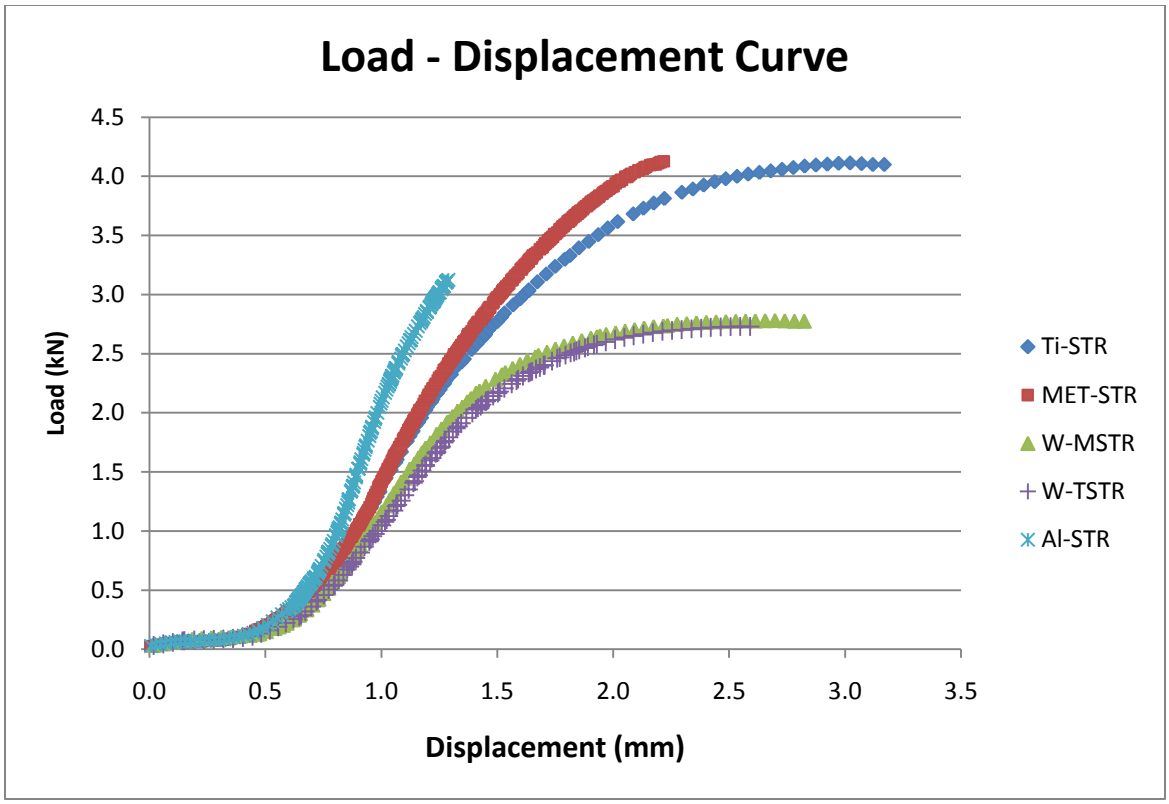

Figure 5.9: Load-displacement curve pattern for the different material types.

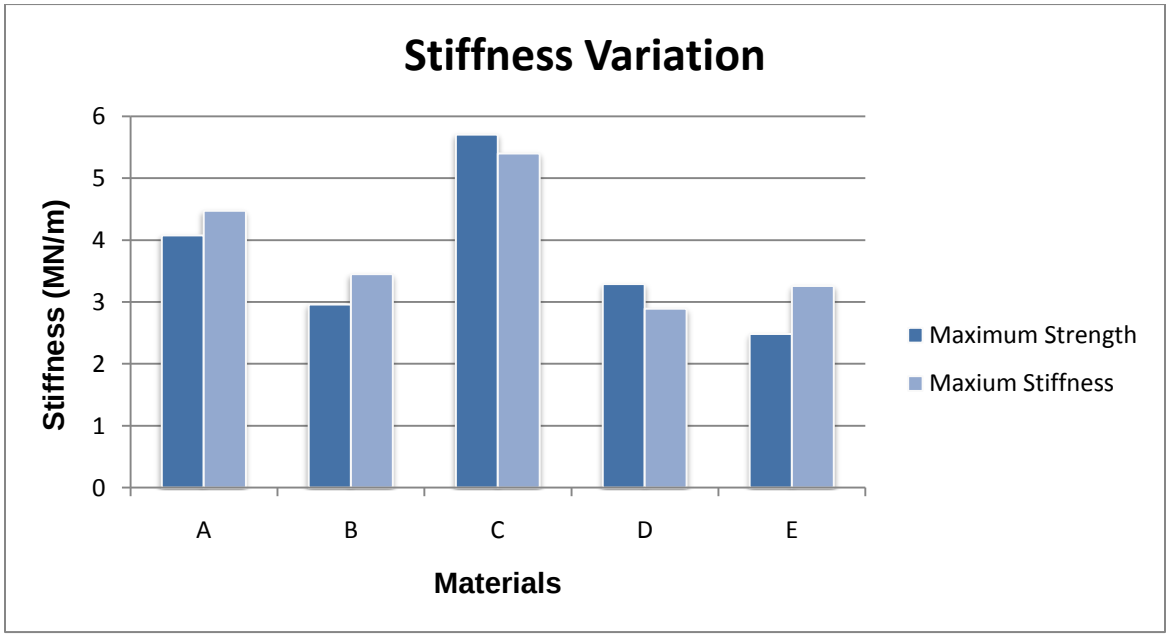

Figure 5.10: Stiffness distribution for structures based upon material type and design criteria.

5.3.3 Statistical Analysis of the Strain Energy Density

The results of the strain energy densities presented above were analyzed statistically using SAS 9.2 to verify whether or not their differences are significant. The experiment was a two way factorial design with three replicates. Material and design comprise the two fixed factors with five and two levels respectively as earlier defined in sub-section 5.3.2. The analyses combine the results of the MetPreg®/Al3003 and Ti/Al3003 based structures all in one.

The result of the analysis shows that the data satisfies the assumption of approximate normality and homoscedasticity. Analysis of variance (ANOVA) in Table 5.8 shows that the interactions between the two fixed factors with p-value of 0.1856 does not have statistically significant effects on the response variable. Among the individual factors, design, with a p-value of 0.2815 does not have statistically significant effects on the response variable. However, material, with p-value of <0.0001 has statistically significant effects. The R-square for the model is 0.9182. This shows that the variability due to error is small.

Since design does not have statistically significant effects on the strain energy densities, it means any of the design criteria (maximum strength or maximum stiffness) can be used to fabricate the dual-material minimum weight structures using UC for a given application. The averages of strain energy densities for structures fabricated using the two designs are compared in Fig. 5.8. Post hoc means analysis data (Table 5.9) for material (the only factor with statistically significant effects) shows that Ti reinforced structures have statistically significant higher average strain energy densities than MetPreg® reinforced structures. Copies of Ti and MetPreg® reinforced structures directly

machined out of wrought Al 3003 plates do not have any statistically significant different strain energy densities. UC fabricated unreinforced Al 3003 copies of MetPreg® structures (C structures) have statistically significant lower average strain energy density compared to all other structures.

From this analysis, it can be inferred that UC fabricated structures with appropriate reinforcement leads to significant improvement of their load bearing capabilities compared to fabrications with the matrix materials only. Although MetPreg® reinforced structures have 60% volume fraction of the reinforcing material compared to 25% for Ti reinforced structures, it means the use of ductile materials for reinforcements should be preferred to brittle materials in UC fabricated structures.

Table 5.8: Analysis of Variance of the Experimental Data

Source	DF	Type I SS	Mean Square	F Value	Pr > F
material	4	1.9238906E13	4.8097265E12	54.08	<.0001
design	1	108962133333	108962133333	1.23	0.2815
material*design	4	611121866667	152780466667	1.72	0.1856

Table 5.9: Post Hoc Means Analysis for the Material-Factor Levels

Means with the same letter are not significantly different.			
REGWQ Grouping	**Mean**	**N**	**material**
A	3053333	6	B
B	2336667	6	A
C	1878333	6	D
C			
C	1815000	6	E
D	602000	6	C

5.3.4 Failure Features

The failure features of the structures depend mostly on the design criterion used. Most of those designed based on maximum stiffness criterion failed at the flange as shown in Fig. 5.11 for any material combination. Their flange widths are generally smaller than those designed based on maximum strength criterion. It shows that higher stresses are concentrated at the neck of the flanges. Rather than fracture by tearing the materials, most of them deform and in some cases, the consolidated foils delaminate as shown Fig. 5.12. However, none of the maximum strength structures failed at the flange. MetPreg® reinforced maximum strength structures generally failed at the left hand side tension members. The failures occurred at the edge-to-edge foil joints of the Al 3003 matrix materials and/or at the edge-to-edge joints of the reinforcing MetPreg® materials. The right hand side tension members did not have any foil joint; as such no fracture occurred on them. The left tension members were perpendicular to the direction of consolidated foils, this make them to have intra-layer edge-to-edge joints of the matrix foil materials. The right hand tension members were however, cut along the direction of foil consolidation. The properties of the joints have been characterized in earlier work (chapter 4).

Figures 5.13 to 5.15 illustrate the modes of failure for the maximum strength MetPreg®/Al3003 reinforced structures. In Fig. 5.13, failure occurred at the foil edge-to-edge joints of the matrix material. The stress on the tension member for this structure at failure was 313MPa. A weaker matrix material foil joint must have exposed the reinforcing brittle MetPreg® foil to failure. Figure 5.14 shows a combination of failures at the matrix foil joints and the joints of the reinforcing materials. There were inter-lamina

foil delaminations between the fracture locations. The stress on the tension member at the point of fracture was 320MPa. In Fig. 5.15, failure occurred at the edge-to-edge joint of the reinforcing MetPreg® foils only. The tension member failed at 309MPa. It is worthy of note that most ultrasonically consolidated MetPreg®/Al3003 composite tensile specimens (with 60% volume fraction) preliminarily tested failed prematurely at stresses ranging from 300 to 450MPa. Some of the Al_2O_3 reinforcing fibers in the MetPreg® foils may have been damaged under the action of the applied ultrasonic energy through the sonotrode during welding, resulting in premature brittle failures.

Figure 5.11: Failure feature of a structure designed based upon maximum stiffness criterion.

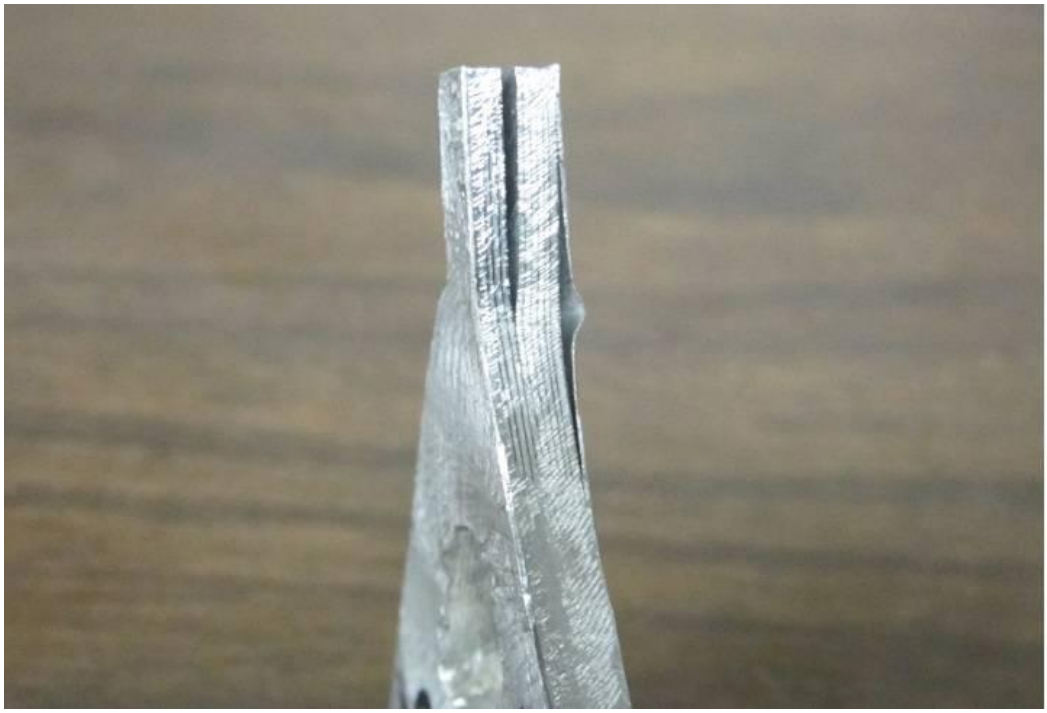

Figure 5.12: Delamination at the flange for some of the structures designed based on maximum stiffness criterion.

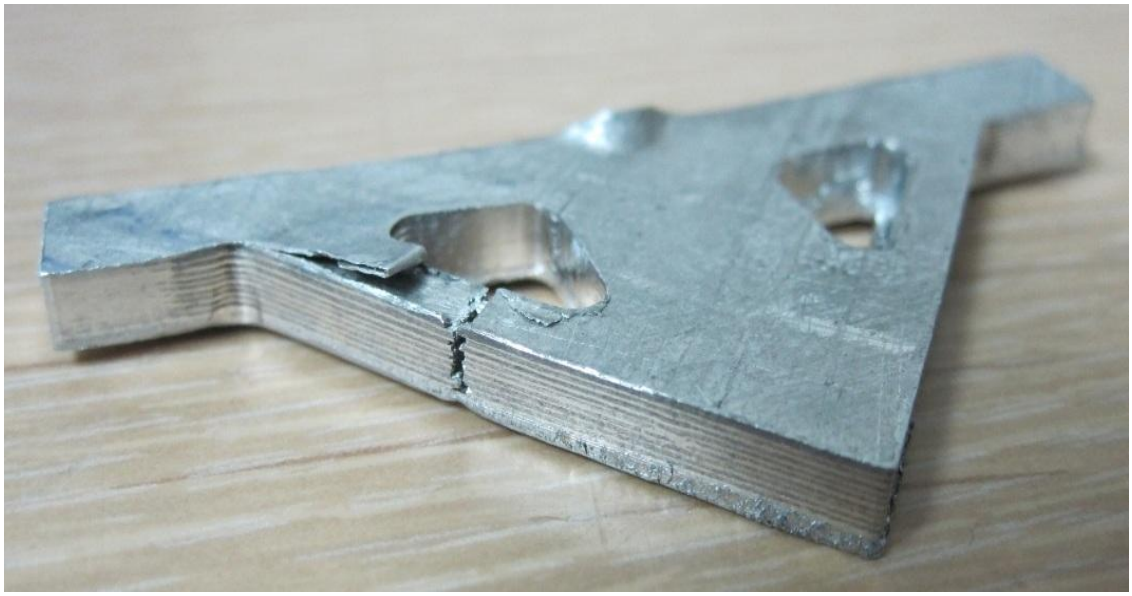

Figure 5.13: Fracture at the edge-to-edge foil joint of the matrix material on a MetPreg® reinforced tension member.

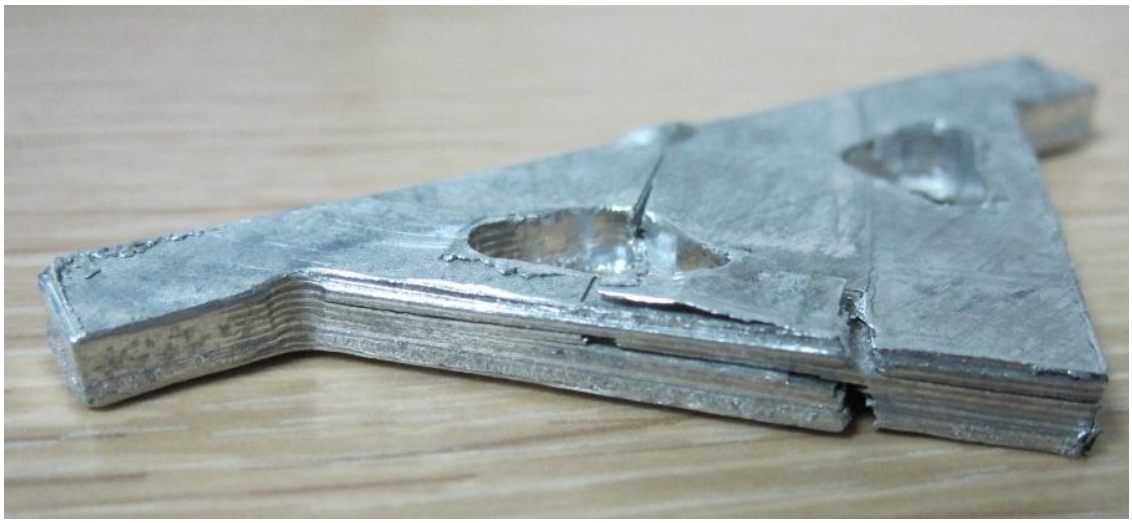

Figure 5.14: Fracture at both the edge-to-edge foil joint of the matrix material and the edge-to-edge joint of the reinforcing foils on a MetPreg® reinforced tension member.

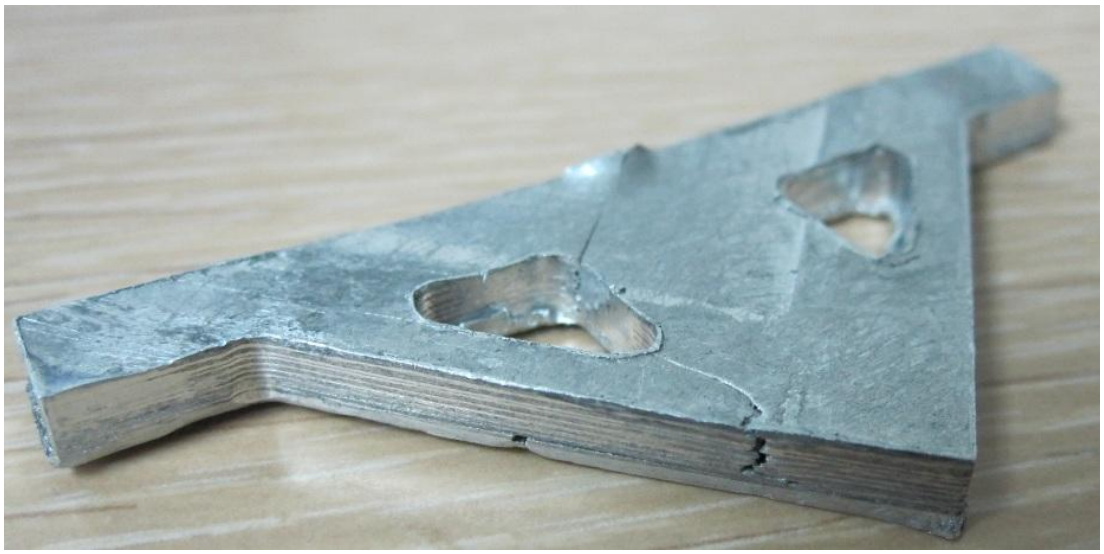

Figure 5.15: Fracture at the edge-to-edge joint of the reinforcing foils on a MetPreg® reinforced tension member.

Details of the failure stresses on the tension members for structures designed with MetPreg®/Al3003 using maximum strength criterion and their single material structure copies are shown in Fig. 5.16 (that is, those described with STR labels). The stresses were calculated using the load relations in Table 5.1. Al-STR structures ultrasonically

consolidated exclusively with Al3003 foils and default foil overlap setting of width 23.90mm fractured at the tension member at an average stress of 169MPa. This fracture stress is within the range of tensile strengths obtained for tensile specimens fabricated with the same machine parameters in earlier work (chapter 4). Also, the W-Al-MSTR structures fabricated exclusively with the wrought Al3003 material failed at the tension member at an average stress of 205MPa, which is within the range of the tensile strengths obtained for the parent material.

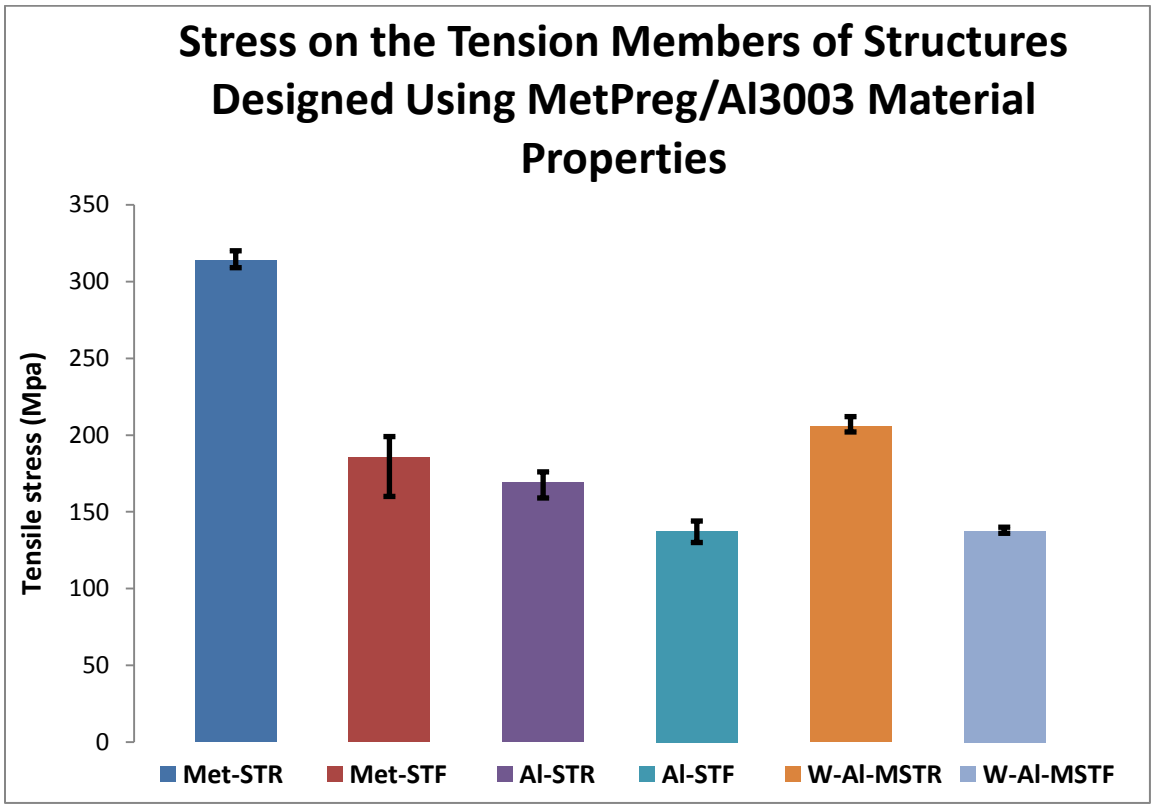

Figure 5.16: Calculated stresses on the tension members of structures designed using MetPreg®/Al 3003 material properties at the point of failure.

5.4 Conclusions

The use of the ultrasonic consolidation process for the fabrication of multi-material minimum weight structures has been demonstrated. A fabrication methodology for joining foils of different materials to make dual-material structures was developed. Test results show that there are significantly higher strain energy densities at the point of failure in structures with reinforced members compared to unreinforced Al 3003 matrix materials. As a result, their load carrying capacities were greatly improved. It was observed that the failure mode of the structures is generally dependent upon the design criteria and the materials used. Structures fabricated based upon maximum strength criterion using MetPreg®/Al3003 composite materials as the tension members exhibited brittle failures at edge-to-edge foil joints. Those designed based upon maximum stiffness criterion generally failed at the flange of the triangular structures irrespective of the material combination. Ductile materials are better for UC structures reinforcements than brittle materials. Structures fabricated with 25% Ti volume fractions yielded statistically significant higher strain energy densities than those fabricated with 60% volume fraction of MetPreg®. From the results of this work, it is believed that multi-material structures can be fabricated for real life applications using appropriate material combinations.

References

Arcaute, K., Mann, B., Wicker, R., 2009. Stereolithography of spatially controlled multi-material bioactive poly(ethylene glycol) scaffolds. Acta Biomaterialia 6, 1047-1054.

Cohen, D.L., Malone, E., Lipson, H., Bonassar, L.J., 2006. Direct freeform fabrication of seeded hydrogels in arbitrary geometries. Tiss. Eng. 12, 1325-1335.

Dewhurst, P., 2001. Analytical solutions and numerical procedures for minimum-weight Michell structures. J. Mech. Phys. Solid. 49, 445–467.

Dewhurst, P., 2005. A general optimality criterion for strength and stiffness of dual-material property structures, Int. J. Mech. Sci. 47, 293-302.

Domack, M.S., Baughman, J.M., 2005. Development of nickel-titanium graded composition components. Rapid Protot. J. 11, 41-51.

Foroozmehr, E., Sarrafi, R., Hamid, S., Kovacevic, R., 2009. Synthesizing of functionally graded surface composites by laser powder deposition process for slurry erosion applications. In: Proceedings of 20th Solid Freeform Fabrication Symposium, Austin, TX, USA, August 3-5.

Griffith, M.L., Harwell, L.D., Romero, J.T., Schlienger, E., Atwood, C.L., Smugeresky, J.E., 1997. Multi-material processing by LENS. In: Proceedings of the 8th Solid Freeform Fabrication Symposium, Austin, TX, USA. August 11-13.

Inamdar, A., Magan, M., Medina, F., Grajeda, Y., Wicker, R., 2006. Development of automated multiple material stereolithography machine. In: Proceedings of the 17th Solid Freeform Fabrication Symposium, Austin, TX, USA, August 14-16.

Jae-Won Choi, J., MacDonald, E., Wicker, R., 2009. Multiple material microstereolithography. In: Proceedings of the 20th Solid Freeform Fabrication Symposium, Austin, TX, USA, August 3-5.

Janaki Ram, G.D., Stucker, B.E., 2008. LENS® deposition of CoCrMo coatings on titanium implant structures. J. manuf. Sci. Eng. 130, 024503-1 - 024503-5.

Janaki Ram, G.D., Robinson, C., Yang, Y., Stucker, B.E., 2007. Use of ultrasonic consolidation for multi-material structures. Rapid Protot. J. 13, 226-235.

Kruger, S., Wagner, G., Eifler, D., 2004. Utrasonic welding of metal/composite joints. Adv. Eng. Mater. 6, 157-159.

Liu, W., DuPont, J.N., 2003. Fabrication of functionally graded TiC/Ti composites by laser engineered net shaping. Scr. Mater. 48, 1337-1342.

Malone, E., Rasa, K., Cohen, D., Isaacson, T., Lashley, H., Lipson H., 2004. Freeform fabrication of zinc-air batteries and electromechanical assemblies. Rapid Protot. J. 10, 58-69.

Michell, A.G.M., 1904. Limits of economy of material in frame-structures. Philosophical Magazine, 8, 589-597.

Obielodan, J.O., Stucker, B.E., 2009. Effects of post processing heat treatments on the bond quality and mechanical strength of Ti/Al3003 dual materials fabricated using ultrasonic consolidation. In: Proceedings of the 20th Solid Freeform Fabrication Symposium, Austin, TX, USA, August 3-5.

Selyugin, S.V., 2004. Some general results for optimal structures. Struct. Multi-Disc. Optimiz. 26, 357-366.

White D.R., 2003. Ultrasonic consolidation of aluminum tooling, Adv. Mater. Process. 161, 64-65.

Wicker, R., Medina, F., Elkins, C., 2004. Multiple material micro-fabrication: extending stereolithography to tissue engineering and other novel applications. In: Proceedings of the 15th Solid Freeform Fabrication Symposium, Austin, TX, USA, August 2-4.

CHAPTER 6

CHARACTERIZATION OF THE STRENGTHS OF DUAL-MATERIAL JOINTS FABRICATED USING LASER-ENGINEERED NET SHAPING

This chapter has been prepared for publication in the Journal of Engineering Materials and Technology

Abstract

Joints between dissimilar material systems made using laser metal deposition processes have been investigated. The fusion of materials with different physical properties and chemical compositions under high laser power often results in defects at the joints. Although some solutions have been suggested in previous work for defect-free fabrications, most of the joints studied have been characterized using qualitative techniques only. Quantitative study is imperative for predicting the mechanical behavior of fabricated structures for real life applications. In this work, tensile and flexural specimens made of different Ti6Al4V and Ti6Al4V/10%TiC dual-material transition joint designs were fabricated using laser-engineered net shaping (LENS) and tested. It was found that transition joint design has a significant effect on the mechanical strength of dual-material structures.

6.1 Introduction

The capabilities of additive manufacturing (AM) technologies to fabricate complex geometries have been widely demonstrated. AM has also been shown to enable the fabrication of heterogeneous materials and microstructural mixes in a single component. Some technologies like 3D printing [1-2], stereolithography [3-4], selective laser sintering [5], ultrasonic consolidation [6-8], direct laser metal deposition processes [8-11] and others have been used to demonstrate the multi-material capabilities of AM. The materials used range from polymers to metals and ceramics; and in some cases are process-specific. The chemical and physical compatibilities of the material systems are important factors that determine the qualities of the joint between multiple materials. The use of difficult-to-join material systems is a challenge; however several solutions have been shown to enable the successful fabrication of some multi-material systems. Two examples are the use of gradient transitions from one material to the other [12, 13] and the use of compatible intermediate materials [chapter 2].

Inter-material joint problems are common in fusion-based processes such as direct laser metal deposition processes. The processes include laser-engineered net shaping (LENS) and its variants, like direct light fabrication (DLF), epitaxial laser metal forming (E-LMF), laser direct forming (LDF), laser rapid forming (LRF) and others. Good selection of process parameters are required in order to achieve defect free component fabrication in all cases.

LENS possesses the capabilities to fabricate fully dense structures using powder materials. It fabricates solid objects in a layer-wise fashion from computer aided design (CAD) models that are first numerically sliced to predetermined thickness. Each layer is

fabricated by melting powder materials delivered to the focus of the laser beam on a substrate that is mounted on an x-y stage. The stage moves in a raster fashion according to the tool paths generated using the sliced CAD models. The fabrication takes place under a controlled, inert atmosphere in a glove box. The process is schematically illustrated in Fig. 6.1. Some of the important process parameters are laser power, powder flow rate, layer thickness, hatch width, deposition speed and oxygen level in the glove box. The capabilities of LENS for multi-material fabrication have been demonstrated. It is used for composite material fabrication [14-15], functionally gradient structures [11-13], multi-materials processing [10] surface cladding for corrosion resistance [11], and biomedical applications [16-17].

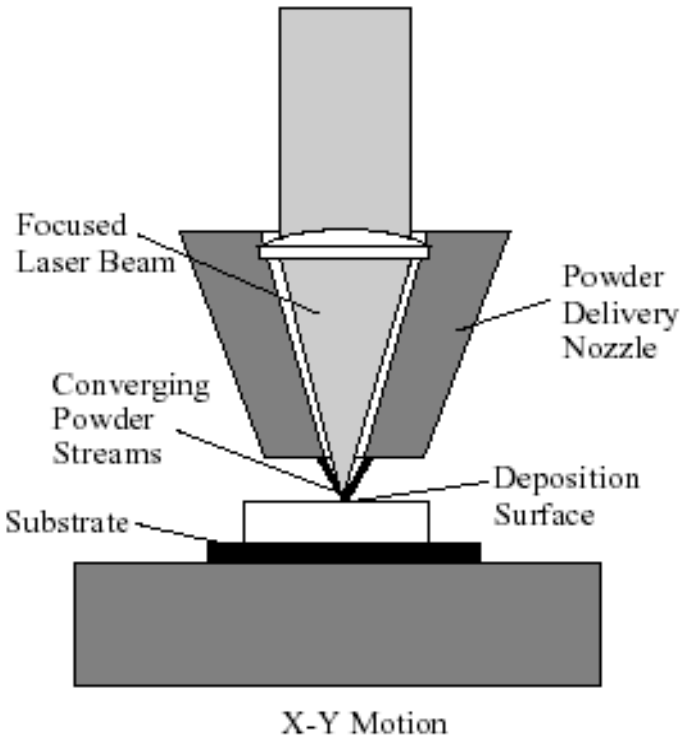

Figure 6.1: Schematic illustration of LENS deposition process.

Most of the earlier work on multi-material fabrication using direct laser metal deposition processes did not go beyond establishing successful fabrication of different material systems through qualitative characterizations using microstructure studies. However, its potential for fabricating multi-material structures for load carrying applications will not be fully achieved without establishing the mechanical properties of transition joints between the materials.

Dual-material minimum weight structure design [18-20] is one of the evolving application areas of AM fabricated multi-material structures. They are both geometrically and materially complex, and thus are difficult or impossible to fabricate using conventional processes. They have multiple, thin members that are preferably made from light weight materials with high specific strength and stiffness. Such structures are readily applicable to the aerospace and automotive industries, where there is continuous emphasis on higher strength and lower weight structures for improved fuel efficiency and performance. Figure 6.2 shows an example of a complex minimum weight structure with members that could be made of different materials based upon Michell theory [20]. In the illustrated structure, if the structure is pinned at points A and B and a load is placed at C, parallel to a line between A&B, as shown with the arrow, the outer member labeled D will be in pure compression, as well as all the inner members that join D tangentially. Those inner network members that are perpendicular to D, and the member between A and C will be in pure tension. In order to optimize a structure to its fullest extent, the members in tension can be made of materials different from those in compression. In this case, the strength of the intersections between the tension and compression members is of critical importance for the structure's reliability and performance.

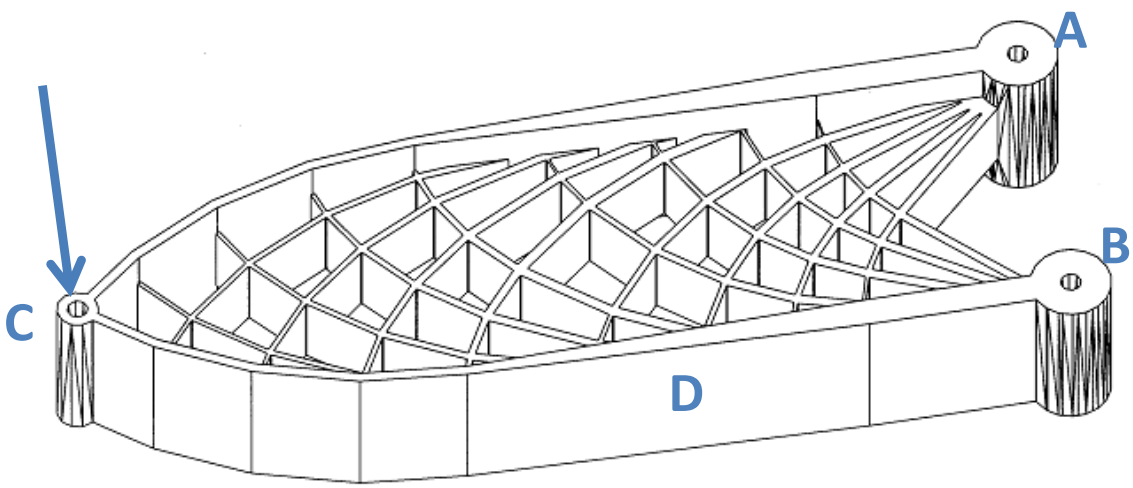

Figure 6.2: A minimum weight structure design [21].

Simplified minimum weight structures that are representative of the more complex design shown in Fig. 6.2 were designed based on maximum strength and maximum stiffness criteria [18] and fabricated. Figure 6.3 shows a free body diagram of a simplified structure design with *oa*, *ob* and *oc* as compression members and *ab* and *ac* as tension members when subjected to compressive load *F* with simple supports at *b* and *c*. Given such a design with

span = L,

applied force = F,

$$F = f\sqrt{2}\ ,$$

Where f is the stress acting on the tension members at any point during loading, Table 6.1 shows the load relationships existing in the structure members. Structures designed based on maximum stiffness criterion must satisfy the following strain ratio [18].

$$\frac{\varepsilon_T}{\varepsilon_C} = \left[\frac{\left(\rho_T / E_T\right)}{\left(\rho_C / E_C\right)}\right]^{\frac{1}{2}} = \left(\frac{E_C \rho_T}{E_T \rho_C}\right)^{\frac{1}{2}} \qquad \text{(i)}$$

Table 6.1: Load and Size Relationship for Minimum Weight Structure

Element	Length	Force	Cross-sectional area
oc	$L/2$	$F/2 = f/\sqrt{2}$	$F/(2\sigma_C)$
oa	$L/2$	$F = f\sqrt{2}$	$F/(\sigma_C)$
ac	$L/\sqrt{2}$	$F/\sqrt{2} = f$	$F/(\sqrt{2}\sigma_T)$

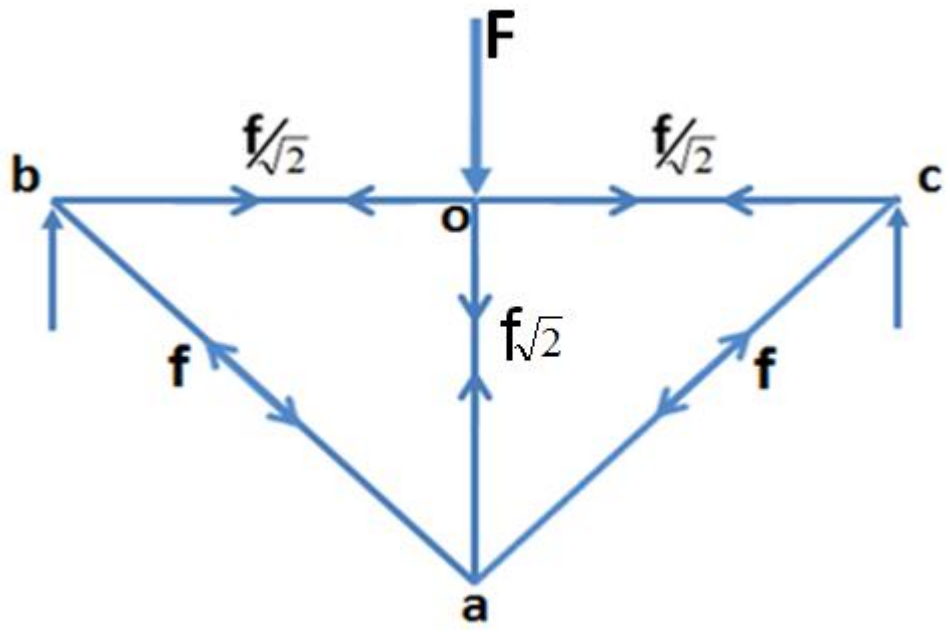

Figure 6.3: Free body diagram of the dual-material minimum weight structure.

This work is aimed at characterizing the failure characteristics and strengths of dual-material systems using different material transition designs at the joints between tensile and compressive members. Ti6Al4V/TiC composite and Ti6Al4V materials were used for the study. Different material transition joints were designed and tested for flexural and tensile strengths. Optimal designs were applied for the fabrication of dual-material minimum weight structures and tested.

6.2 Experimental Procedures

A laser-engineered net shaping (LENS 750) machine made by Optomec Inc., Albuquerque, USA, was used for this experiment. The machine uses a continuous wave ND:YAG laser with a capacity of up to 400 watts. The laser power used ranged from 200 to 270 watts depending upon the powder feed rate and traverse speed. The machine has a dual powder feeder system that allows the simultaneous delivery of two different material mixtures. The powder is delivered by argon carrier gas to the focus of the laser beam, and deposits were made on a 6mm thick commercially pure (CP) titanium substrate. The machine has a 3- axis motion system consisting of an x-y motion stage and a z-axis for integrated laser and powder delivery system. The oxygen level was maintained under 10 parts per million (ppm) in the glove box. Deposition layer were of 0.25mm thickness and 0.38mm hatch width for all fabrications. The deposition nozzle stand-off distance from the deposit was maintained at 10mm.

Spherical Ti6Al4V powder material of 125 – 210 microns diameter supplied by Advanced Specialty Metals (ASM), New Hampshire, USA and TiC powder of 45 – 150 micron particle size, supplied by Pacific Particulate Materials (PPM) Limited, Canada, were used. Although the recommended powder particle size for LENS fabrication is 45 –

150 microns diameter, the Ti6Al4V size used was found to flow well through the delivery system. Two sets of dual-material test specimens were fabricated for joint strength characterization. A set was fabricated for flexural strength determination and another set of corresponding joint designs for tensile properties determination.

In each test type, six different joint designs were fabricated with three replicates. The designs, as shown in Fig. 6.4 below are: butt joint; gradient transition joint; interlocked material joint, randomly interlocked material joint, scarf joint and v-groove joint. The joints are respectively labeled butt, gradient, interlock, random, scarf, and v-groove in this work. The specimens were fabricated with Ti6Al4V material at one end and Ti6Al4V/10wt%TiC at the other. The joint designs define the transition from one material to the other. The butt joint was designed for an abrupt transition from one material to the other. Interlock joints were fabricated with interlocking strips of materials of 1mm thickness. They were made by depositing four layers of materials for each strip. Random joints were designed with random lengths of interlocking strips of 0.5mm. They were made by depositing two layers of materials for each strip. The scarf joint was designed with a lap angle of 45^{o} while the included angle of the v-groove joint design is 90^{o}. The gradient transition joint was designed to vary TiC composition linearly from zero to 10wt%TiC in Ti6Al4V at a step interval of 0.25mm over a total length of 5mm.

Material-specific STL CAD files were developed for the fabrication of the dual-material test specimens. Two different material mixtures were automatically deposited side-by-side in each layer following the spatial relationship specified in the machine code, which was dependent on the joint design. The gradient transition joint specimens were fabricated parallel to the deposition z-axis direction, as more than three axes would

be required for its deposition in any other direction. Specimens with other joint designs were deposited perpendicular to the deposition nozzles. Single material specimens were fabricated to determine the as-deposited tensile properties of the two base material mixtures (Ti6Al4V and Ti6Al4V/10wt%TiC). A combination of computer numerical control (CNC) milling and wire electrical discharge machining (EDM) were used to finish up the specimens to final size and to remove them from the substrate.

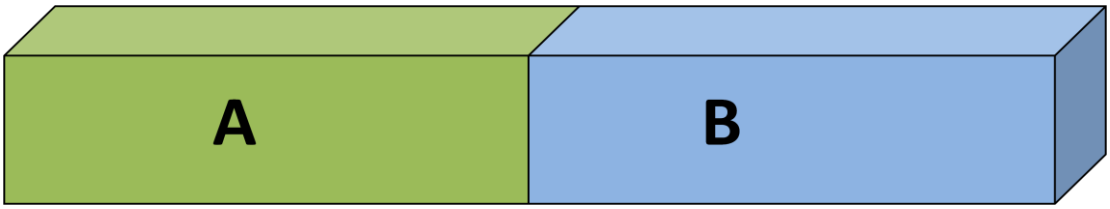

(a) Butt joint.

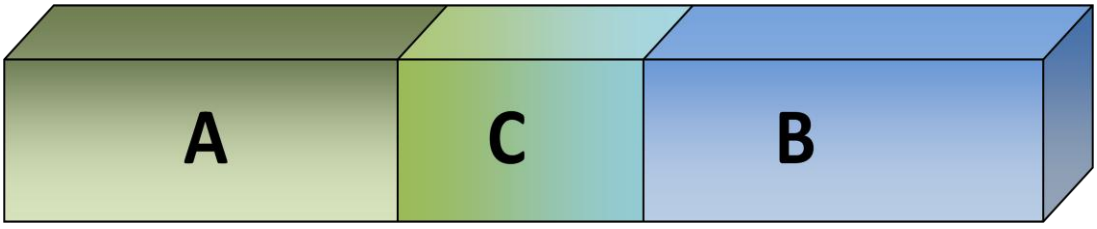

(b) Gradient joint.

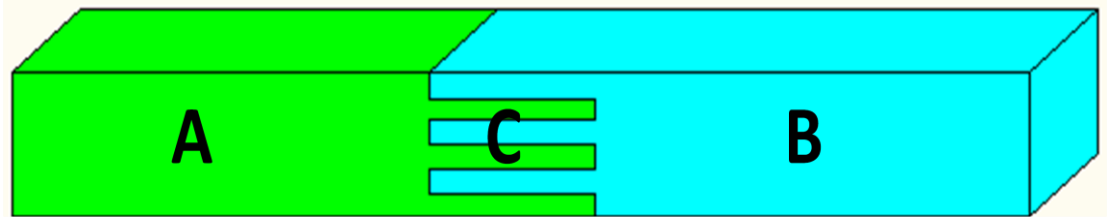

(c) Interlocking joint.

Figure 6.4: Multi-material interface designs for LENS deposition.

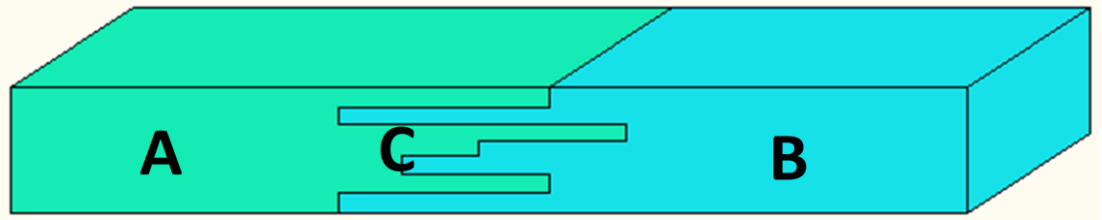

(d) Random interlock joint.

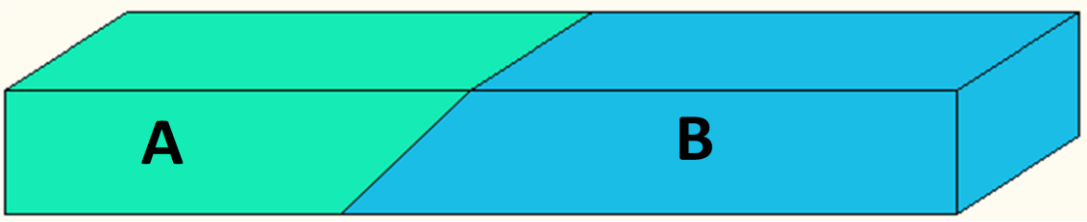

(e) Scarf joint.

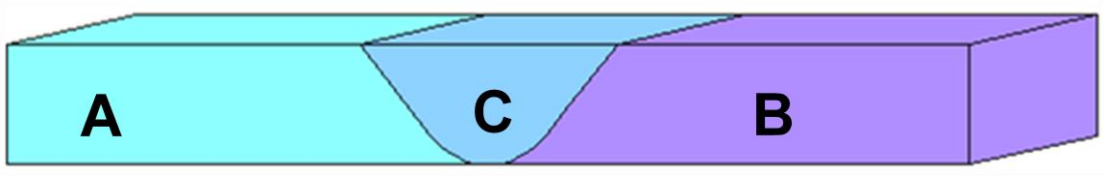

(f) V-groove joint.

All tensile specimens were made in accordance with ASTM E 8_E 8M. 3-point bend specimens were sized based on ASTM C1341-06. The flexural strengths were calculated using

$$\sigma_f = \frac{3FL}{2bd^2} \qquad \text{(ii)}$$

where σ_f = flexural strength

F = load at failure

L = specimen support span

b = specimen width, and

d = specimen thickness.

An ASTM D 2344 short beam 3-point test fixture was used for the flexural strength tests. A 50kN Tinius Olsen tensile testing machine was used for all tests at a crosshead speed of 0.5mm/minute.

Dual-material minimum weight structures designed based upon maximum strength and maximum stiffness criteria were fabricated using selected material transition joint designs. This selection was based on the results of the joint design characterizations just described. The structures were meant to test the performance of the joint designs in practical applications. They were fabricated using Ti6Al4V as the compression member material and Ti6Al4V/10wt%TiC as the tension member material. An initial attempt to fabricate the structures with Ti6Al4V/10wt%TiC composite as the tension member using the T- and V-shaped material models shown in Fig. 6.5 was unsuccessful as cracks developed during deposition, mostly after the eighth layer. The cracks initiated and propagated at the Ti6Al4V/10wt%TiC composite side at the joints. Butt and scarf joints shown in Fig. 6.5 were used during those trials. The cracks developed irrespective of the joint design used. However, structures fabricated with 5wt%TiC composition in the tension material members using the same material models did not crack.

The problem with cracks necessitated a change in the design of the material models to allow for a combination of butt and interlock joints at all the material intersections as shown in Fig. 6.6. Figure 6.6a is a fork shaped Ti6Al4V material model with arms extending through the triangular shaped structure. The two lower arms in Fig. 6.6 are of 0.5mm thickness, while the topmost arm is of 1mm thickness. The arms were

intended to separate Ti6Al4V/10wt%TiC composite tension members (with material model shown in Fig. 6.6b) into three discrete partitions with Ti6Al4V as 0.5mm thick inter-layers. However, during the fabrication, rather than deposit two layers of Ti6Al4V materials consecutively at the inter-layer, they were alternated with Ti6Al4V/10wt%TiC composite layers. This deposition method significantly reduced the occurrence of cracks in the deposits. Fabricated minimum weight structures were tested with an ASTM D 2344 short beam test fixture as illustrated in Fig. 6.7. The load at failure was obtained for analysis. Also, the mode of failure, especially the fracture location, was studied.

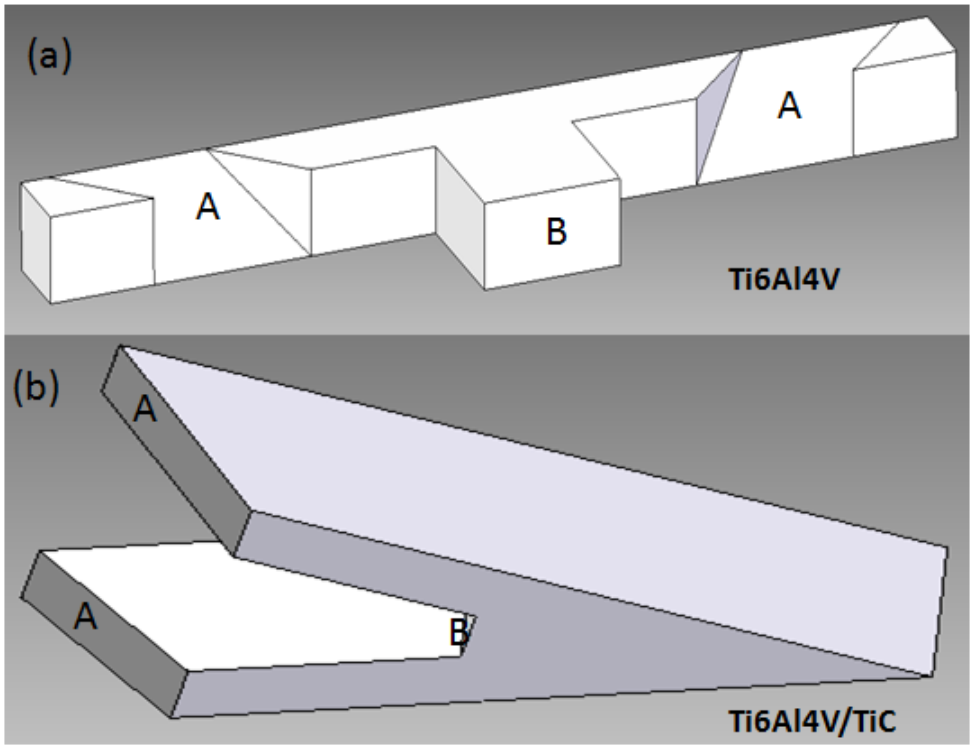

Figure 6.5: T- and V-shaped CAD material models.

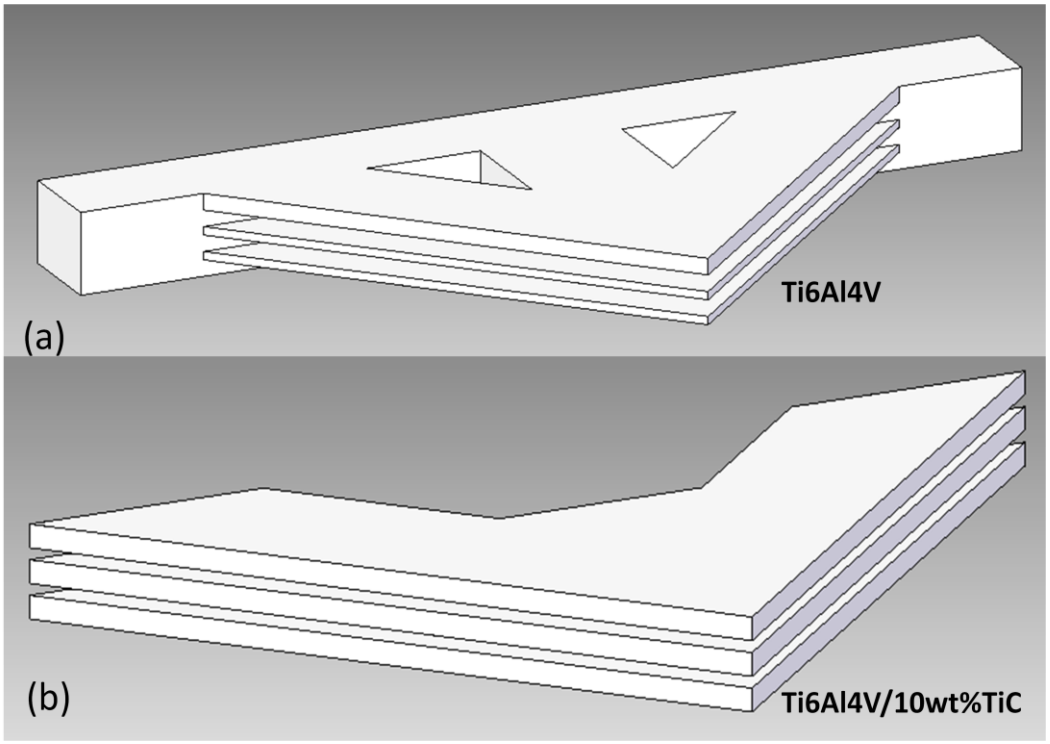

Figure 6.6: Material specific CAD models.

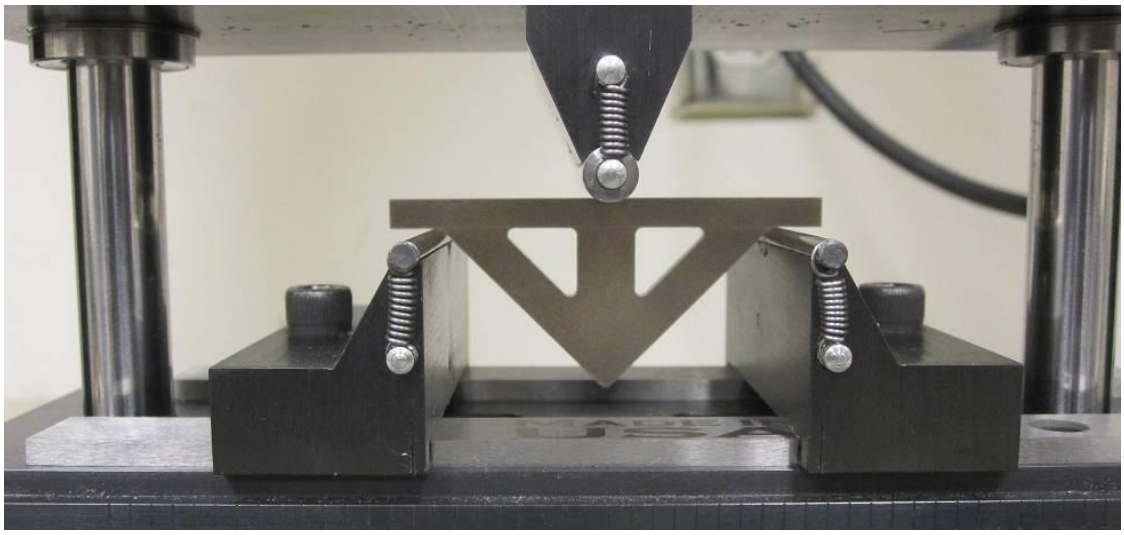

Figure 6.7: Structure under test using a 3-point bend test fixture.

6.3 Results and Discussion

6.3.1 Microstructures

Some of the micrographs of deposited specimens are shown in Fig. 6.8 below. Figures 6.8a and 6.8b shows butt joint interface with some level of interlock. The interlock is due to the fact that the two material models used for the dual material specimens share the same contour boundary line, and in every layer, each of the materials is deposited at the common boundary resulting in small amount of interlock. Figure 6.8c shows a sandwiched strip of Ti6Al4V/10wt%TiC composite in an interlock material joint.

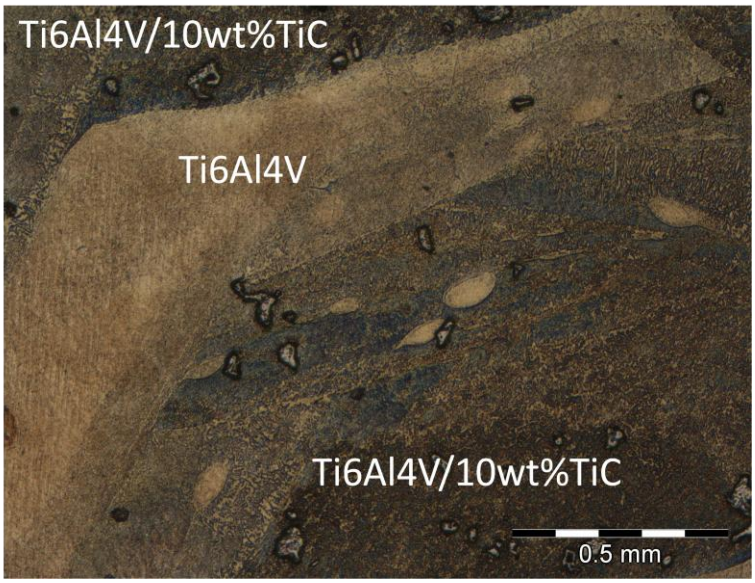

(a): Butt joint showing small interlock at the boundary contour deposit.

Figure 6.8: Micrographs of some of the dual-material test specimens.

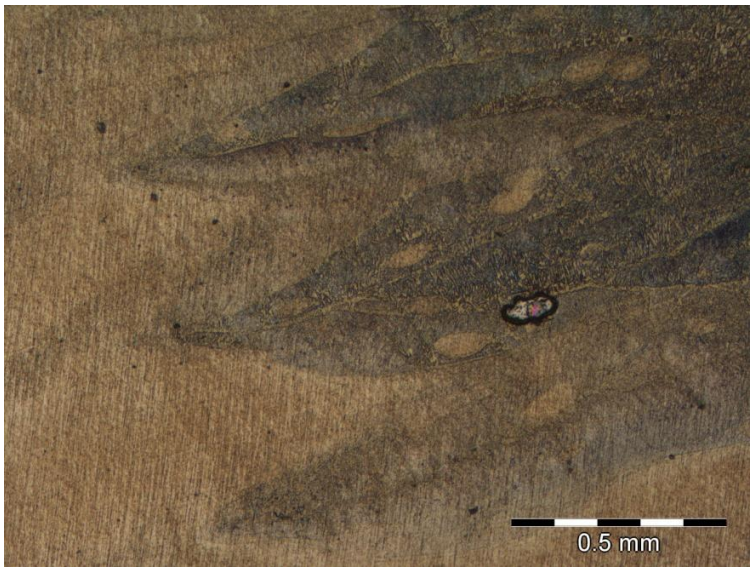

(b): Butt joint showing material mixing at the interface.

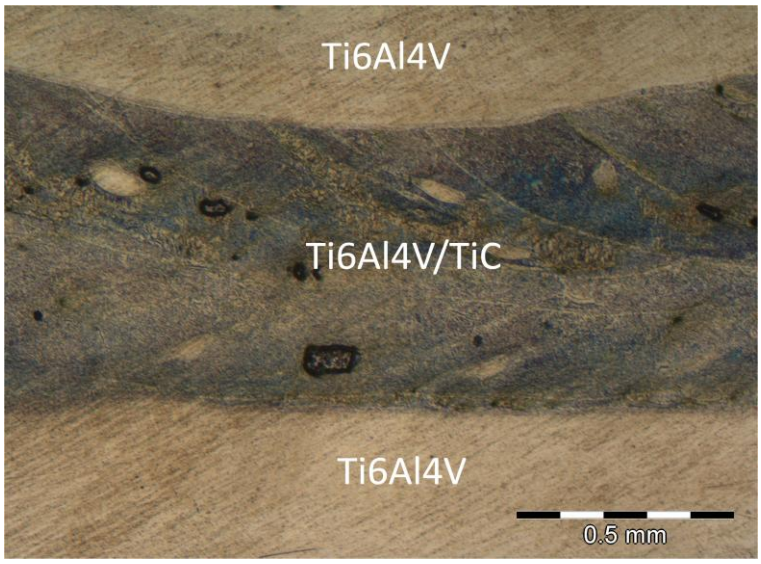

(c): Interlocked joint showing a sandwiched Ti6Al4V/10wt%TiC strip.

6.3.2 Flexural and Tensile Strengths

The flexural strength data obtained are shown in Table 6.2 and graphically in Fig. 6.9. The flexural strengths of the base materials (Ti6Al4V and Ti6Al4V/10wt%TiC) are included. It can be seen from the data that under the bending load condition, the scarf

joint design yielded the highest average flexural strength. It also has one of the lowest strength variations. The butt joint design yielded the lowest average strength. The result of a statistical analysis of the data using SAS 9.2 show that joint design (with a p-value of 0.2268) does not have statistically significant effect on the flexural strength of the LENS fabricated specimens. It means for an application requiring lateral loading, any of the material transition joint designs can be used. The ease of fabrication will therefore be a major consideration for such applications.

The tensile strengths data for corresponding joints designs are shown in Table 6.3 and Fig. 6.10. The results of the analysis of the data show that joint design as a factor, statistically significant effect on the tensile strengths of LENS fabricated dual-material structures with a low p-value of 0.0002 as shown in the analysis of variance (ANOVA) Table 6.4. Single material specimens with Ti6Al4V and Ti6Al4V/10wt%TiC expectedly have the highest average tensile strength values. According to the Ryan-Einot-Gabriel-Welsch (REGWQ) post hoc means analysis table shown in Table 6.5, both interlock and butt joint designs have statistically significant higher average tensile strengths than random and v-groove designs. Although the former pair yielded higher average tensile strengths than gradient and scarf joints, the differences are not statistically significant. It means any of those four designs can be used in place of another in LENS fabricated dual-material structures. One of the major defects that might have resulted in low tensile strengths recorded for the v-groove joint design is shown in Fig. 6.11. In this design, the two principal materials are first deposited completely before the transition joint material is deposited in the groove. With the as-deposited rough surfaces of the principal materials, sometimes the laser does not have all the surfaces exposed for re-melting and

deposition with the filler transition material. Voids are therefore created in the process. The voids act as stress raisers that cause weakening of the joints and early failure.

Table 6.2: Flexural Strength (MPa) Data

Material/Joint Design	Samples 1	2	3	Average
Butt	1790.04	1686.56	1264.48	1580.36
Gradient	1996.37	1875.49	2003.27	1958.38
Interlock	1864.19	2389.45	1837.56	2030.40
Random	1885.64	1610.98	1865.32	1787.31
Scarf	2093.81	2091.60	2251.95	2145.79
Ti64	2163.86	1895.14	1896.96	1985.32
Ti64/10wt%TiC	1578.96	2033.35	1388.11	1666.81
V-Groove	1449.64	2026.20	2422.69	1966.18

Table 6.3: Tensile Strength (MPa) Data

Material/Joint Design	Samples 1	2	3	Average
Butt	1138	1124	1096	1119.33
Gradient	1055	1080	1035	1056.67
Interlock	1186	1163	1090	1146.33
Random	855	935	834	874.66
Scarf	1089	1021	1034	1048.00
Ti64	1119	1196	1192	1169.00
Ti64/10wt%TiC	1225	1240	1124	1196.33
V-Groove	770	978	1069	939.00

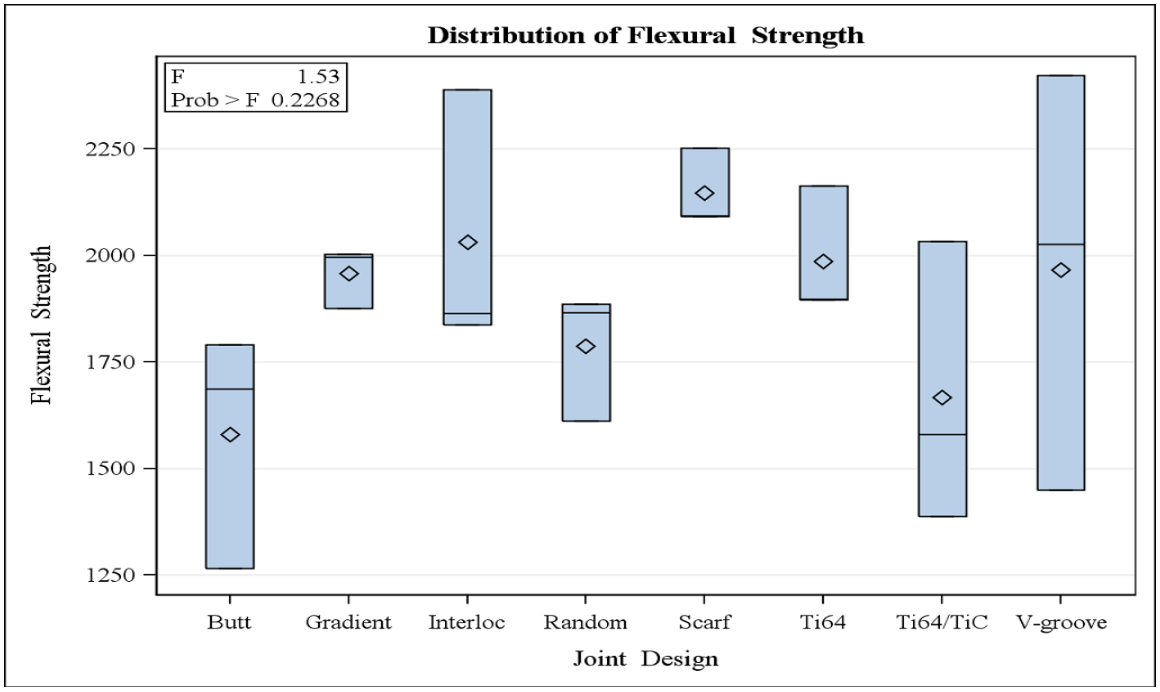

Figure 6.9: Comparison of flexural strengths (MPa) of LENS fabricated dual-material joint designs.

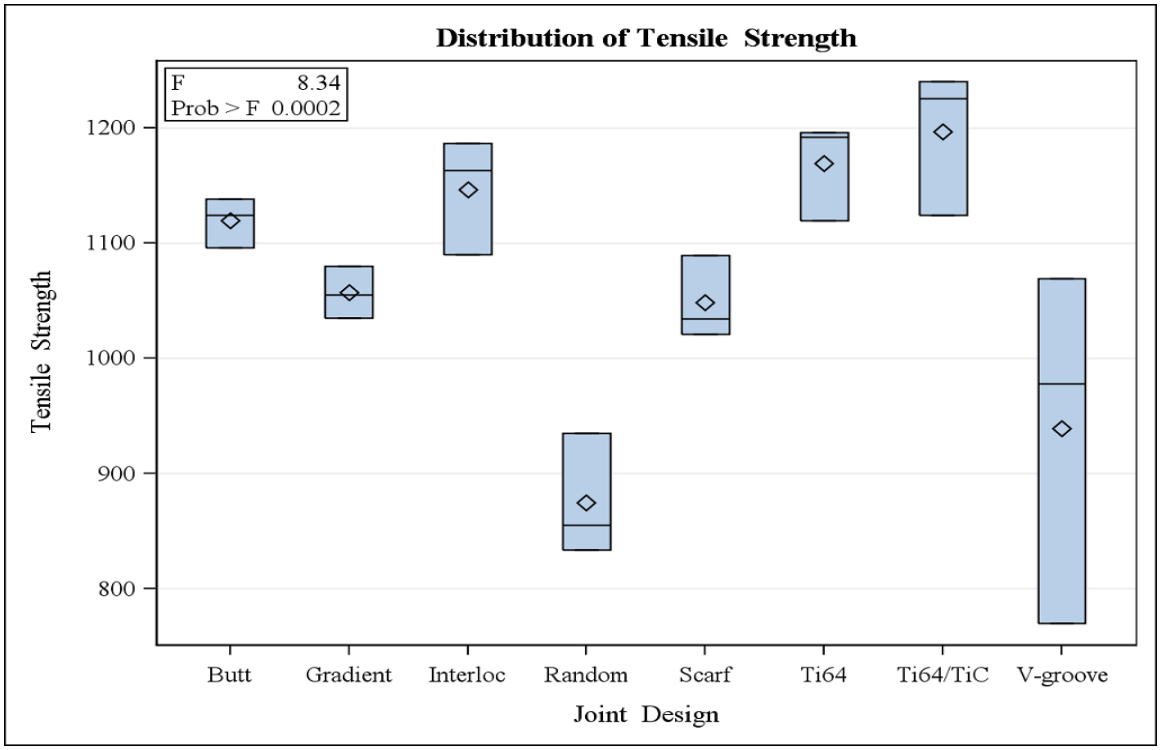

Figure 6.10: Comparison of tensile strengths of LENS fabricated dual-material joint designs.

Table 6.4: Analysis of Variance.

Source	DF	Type III SS	Mean Square	F Value	Pr > F
Joint Design	7	269956.0000	38565.1429	8.34	0.0002

Table 6.5: REGWQ Multiple Range Test for Tensile Test Data.

Means with the same letter are not significantly different.				
REGWQ Grouping		**Mean**	**N**	**Joint Design**
	A	1196.33	3	Ti64/TiC
	A			
	A	1169.00	3	Ti64
	A			
	A	1146.33	3	Interlock
	A			
	A	1119.33	3	Butt
	A			
B	A	1056.67	3	Gradient
B	A			
B	A	1048.00	3	Scarf
B				
B	C	939.00	3	V-groove
	C			
	C	874.67	3	Random

.

6.3.3 Dual-Material Minimum Weight Structures Test Results

A sample of the fabricated minimum weight structures is shown in Fig. 6.12. The joint locations are marked with letters A and B. Data obtained from the loading tests are shown in Tables 6.7 to 6.9. For ease of representation, the structures are labeled as follows: maximum strength criterion structures with 5wt%TiC in the tension members are denoted STR5; maximum stiffness criterion structures of the same composition are

STF5; and the corresponding structures with 10wt%TiC are STR10 and STF10. Table 6.5 shows the member (*oa*, *oc* and *ac* illustrated in Fig. 6.3) sizes for each of the fabricated structures.

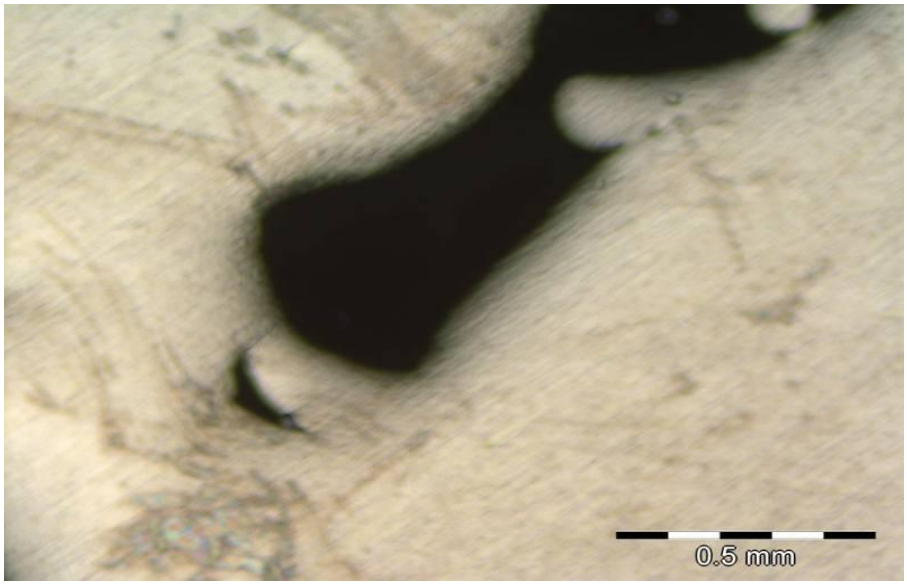

Figure 6.11: Defect on a V-groove joint design.

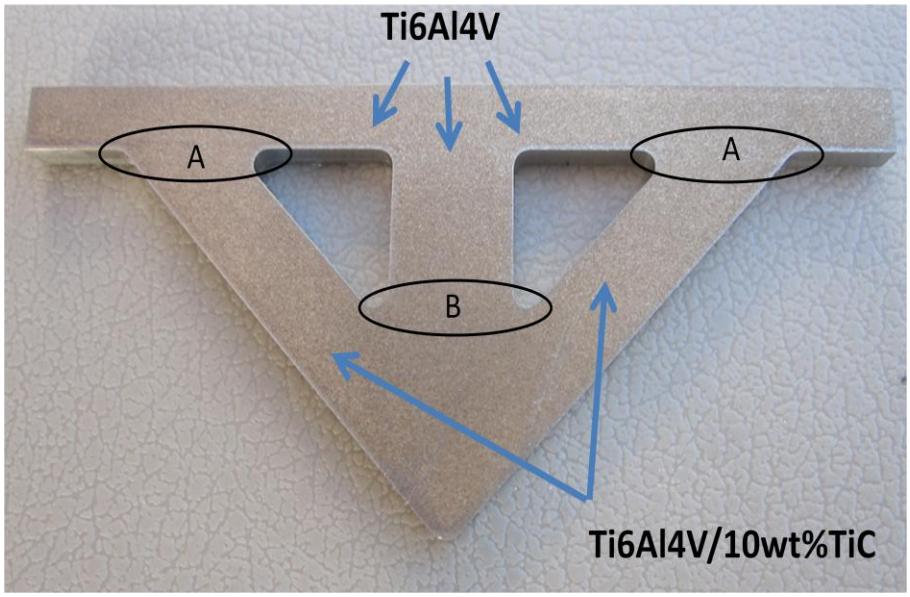

Figure 6.12: LENS fabricated dual-material minimum weight structure.

Table 6.6: Member Sizes for Fabricated Minimum Weight Structures

Structure	Sample	Member width (mm)			Thickness
		oa	***oc***	***ac***	
STR5	1	8.00	4.00	6.00	3.20
	2	8.00	4.00	6.00	3.20
	3	8.00	4.00	6.00	3.20
STF5	1	7.14	3.57	6.40	4.00
	2	7.14	3.57	6.40	3.60
	3	7.14	3.57	6.40	4.00
STR10	1	8.00	4.00	5.50	2.90
	2	8.00	4.00	5.50	3.00
	3	8.00	4.00	5.50	2.84
STF10	1	7.00	3.50	4.77	3.25
	2	7.00	3.50	4.77	3.35
	3	7.00	3.50	4.77	3.39

Table 6.7: Failure Loads (kN)

Structure	Samples			Average
	1	**2**	**3**	
STR5	13.87	7.44	12.77	11.36
STF5	21.3	13.06	18.14	17.50
STR10	14.2	11.81	13.25	13.08
STF10	12.1	13.76	14.96	13.61

Table 6.8: Stresses (MPa) Acting on the Tension Members at the Time of Failure

Structure	Samples			Average
	1	**2**	**3**	
STR5	511	274	470	418.33
STF5	588	401	501	496.67
STR10	630	506	600	578.67
STF10	552	609	654	605.00

Table 6.9: Strain Energy Densities (MJ/m^3) Data for LENS Fabricated Minimum Weight Structures

Structure	Samples			Average
	1	2	3	
STR5	6.28	6.71	5.91	6.30
STF5	13.4	4.51	4.71	7.54
STR10	10.3	4.72	7.64	7.56
STF10	6.86	9.30	9.51	8.56

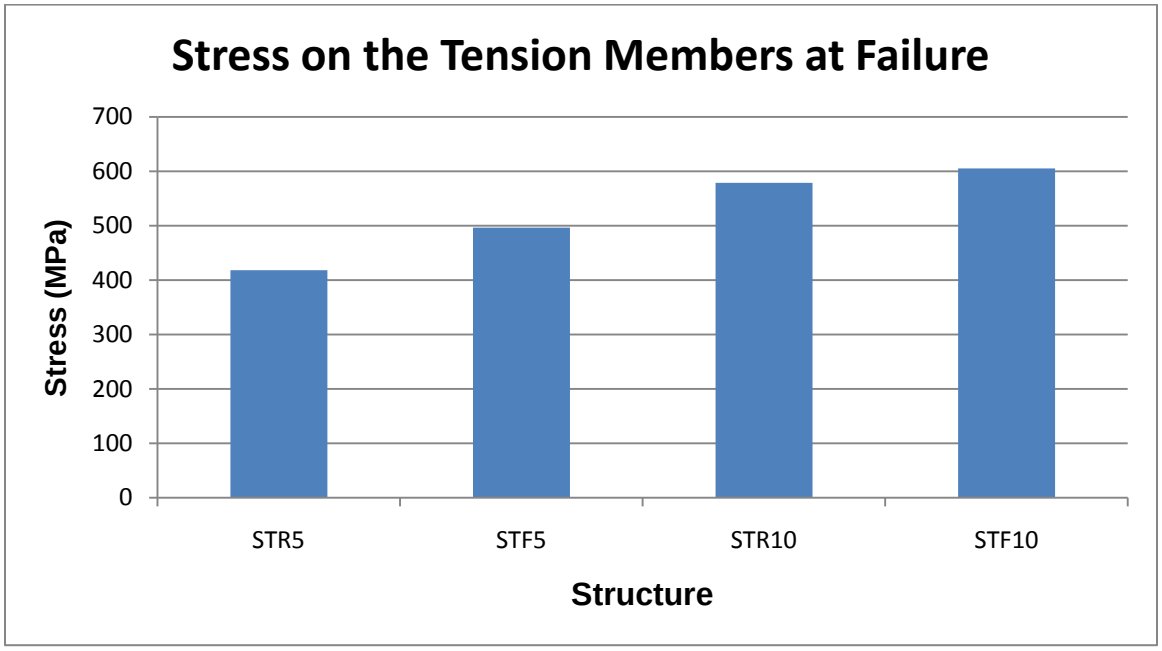

Figure 6.13: Stresses on the tension members at failure.

The load *F* (as illustrated in Fig. 6.3) applied at the time of failure for each structure is shown in Table 6.7. Table 6.8 shows the stress on the tension members at failure, while Table 6.9 shows the calculated strain energy density for each structure. The strain energy densities were calculated by dividing the area under the load-displacement curve by the volume of the respective structures. The areas were obtained by numerical

integration using the data generated during testing. The load applied at failure for both 5wt%TiC and 10wt%TiC material structures, seen graphically in Fig. 6.13, are close in value, although they are not directly comparable. The stresses on the tension members (*ac* or *ab* in Fig. 6.3) for each structure are shown in Table 6.8 and Fig. 6.13. The stress in each member at the point of failure was calculated by normalizing the resolved load (based on Table 6.1 relationships) with respect to cross-sectional area.

STR10 and STF10 structures failed at slightly higher stresses in the tension members than corresponding STR5 and STF5 structures. The stress values are about 50% of the tensile strength of the respective materials. The tensile strengths as experimentally determined are shown in Table 6.10. It is noteworthy that no failure occurred at the joints in any of the structures. As shown in Fig. 6.14, the strain energy densities for the structures based upon the applied design criteria have close values. The maximum stiffness structures have slightly higher average strain energy densities than maximum strength structures. This could be in part because of the fact that the structures failed at relatively low stresses. To achieve failure at higher stresses for this LENS fabricated structures and more accurate assessment of their performance based on the two design criteria, the differences between compression and tension member sizes for each material system must be more than shown in Table 6.8. This can be achieved with higher stiffness ratio between the compression and tension members. Table 6.10 shows the mechanical properties of the materials used.

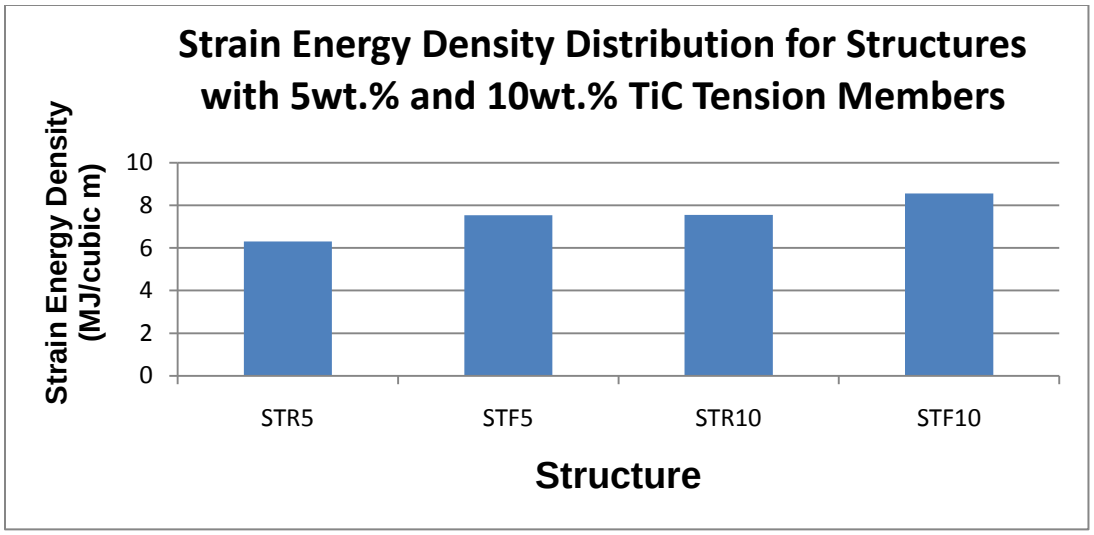

Figure 6.14: Strain energy densities at failure.

Table 6.10: Average Tensile Properties of Materials Used

Material	Yield strength (MPa)	Tensile strength (MPa)	Modulus (GPa)
Ti6Al4V	1072	1169	111
Ti6Al4V/5wt%TiC	985	1099	114
Ti6Al4V/10wt%TiC	1089	1196	154

(a): Failure at a tension member on an STR10 structure.

Figure 6.15: Fracture locations in LENS fabricated minimum weight structures.

(b): Failure at the flange obtained in most structures.

6.4 Conclusions

It has been shown experimentally in this work that transition joint design does not have significant effect on the flexural strengths of LENS fabricated dual-material structures made of compatible materials. In contrast, it has significant effect on their tensile strengths. V-grooved and randomly interlocked joint designs yielded poor tensile strengths when compared to interlocked, butt, gradient and scarf joints. Among the later four design types, the interlock design yielded the best average tensile strength. It also performed well under flexural loading. However, any of the four designs can be used for structural applications. Interlock transition joint designs helps in relieving the buildup of residual stresses and minimizing the formation and propagation of cracks in the transition joints in dual-material structures. None of the LENS fabricated minimum weight structures fail at the material transition joints under 3-point loading conditions. This work has shown that several different types of joint designs can work reliably for multi-material components.

References

[1] Cohen, D.L., Malone, E., Lipson, H. and Bonassar, L.J., 2006, "Direct Freeform Fabrication of Seeded Hydrogels in Arbitrary Geometries," Tissue Eng., **12**(5), pp. 1325-1335.

[2] Malone, E., Rasa, K., Cohen, D., Isaacson, T., Lashley, H., and Lipson H., 2004, "Freeform Fabrication of Zinc-air Batteries and Electromechanical Assemblies," Rapid Protot. J., **10**(1), pp. 58-69.

[3] Inamdar, A., Magana, M., Medina, F., Grageda, and Wicker R., 2006, "Development of Automated Multiple Material Stereolithography Machine," *Proceedings of 17th Solid Freeform Fabrication Symposium*, Austin, TX, USA, August 14-16.

[4] Jae-Won Choi, J., MacDonald, E., and Wicker, R., 2009, "Multiple Material Microstereolithography," *Procedings of the 20th Solid Freeform Fabrication Symposium*, Austin, TX, USA, August 3-5.

[5] Liew, C.L., Leong, K.F., Chua, C.K., and Du, Z., 2001, "Dual-Material Rapid Prototyping Techniques for the Development of Biomedical Devices. Part 1: Space Creation," The int. J. Adv. Manuf. Technol., **18**(10), pp. 717-723

[6] Janaki Ram, G.D., Robinson, C., Yang, Y., and Stucker, B.E., 2007, "Use of Ultrasonic Consolidation for Multi-Material Structures," Rapid Protot. J., **13**(4), pp. 226-235.

[7] Obielodan, J.O., and Stucker, B.E., 2009, "Effects of Post Processing Heat Treatments on the Bond Quality and Mechanical Strength of Ti/al3003 Dual-Materials Fabricated Using Ultrasonic Consolidation," *Proceedings of the 20th Solid Freeform fabrication Symposium*, Austin, TX, USA, August 3-5.

[8] Choi, J., and Chang, Y., 2005, "Characteristics of Laser Aided Direct Metal/Material Deposition Process for Tool Steel," Int. J. Mach. Tool Manuf., **45**, pp.597-607.

[9] Wang, F., Mei, J., Jiang, H., and Wu, X., 2007, "Laser Fabrication of Ti6Al4V/TiC Composites Using Simultaneous Powder and Wire Feed," Mater. Sci. and Eng. A, **445-446**, pp. 461-466.

[10] Griffith, M.L., Harwell, L.D., Romero, J.T., Schlienger, E., Atwood, C.L., and Smugeresky, J.E., 1997, "Multi-Material processing by LENS," *Proceedings of the 6th Solid Freeform Fabrication Symposium*, Austin, TX, USA., August 11-13.

[11] Lin, X, Yue, T.M., Yang, H.O., and Huang, W.D., 2006**,** "Microstructure and Phase Evolution in Laser Rapid Forming of a Functionally Graded Ti–Rene88DT alloy," Acta Mater., **54**(7), pp. 1901-1915.

[12] Foroozmehr, E., Sarrafi, R., Hamid, S., and Kovacevic, R., 2009, "Synthesizing of Functionally Graded Surface Composites by Laser Powder Deposition Process for Slurry Erosion Applications," *Proceedings of the 20th Solid Freeform Fabrication Symposium*, Austin, TX, USA, August 3-5.

[13] Liu, W., and Dupont, J.N., 2003, "In-Situ Reactive Processing of Nickel Aluminides by Laser-Engineered Net Shaping, "Metall. Mater. Trans. A, **34**(11), pp. 2633-2641

[14] Banerjee, R., Collins, P.C., Genc¸ A., and Fraser, H.L., 2003, "Direct Laser Deposition of In Situ Ti_ 6Al_ 4V_ TiB Composites", Mater. Sci. Eng. A, **358**, pp.343-349

[15] Banerjee, R., Collins, P.C., and Fraser, H.L., 2002, "Laser Deposition of In Situ Ti–TiB Composites," Adv. Eng. Mater., **4**(11), pp. 847-851.

[16] Janaki Ram, G.D., and Stucker, B.E., 2008, "LENS® Deposition of CoCrMo Coatings on Titanium Implant Structures," J. Manuf. Sci. Eng., **130**(2), pp. 024503-1 to 024503- 5, 2008.

[17] Janaki Ram, G.D., Carson, E., and Stucker, B.E., 2008, "Microstructure and Wear Properties of LENS® Deposited Medical Grade CoCrMo," J. Mater. Sci.: Mater. Medicine, **19**(5), pp. 2105-2111.

[18] Dewhurst, P., 2005, "A General Optimality Criterion for Strength and Stiffness of Dual-Material Property Structures," Int. J. Mech.l Sci., **47**(20), pp. 293- 302.

[19] Selyugin, S.V., 2004, "Some General Results for Optimal Structures," Struct. Multi-Disc. Optimiz., **26**(5), pp. 357-366.

[20] Michell, A.G.M., 1904, "Limits of Economy of Material in Frame-Structures," Philosophical Magazine, **8**(47), pp. 589-597.

[21] Dewhurst, P., 2001, "Analytical Solutions and Numerical Procedures for Minimum-Weight Michell Structures," J. Mech. Phys. Solids, **49**(3) pp. 445 – 467

CHAPTER 7

CONCLUSIONS AND FUTURE WORK

7.1 Summary of Results

The research goal of developing methodologies for fabricating multi-material structures having effective material transition joints have been achieved.

Several engineering materials were successfully bonded using ultrasonic consolidation. This included various combinations of molybdenum; tantalum; titanium; silver; copper; MetPreg®; Nickel; stainless steel 316L; boron powder; and aluminum alloys 3003, 1100, and 6061. The list is made up of face centered cubic (FCC), body centered cubic (BCC) and hexagonal close pack (HCP) crystal structured materials. All the FCC materials are relatively softer than other material types and bonded well with each other. However, only the aluminum alloys had good bonding with all other materials. None of molybdenum, tantalum and titanium bonded with itself or other BCC or HCP materials. With the use of 50μm thick Al 1100 foil as an interlayer, any of the difficult to join materials could be effectively bonded either to themselves in similar material system or to other materials.

The shear strengths of UC fabricated Ti/Al 3003 dual-material were characterized using post-consolidation annealing at 480^{o}C at different soaking times in the oven. The soaking times ranged from 30 to 270 minutes. The as-consolidated material yielded average shear strength of 37.78 MPa. All heat treated samples yielded higher average shear strengths than the as-consolidated samples. The highest average value of 72.96 MPa was recorded for 30 minute heat treated samples. Samples heat treated for longer times generally yielded lower shear strength value. The reduction in strength is due to

recrystallization and grain growth with longer soaking time resulting in softening at the interface.

In UC fabricated structures using automatic foil feeding, intra-layer edge-to-edge gaps between foils are common defects. This could result in early failure in fabricated structures if not eliminated or minimized. Characterization of the transverse strengths of fabricated structures using varying foil edge-to-edge gaps was carried out. Specimens fabricated using the default foil overlap setting yielded an average transverse tensile strength of 180 MPa. With wider foil edge-to-edge gaps, lower transverse strength values were obtained. As the edge-to-edge gaps are closed up, transverse strengths progressively increased to a maximum of 201 MPa. Further reduction in edge-to-edge gaps resulted in the reduction of transverse strengths. This is because, it was difficult to bond the foils with further reduction in the edge-to-edge gaps.

A methodology was developed for fabricating dual-material structures. This involved repeated fabrication of a minimum thickness of block of Al 3003 matrix material and using the integrated CNC milling head to create cavities for embedding the second material. After embedding the reinforcing material, another block of the same thickness is fabricated in a cycle until the desired thickness is achieved. Dual-material minimum weight structures made of MetPreg® and titanium reinforcing materials were fabricated and tested. Reinforced structures failed at higher strength values than those made with single matrix materials.

LENS fabricated dual-material structures with different material transition joint designs were tested for flexural and tensile strengths. The results show that joint designs do not have significant effects on the flexural strengths of the structures. However, it has

statistically significant effects on their tensile strengths. Structures with interlocked transition joint design yielded the highest average tensile strength value of 1146 MPa, while v-groove and random joints respectively yielded the lowest strength values of 939 MPa and 875 MPa.

7.2 Conclusions

7.2.1 Multi-Material Bonding Using Ultrasonic Consolidation

The multi-material capabilities of additive manufacturing technologies using ultrasonic consolidation and laser-engineered net shaping have been demonstrated in this work. It has been proven that a wide range of materials can be bonded to fabricate multi-material structures. Within the limits of the process parameters of the Solidica Formation^{TM} used, most of the face centered cubic (FCC) crystal structured materials investigated bonded well with themselves and other FCC materials. It was also found that the ability to plastically deform at least one of a combination of materials is a major requirement for successful UC fabrication of multi-material structures. The possibility of local composition control within a limited area of a structure was demonstrated by successfully embedding fine boron particles in UC structures. This can be an initial step for further processing like heat treatments.

7.2.2 Optimization of the Shear Strengths of Ti/Al 3003 Dual-Material Structures

The bond strengths of Ti/Al 3003 characterized using lap shear testing show that the strengths of as-consolidated structures can be significantly improved by subjecting them to suitable heat treatments. It was found that a 30-minute oven annealing yielded

about twice the shear strength of as-consolidated materials. Longer heat treatment times degraded the strength of the structures. Post consolidation heat treatment synergizes the complex geometry and multi-material capabilities of UC with the good bond strengths obtainable with diffusion bonding. This is especially good for heat treatable material combinations.

7.2.3 Minimizing Defects Between Adjacent Consolidated Foils

UC fabricated structures have some associated intra-layer and interlayer bonding defects. Several authors have been able to develop optimum sets of parameters for specific materials that are able to eliminate or minimize the occurrence of interlayer bonding defects to improve the linear welding density. In this work, it was discovered that optimizing foil overlap settings in a UC machine can minimize the occurrence of edge-to-edge intra-layer gap defects. In complex load carrying structures, it is difficult to avoid stresses in the transverse orientation to the consolidation direction. The optimized overlap setting in the standard Al 3003 foils used for automatic feeds in a Solidica Formation™ machine was found to yield microstructures with the lowest defect incidence and good structure strengths in the transverse direction.

7.2.4 Multi-Material Minimum Weight Structures Fabrication Using UC

Most UC fabricated multi-material structure research studies have been limited to investigations of dissimilar materials that can be welded to each other. They are mostly characterized using different metallographic methods. Methodologies for fabricating actual multi-material structures was developed using MetPreg® and titanium embedded in

Al 3003 matrix materials without the use of any special fixtures like rotary tables. Dual-material minimum weight structures were fabricated and tested to verify their load carrying capabilities. In comparison to structures made of the matrix material only, both titanium and MetPreg based dual-material structures were found to yield statistically significantly higher strain energy densities at failure. The outcome of the study shows that UC can be used for fabricating multi-material components for structural applications.

7.2.5 Characterization of the Strengths of LENS Fabricated Dual-Material Joints

Successful fabrication of multi-materials using fusion based technologies has been a challenge. Differences in physical properties and chemical compositions often result in cracks at the material joints during fabrication. In this work, different material transition joints were designed and fabricated for Ti6Al4V and Ti6Al4V/10wt%TiC dual-materials. The results of flexural tests show that there is no statistically significant difference in the strength of the structures using any of the transition joint designs. However, there is evidence through tests to show that the material transition joint designs have significant effects on the tensile strengths of the structures. Randomly interlocked and v-groove transition joint designs performed poorly in comparison to butt, gradient, interlocked and scarf joints.

Ti6Al4V and Ti6Al4V/10%wt%TiC dual-material structures with a combination of butt and scarf joints were found to develop cracks at any point beyond the eighth layer during deposition. The use of Ti6Al4V interlayers at an interval of every four layers of Ti6Al4V/10wt%TiC minimized the cracking problems.

7.3 Recommendations

Based on the knowledge gained in this work the following recommendations have been considered necessary for their applications and further work.

7.3.1 Use of Interlayer Materials

With Solidica Formation^{TM} machine used in this work, none of the BCC and HCP structured materials bonded well to each other. Interlayer materials were used to bond them to each other. It is believed that with higher ultrasonic energy, those harder materials can be bonded to each other. However, where higher capacity machines are unavailable, suitable materials can be used as interlayer between difficult to joint materials of interest. The interlayer materials should be such that will not negatively affect the functionality of the two principal materials been bonded. In most cases, the interlayer material can bond well with each of the principal materials.

7.3.2 Improving the Bond Strengths of UC Structures

Improved bonding strength in ultrasonically consolidated structures can be achieved by subjecting them to suitable heat treatment. The structures must initially be well bonded ultrasonically before subsequent heat treatment. This will eliminate the need for pressure application during heat treatment. Post-consolidation treatment brings about a synergy of the benefits of the complex geometries possible with additive manufacturing and the strong bonding achievable with diffusion bonding processes.

7.3.3 Reinforcement Materials for UC Structures

Where possible, ductile reinforcing materials are recommended in place of brittle ones in complex UC fabricated multi-material structures for load bearing applications.

The more ductile materials have capabilities to enhance plastic deformation on members with foil edge-to-edge joints. As failures are more likely to occur at the foil edge-to-edge joints on stressed members, the use of brittle materials as reinforcement has been found not to perform well like the less brittle ones. Fractures originate from the foil edge-to-edge joints in most cases. This propagates through brittle materials much more easily. Based upon the results obtained, metallic material reinforcement should be preferred over composite. Further study is however, recommended for better understanding.

7.3.4 Transition Joint Designs in LENS Fabricated Multi-Material Structures

Material transition joint design is an important factor that has effects on the mechanical integrity of LENS fabricated multi-material structures. Interlocked, gradient, scarf and butt joints have been found to work well for dual-material structures subjected to tension load. Where possible, the interlocked joint is preferred as it has been proven to perform better under loading conditions. For material systems that are susceptible to cracking at the joints, the use of alternating strips of the two materials at the transition helps to minimize crack occurrence. Based on the knowledge gained in this work, randomized interlocked and v-groove designs are not recommended for multi-material transition joints in LENS fabricated structures. They are susceptible to fabrication defects that can result in early failures under loading conditions.

7.3.5 Multi-Material Transition Joints for Structures Fabricated Using Other AM Processes

In other additive manufacturing processes like Electron Beam Melting, Fused Deposition Modeling, Stereolithography, 3D Printing and related technologies, regular

interlocked transition joints is recommended as a first choice for multi-material structures fabrication. They enable greater surface area of contact at the transition joints. In fusion based processes, they help in minimizing the occurrence and propagation of cracks.

7.4 Future Work

There are other areas of further research work that can be identified from the outcome of the present work. These are discussed in the following sub-sections.

7.4.1 Higher-Powered Multi-Material UC Bonding

Attempts have been made to bond several dissimilar materials in this work using UC. The result has been varied. In some, very good bondings were achieved, especially in the cases involving aluminum alloys and harder materials. Moderate bonding was achieved in some material combinations, especially Al 6061 and Tantalum. Molybdenum could not be bonded directly with Copper; an interlayer thin foil Al 1100 was used to indirectly weld the two principal materials. Also, none of the body centered cubic (BCC) structured materials could be bonded to each other or to titanium, the only hexagonal close pack (HCP) structured material used in the work.

It is strongly believed that with much higher ultrasonic energies, beyond the capabilities of the Solidica Formation^{TM} used, good bonding can be achieved with more materials.

7.4.2 Characterization of the Bonding Strengths of UC Fabricated Multi-Materials

Most of the multi-material characterizations have been limited to qualitative techniques using metallographic studies. While this is very important, it is not enough for

comprehensive definition of the overall quality of the bonds. Determining the bonding strengths of UC fabricated multi-material components using quantitative testing methods is very important for their potential applications in real life. Limited attention was devoted to this by characterizing the bonding strength of Ti/Al 3003 in this work. It will be necessary to characterize other combinations of materials to ascertain the optimum fabrication conditions that will yield the best bonding strengths. The overall aim is to maximize bonding strengths between the materials joined by using optimized process parameters and to attain shear strength values as close as possible to one of the base materials.

7.4.3 UC Process Improvement for Multi-Material Structures

The dual-material minimum weight structures fabrication in this work were physically exacting, requiring the skill of the fabricator to accurately place the reinforcing materials in their rightful positions. Development of special fixtures or automated handling for that purpose will enhance multi-material consolidation and reduce the level of human attention currently required to put the materials in place accurately.

7.4.4 Crack Formation and Propagation in LENS Fabricated Structures

Higher stiffness values were originally desired for the tension members of the LENS fabricated minimum weight structures in chapter 6. This was intended to be achieved with high TiC compositions in Ti6Al4V/TiC composite. However, cracks developed in 20wt%TiC and higher percentage compositions. Minimum weight structures fabricated with 10wt%TiC composition in the tension materials had to be redesigned to avoid crack formation after initial unsuccessful attempts. For simple tensile

and flexural specimens' fabrications, no crack developed with Ti6Al4V/10wt%TiC materials. This is because there was free room for expansion and contraction in those specimens. However, in complex structures with multiple materials, differential coefficient of expansion results in residual stresses leading to cracks.

In future work, studies on avoiding crack formation and propagation will be necessary in order to be able to fabricate structures with higher stiffness materials made of Ti6Al4V/TiC composite. It is recommended to first develop a finite element model to determine the process windows for crack free LENS fabrications.

APPENDIX

Permissions

All permissions related to the inclusion of Journal articles in this dissertation are presented in subsequent pages.

aggiemail John Obielodan <john.obielodan@aggiemail.usu.edu>

Fwd: ASME PUBLICATIONS PERMISSION REQUEST FORM SUBMISSION

Beth Darchi <DarchiB@asme.org> **Tue, May 18, 2010 at 9:37 AM**
To: john.obielodan@aggiemail.usu.edu

Dear Mr. Obielodan:
It is our pleasure to grant you permission to use ASME paper "Minimizing defects between adjacent foils in ultrasonically consolidated parts," by J.O. Obielodan, G.D. Janaki Ram, B.E. Stucker and D.G. Taggart, Journal of Engineering Materials and Technology, Vol. 132, 2010, cited in your letter for inclusion in a Doctoral Thesis entitled Fabrication of multi-material structures using ultrasonic consolidation and laser-engineered net shaping to be published by Utah State University.

As is customary, we ask that you ensure full acknowledgment of this material, the author(s), source and ASME as original publisher on all printed copies being distributed.

Many thanks for your interest in ASME publications.

Sincerely,
Beth Darchi
Permissions & Copyrights
ASME, 3 Park Avenue
New York, NY 10016
T: 212-591-7700
F: 212-591-7841
E: darchib@asme.org

>>> <webmaster@asme.org> 5/15/2010 4:11 PM >>>

Permissions

Emerald's permissions service is now enhanced with Copyright Clearance Center's Rightslink® service.

"Promoting and protecting the interests of those who create and those who invest in creativity"

Emerald's permission service is now delivered through the Copyright Clearance Center's Rights Link® online system. This new development provides a highly efficient, real time service to clear copyright permission for the lawful re-use, distribution or republication of Emerald's copyright materials.

The quick way to clear permissions

- Locate the abstract of the article you wish to reuse in the Emerald database
- Click on the 'Reprints and Permissions' link
- Select the rights required (following the online instructions)
- Receive an immediate quote (you will be asked to set up a RightsLink® account to pay online)
- Read and accept Emerald's Terms & Conditions

NB: if Emerald does not hold the copyright of an article, the link will not appear. For permission to use these articles contact the copyright holder directly.

Translation rights

For translation rights, please contact permissions@emeraldinsight.com

You can also read further information on Emerald's copyright policy.

Emerald Authors

Please note that when an author publishes in an Emerald publication, they retain the right to:

- ***Distribute copies of their own published article for educational purposes***
- ***Reuse or republish part or all of their article in a presentation, dissertation, journal article or book edited by themselves***
- ***Post the pre-print or final accepted version of their paper (not the journal PDF) in an institutional or subject repository***

Authors do not need to request our permission for any of the above but if you require written permission for your publisher, please contact permissions@emeraldinsight.com

For further information please see Emerald's Authors' Charter.

aggiemail **John Obielodan <john.obielodan@aggiemail.usu.edu>**

Permission for Journal Reprint

John Obielodan <john.obielodan@aggiemail.usu.edu> **Sun, Jun 20, 2010 at 11:51 PM**
To: janakiram_gabbita@yahoo.co.in, Durga Janaki Ram Gabbita <jram@iitm.ac.in>

Dear Dr. Janaki Ram Gabitta,

I will please want you to give me your permission to use the paper we co-authored as follows as a chapter in my multi-paper dissertation.

J.O. Obielodan, G.D. Janaki Ram, B.E. Stucker, D.G. Taggart, 2010. Minimizing defects in adjacent foils in ultrasonically consolidated parts,
Vol.132(1), pp.011006-1 - 011006-8.

The permission is required by Utah State University graduate school policy before I can include the paper as a chapter.

Thank you.
John Obielodan

aggiemail **John Obielodan <john.obielodan@aggiemail.usu.edu>**

Permission for Journal Reprint

David G Taggart <taggart@uri.edu> **Mon, Jun 21, 2010 at 4:09 AM**
Reply-To: taggart@uri.edu
To: John Obielodan <john.obielodan@aggiemail.usu.edu>

Hi John,

It's good to hear from you. Yes, you have my permission to use the paper we co-authored as a chapter in your dissertation.

Thanks,
Dave
[Quoted text hidden]
--
David G. Taggart, Ph.D.
Professor and Chair, Mechanical, Industrial and Systems Engineering
University of Rhode Island
204 Wales Hall, 92 Upper College Road, Kingston, RI 02881
401-874-5934, Fax 401-874-2355, E-mail taggart@uri.edu

aggiemail John Obielodan <john.obielodan@aggiemail.usu.edu>

Permission for Journal Reprint

John Obielodan <john.obielodan@aggiemail.usu.edu> **Sun, Jun 20, 2010 at 11:51 PM**
To: janakiram_gabbita@yahoo.co.in, Durga Janaki Ram Gabbita <jram@iitm.ac.in>

Dear Dr. Janaki Ram Gabitta,

I will please want you to give me your permission to use the paper we co-authored as follows as a chapter in my multi-paper dissertation.

J.O. Obielodan, G.D. Janaki Ram, B.E. Stucker, D.G. Taggart, 2010. Minimizing defects in adjacent foils in ultrasonically consolidated parts,
Vol.132(1), pp.011006-1 - 011006-8.

The permission is required by Utah State University graduate school policy before I can include the paper as a chapter.

Thank you.
John Obielodan

aggiemail John Obielodan <john.obielodan@aggiemail.usu.edu>

Permission for Journal Reprint

Durga Janaki Ram Gabbita <jram@iitm.ac.in> **Tue, Jun 22, 2010 at 12:52 PM**
To: John Obielodan <john.obielodan@aggiemail.usu.edu>

Hi John,
I remember James obtained these permissions on a specific form. Please verify. In any case, this paper can form a part of your thesis.
Good luck with your thesis.
With kind regards,
Janaki Ram

_____
From: John Obielodan [john.obielodan@aggiemail.usu.edu]
Sent: Monday, June 21, 2010 11:21 AM
To: janakiram_gabbita@yahoo.co.in; Durga Janaki Ram Gabbita
Subject: Permission for Journal Reprint
[Quoted text hidden]

aggiemail John Obielodan <john.obielodan@aggiemail.usu.edu>

Permission for Journal Reprint

John Obielodan <john.obielodan@aggiemail.usu.edu> **Sun, Jun 20, 2010 at 12:55 AM**
To: "Murr, Lawrence E." <lemurr@utep.edu>

Dear Dr. Murr,

I appreciate your expedited response to the paper I sent. Please, I have a VERY URGENT request from you before you go to the laboratory you mentioned in your mail where you may not have internet service. I am about to defend my dissertation. The papers I have had with you will be included in my multi-paper dissertation, and I am required by our graduate school to obtain written permission from all co-authors to all papers to be included.

I will be glad if you can reply me with a mail granting me the permission to use the papers for my dissertation. The titles of the papers are as follows:

(i) Multi-material bonding in ultrasonic consolidation, published in Rapid prototyping Journal, Vol.16(3), pp.180-188, 2010.

(ii) Optimization of the shear strengths of ultrasonically consolidated Ti/Al3003 dual-material structures, to be submitted to the Journal of materials processing technology

I will also need the email adresses of all your students whose names appear on the last journal, in order for me to request for their permission also.

Thank you.
John

aggiemail **John Obielodan <john.obielodan@aggiemail.usu.edu>**

Permission for Journal Reprint

Murr, Lawrence E. <lemurr@utep.edu> **Tue, Jun 22, 2010 at 12:34 AM**
To: John Obielodan <john.obielodan@aggiemail.usu.edu>

John,
I am pleased to give you permission to use our joint work as necessary.
L. E. Murr,
Murchison Professor and Chairman
Department of Metallurgical and Materials Engineering
The University of Texas at El Paso

You can email my principal student, Sara Gaytan, and she will provide the email info. You might send her the names of students involved.
(smgaytan@miners.utep.edu)

Best wishes,
L. E. Murr

From: John Obielodan [john.obielodan@aggiemail.usu.edu]
Sent: Sunday, June 20, 2010 12:55 AM
To: Murr, Lawrence E.
Subject: VERY URGENT REQUEST!
[Quoted text hidden]

Dear Sir/Madam,

I would like to give my permission to J.O. Obielodan to use the paper named as "Multi-material bonding in ultrasonic consolidation, Rapid Prototyping Journal, vol. 16(3), pp. 180-188" in any place of scientific field.

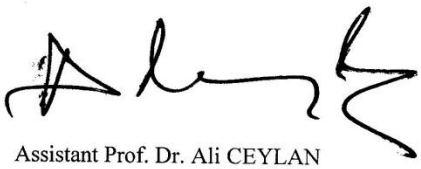

Assistant Prof. Dr. Ali CEYLAN

Dumlupinar university,

Ceramic Engineering Department

Kutahya / Turkey

aggiemail **John Obielodan <john.obielodan@aggiemail.usu.edu>**

Permission for paper inclusion in dissertation

John Obielodan <john.obielodan@aggiemail.usu.edu> **Mon, Jun 21, 2010 at 12:11 PM**

To: emartinez21@miners.utep.edu, jlmartinez6@miners.utep.edu, Hernandez.h.daniel@gmail.com, daramirez2@miners.utep.edu

Dear All:

I will please want you to give me your permission to use the paper we co-authored as follows as a chapter in my multi-paper dissertation.

J.O. Obielodan, B.E. Stucker, E. Martinez, J.C. Martinez, D.H. Hernandez, and L.E. Murr. "Optimization of the Shear Strengths of Ultrasonically Consolidated
Ti/Al 3003 Dual-Material Structures", Journal of Materials Processing Technology

The permission is required by Utah State University graduate school policy before I can include the paper as a chapter.

You can give your permission through individual reply to this mail.

Thank you.
John

aggiemail **John Obielodan <john.obielodan@aggiemail.usu.edu>**

Permission for paper inclusion in dissertation

Edwin Martinez <emartinez21@miners.utep.edu> **Mon, Jun 21, 2010 at 12:25 PM**
To: john.obielodan@aggiemail.usu.edu

yes you may use the paper
E. Martinez

> Date: Mon, 21 Jun 2010 12:11:41 -0600
> Subject: Permission for paper inclusion in dissertation
> From: john.obielodan@aggiemail.usu.edu
> To: emartinez21@miners.utep.edu; jlmartinez6@miners.utep.edu; Hernandez.h.daniel@gmail.com; daramirez2@miners.utep.edu
[Quoted text hidden]

aggiemail **John Obielodan <john.obielodan@aggiemail.usu.edu>**

Permission for paper inclusion in dissertation

John Obielodan <john.obielodan@aggiemail.usu.edu> **Mon, Jun 21, 2010 at 12:11 PM**

To: emartinez21@miners.utep.edu, jlmartinez6@miners.utep.edu, Hernandez.h.daniel@gmail.com, daramirez2@miners.utep.edu

Dear All:

I will please want you to give me your permission to use the paper we co-authored as follows as a chapter in my multi-paper dissertation.

J.O. Obielodan, B.E. Stucker, E. Martinez, J.C. Martinez, D.H. Hernandez, and L.E. Murr. "Optimization of the Shear Strengths of Ultrasonically Consolidated
Ti/Al 3003 Dual-Material Structures", Journal of Materials Processing Technology

The permission is required by Utah State University graduate school policy before I can include the paper as a chapter.

You can give your permission through individual reply to this mail.

Thank you.
John

aggiemail **John Obielodan <john.obielodan@aggiemail.usu.edu>**

Permission for paper inclusion in dissertation

Daniel Hernandez <hernandez.h.daniel@gmail.com> **Tue, Jun 22, 2010 at 9:37 AM**
To: John Obielodan <john.obielodan@aggiemail.usu.edu>

Yes, you have my permission to use the paper.

Daniel Hernandez

Sent from my iPhone
[Quoted text hidden]

aggiemail **John Obielodan <john.obielodan@aggiemail.usu.edu>**

Permission for paper inclusion in dissertation

John Obielodan <john.obielodan@aggiemail.usu.edu> **Mon, Jun 21, 2010 at 12:11 PM**

To: emartinez21@miners.utep.edu, jlmartinez6@miners.utep.edu, Hernandez.h.daniel@gmail.com, daramirez2@miners.utep.edu

Dear All:

I will please want you to give me your permission to use the paper we co-authored as follows as a chapter in my multi-paper dissertation.

J.O. Obielodan, B.E. Stucker, E. Martinez, J.C. Martinez, D.H. Hernandez, and L.E. Murr. "Optimization of the Shear Strengths of Ultrasonically Consolidated
Ti/Al 3003 Dual-Material Structures", Journal of Materials Processing Technology

The permission is required by Utah State University graduate school policy before I can include the paper as a chapter.

You can give your permission through individual reply to this mail.

Thank you.
John

aggiemail **John Obielodan <john.obielodan@aggiemail.usu.edu>**

Permission for paper inclusion in dissertation

Diana Ramirez <daramirez2@miners.utep.edu> **Tue, Jun 22, 2010 at 11:16 AM**
To: John Obielodan <john.obielodan@aggiemail.usu.edu>

Hi,
Yes that will be fine. I would like to have a copy of the paper if possible to read as well.

Diana A Ramirez
Sent via BlackBerry from T-Mobile

-----Original Message-----
From: John Obielodan <john.obielodan@aggiemail.usu.edu>
Date: Mon, 21 Jun 2010 18:11:41
To: <emartinez21@miners.utep.edu>; <jlmartinez6@miners.utep.edu>; <Hernandez.h.daniel@gmail.com>; <daramirez2@miners.utep.edu>
Subject: Permission for paper inclusion in dissertation

[Quoted text hidden]

aggiemail **John Obielodan <john.obielodan@aggiemail.usu.edu>**

Permission for paper inclusion in dissertation

John Obielodan <john.obielodan@aggiemail.usu.edu> **Mon, Jun 21, 2010 at 12:11 PM**

To: emartinez21@miners.utep.edu, jlmartinez6@miners.utep.edu, Hernandez.h.daniel@gmail.com, daramirez2@miners.utep.edu

Dear All:

I will please want you to give me your permission to use the paper we co-authored as follows as a chapter in my multi-paper dissertation.

J.O. Obielodan, B.E. Stucker, E. Martinez, J.C. Martinez, D.H. Hernandez, and L.E. Murr. "Optimization of the Shear Strengths of Ultrasonically Consolidated
Ti/Al 3003 Dual-Material Structures", Journal of Materials Processing Technology

The permission is required by Utah State University graduate school policy before I can include the paper as a chapter.

You can give your permission through individual reply to this mail.

Thank you.
John

aggiemail **John Obielodan <john.obielodan@aggiemail.usu.edu>**

Permission for paper inclusion in dissertation

LOUIE MARTINEZ <jlmartinez6@miners.utep.edu> **Tue, Jun 22, 2010 at 1:28 PM**
To: john.obielodan@aggiemail.usu.edu

It is J.L. Martinez and yes for me!

> Date: Mon, 21 Jun 2010 12:11:41 -0600
> Subject: Permission for paper inclusion in dissertation
> From: john.obielodan@aggiemail.usu.edu
> To: emartinez21@miners.utep.edu; jlmartinez6@miners.utep.edu; Hernandez.h.daniel@gmail.com; daramirez2@miners.utep.edu
>
[Quoted text hidden]

CURRICULUM VITAE

John Olorunshola Obielodan
(September 2010)

EDUCATION

Doctor of Philosophy, Mechanical Engineering September 2010
Utah State University, Logan, UT.
Dissertation: Fabrication of Multi-Material Structures Using Laser-Engineered Net Shaping and Ultrasonic Consolidation. Chair: Dr. Brent Stucker

Advanced Postgraduate Course in Tool, Die & Mold Design 1994-1996
Central Institute of Tool Design, Hyderabad, India.
Research: Design of Die-Casting Die for an Automotive Cylinder Head

Bachelor of Engineering, Mechanical 1984-1989
University of Ilorin, Nigeria.
Research: Design and Manufacture of Engineering Components by Squeeze Casting and Gravity Die Casting Processes

RESEARCH EXPERIENCE

Research Assistant, Advanced Manufacturing and Materials Laboratory, Mechanical & Aerospace Engineering Department, Utah State University, USA, 2007-2010.

- Designed and analyzed experiments using statistical tools
- Fabricated multi-material structures using ultrasonic consolidation (UC) and laser-engineered net shaping (LENS)
    - Structures were fabricated using selected material combinations from CP Titanium; Ti6Al4V; Ti6Al4V/TiC composites; MetPreg®; Molybdenum; Nickel; Silver; Boron; Tantalum; Copper; Stainless Steel 316L; and Aluminum Alloys 1100, 3003 and 6061
- Determined optimum multi-material joint designs for LENS fabricated structures
- Characterized material bonding qualities using optical and scanning electron microscopy
- Performed mechanical properties testing and characterization
- Performed failure analysis
- Studied microstructure-property correlation

RESEARCH INTERESTS

- Multi-material additive manufacturing for complex structure designs
    - For aerospace, automobile, medical, nuclear and other industrial applications
- Rapid tooling
- Tool, die and mold design
- Metal and polymer forming processes

TEACHING EXPERIENCE

Visiting Assistant Professor, Ohio Northern University August 2010 - Present
Computer-Aided Design
Engineering Analysis

Adjunct Lecturer, Ahmadu Bello University, Zaria, Nigeria 1997-2006
Taught the following undergraduate courses:

- Mechanics and Properties of Materials
- Manufacturing Processes
- Machine Design I
- Machine Design II
- Tribology

Teaching Assistant, Utah State University, Logan January 2007 – May 2010

- **Laboratory Teacher,** Material Science and Engineering, Spring 2007, Fall 2007, Spring 2008 and Spring 2010.
- **Grader,** Advanced Dynamics, Fall 2008 and Fall 2009
- **Grader**, Machine Design, Spring 2009
- **Grader,** Mechanics of Solids, Summer 2009
- **Grader,** Thermodynamics, Summer 2009

INDUSTRY EXPERIENCE

Assistant Director, Design and Production, Center for Automotive Design & Development, Ahmadu Bello University, Zaria, Nigeria, January 2004 - December 2006

- Actively involved in the hands-on design activities listed under Principal Engineer position below
- Supervised automotive component, systems and tool design activities
- Oversaw manufacturing activities for prototype vehicle components and assemblies
- Served as a member of management

Principal Engineer, Center for Automotive Design & Development, Ahmadu Bello University, Zaria, Nigeria, January 2000 - December 2003

- Designed more than 120 stamping tools for automotive body, chassis and suspension components
- Designed and fabricated automotive components measuring fixtures
- Frequently traveled to supervise the manufacturing of tools and automotive components contracted to companies in six different states in Nigeria, the tools and components were designed in-house

Senior Engineer, Center for Automotive Design & Development, Ahmadu Bello University, Zaria, Nigeria, July 1993 - December 1999

- Designed automotive body, chassis and power train components and systems
- Involved in the fabrication and testing of mock-ups of designed automobile body and chassis systems

- Performed automotive components measurement in the metrology laboratory
- Was on study leave from August 1994 – January 1996

Assistant Territorial Manager, Soko-Tech Nigeria Limited, Jos, Nigeria, January 1993 - June 1993

- Managed the northeastern branch of the company in Jos, Nigeria with 34 technical and non-technical employees
- Coordinated all electrical, mechanical and telecommunication engineering projects in the company branch
- Prepared bill of materials and tendered for ventilation, air-conditioning and plumbing services for public buildings

Project Engineer, Soko-Tech Nigeria Limited, Jos, Nigeria, October 1990 - December 1992

- Designed plumbing systems for public buildings
- Supervised ventilation, air-conditioning and plumbing installation projects
- Maintained central air-conditioning systems

National Youth Service, Peugeot Automobile Nigeria Limited, Kaduna, Nigeria, October 1989 - September 1990

- Designed and fabricated material handling equipment
- Involved in time and motion studies for automotive assembly activities

SERVICE AND LEADERSHIP

Undergraduate Recruitment Summer 2008

- Participated in advanced manufacturing equipment demonstrations to high school students from Wyoming, Idaho and Utah states as part of a week-long Utah State University engineering state program designed for enlightening prospective undergraduate students.

Chairman, **"The Zaria Professionals"**, a non-profit multi-disciplinary community based professional development body, 1999 - 2006

- Organized many successful professional workshops in which industry leaders and professionals in engineering, business, agriculture, academia and others were invited for talks to members and other invited professionals
- Successfully coordinated the activities of the more than 60-member multi-disciplinary professionals

Chairman, Senior Staff Association, Centre for Automotive Design & Development, Zaria (2000 - 2003)

- Successfully coordinated the activities of this workplace welfare association

REVIEWER FOR

- International Journal of Materials and Structural Integrity
- Solid Freeform Fabrication Symposium

PUBLICATIONS

Journal/Conference Papers

- Obielodan, J.O., Ceylan, A., Murr, L.E., and Stucker, B.E., **(**2010), 'Multi-material bonding in ultrasonic consolidation," *Rapid Prototyping Journal,* **16**(3), pp.180-188.

- Obielodan, J.O., Janaki Ram, G.D., Stucker, B.E., and Taggart, D.G. (2010), "Minimizing defects between adjacent foils in ultrasonically consolidated parts," *Journal of Engineering Materials and Technology,* **132** (1), pp. 011006-1 - 011006-8.

- Obielodan, J.O., Stucker, B.E., Martinez, E., Martinez, J.C., Hernandez, D.H., Ramirez, D.A., and Murr, L.E., "Optimization of the shear strengths of ultrasonically consolidated Ti/Al dual-material structures," *Journal of Materials Processing Technology,* under review.

- Obielodan, J.O., and Stucker, B.E., "Multi-material minimum weight structures fabrication using ultrasonic consolidation," *Proceedings of 21st International Solid Freeform Fabrication Symposium*, Austin, TX, USA, August 9-11, 2010.

- Obielodan, J.O., and Stucker, B.E., "Characterization of the strengths of dual-material joints fabricated using laser-engineered net shaping," *Proceedings of 21st International Solid Freeform Fabrication Symposium,* Austin, TX, USA, August 9-11, 2010.

- Obielodan, J.O., and Stucker, B.E., "Effects of post processing heat treatments on the bond quality and mechanical strength of Ti/Al3003 dual materials fabricated using ultrasonic consolidation," *Proceedings of 20th International Solid Freeform Fabrication Symposium,* Austin, TX, USA, August 3-5, 2009.

- Obielodan, J.O., and Stucker, B.E., "Further exploration of multi-material fabrication capabilities of ultrasonic consolidation technique," *Proceedings of 20th International Solid Freeform Fabrication Symposium,* Austin, TX, USA, August 3-5, 2009.

- Peter Dewhurst, David Taggart, Ning Fang, Brent Stucker, Stefan Heinemann, Taylor Spalt, Denis Jahns, Sriruk Srithongchai, and John Obielodan. Procedures for the design and manufacture of dual-material minimum weight structures," *Proceedings of 2009 NSF Engineering Research and Innovation Conference,* Honolulu, Hawaii, USA, June 22-25, 2009

- Obielodan, J.O., Janaki Ram, G.D., and Stucker, B.E., "An experimental determination of optimum foil joint conditions for structural parts fabricated by ultrasonic consolidation," *Proceedings of 19th International Solid Freeform Fabrication Symposium,* Austin, TX, USA, August 4-6, 2008.

Trade Articles

- John Obielodan and Brent Stucker, "US Sponsored R&D", *Wohlers report 2010: rapid prototyping and tooling, state of the industry,* Wohlers Associates Inc., Fort Collins, CO, USA, pp.195-200

- **John Obielodan** and Brent Stucker, "US Sponsored R&D", *Wohlers report 2009*: *rapid prototyping and tooling, state of the industry, Wohlers* Associates Inc., Fort Collins, CO, USA, pp.202-206.

- **John Obielodan.** "Tool engineering in the automotive industry", *CADD News,* Vol.1 No.4, 1998.

Technical Books/Reports with Significant Contribution

- "Design and specifications for CADD MARK II", *Publications of the Center for Automotive Design & Development,* Zaria, Nigeria, August, 1994.

- "Book of specification for CADD MARK I revised Edition", *Publications of the Center for Automotive Design & Development*, Zaria, Nigeria, December, 1993.

- "Design calculations for CADD MARK I", *Publications of the Center for Automotive Design & Development,* Zaria, Nigeria, December, 1993.

- "Report on industrial survey", *Publications of the Center for Automotive Design & Development,* Zaria, Nigeria, December, 1993.

HONORS AND AWARDS

- **Outstanding Paper Award**, 20th International Solid Freeform Fabrication Symposium, University of Texas at Austin, TX, USA, August 3-5, 2009
- **Graduate Student Senate Enhancement Award**, Utah State University, 2009
- **Special Commonwealth African Assistance Plan** (scholarship), 1994

PROFESSIONAL AFFILIATIONS AND LICENSING

- **Member,** Society of Manufacturing Engineers (SME), 2009
- **Member,** American Society of Mechanical Engineers (ASME), 2009
- **Member,** Nigerian Society of Engineers (NSE), 1997
- **Registered Professional Engineer,** Council for the Regulation of Engineering in Nigeria (COREN), 2002